The Dissertation Committee for Talha Ahmed Khan
certifies that this is the approved version of the following dissertation:

Analysis and Design of Energy Harvesting Wireless Communication Systems

Committee:

Robert W. Heath Jr., Supervisor

Jeffrey G. Andrews

Edison Thomaz Jr.

Haris Vikalo

Philip Orlik

Analysis and Design of Energy Harvesting Wireless Communication Systems

by

Talha Ahmed Khan

DISSERTATION

Presented to the Faculty of the Graduate School of

The University of Texas at Austin

in Partial Fulfillment

of the Requirements

for the Degree of

DOCTOR OF PHILOSOPHY

THE UNIVERSITY OF TEXAS AT AUSTIN

December 2017

Dedicated to my family - living and deceased.

Acknowledgments

First of all, I would like to express my deepest gratitude to my supervisor Prof. Robert W. Heath, Jr. for his valuable insights, constant support, and encouragement during the course of my PhD. Working with Prof. Heath has been a wonderful experience both professionally and personally. I would also like to thank my other professors at UT especially Prof. Jeffrey G. Andrews and Prof. Francois Baccelli. The courses offered by Prof. Heath, Andrews, and Baccelli laid a solid foundation for my research. I would like to take this opportunity to thank my committee members Prof. Edison Thomaz Jr. and Prof. Haris Vikalo for their constructive feedback that helped refine this work. I am also grateful to Dr. Philip Orlik for hosting me at Mitsubishi Electric Research Labs (MERL). His priceless advice and support helped steer my research early on in my graduate studies. I am also thankful to Dr. K. J. Kim and other staff members at MERL for their help and support while I was interning at MERL. I am grateful to Prof. Petar Popovski for his insightful feedback on my research. I also appreciate the support of Dr. Ali Yazdan, Dr. Yael Maguire, and other staff members at Facebook for facilitating my research. I also appreciate the help provided by all the staff members at UT, especially Melanie Gulick, Melody Singleton and Karen Little. I am thankful to my friends and colleagues at UT Austin particularly my lab mates at WSIL. I also appreciate MERL and the Army Research Office for funding my research. Special thanks to all my family members to whom I will ever be indebted. Last but not least, I would like to thank the Almighty for

making all of this possible.

Talha Ahmed Khan

The University of Texas at Austin

September 2017

Analysis and Design of Energy Harvesting Wireless Communication Systems

Talha Ahmed Khan, Ph.D.
The University of Texas at Austin, 2017

Supervisor: Robert W. Heath Jr.

Wireless-powered communication is an emerging technology for powering the large number of miniature devices of the future. In a wireless-powered communication system, low-power sensors extract energy from the incident wireless signals to power their operations such as information transmission, sensing or reception. Due to sporadic energy availability, however, such a system is fundamentally different from a traditionally-powered communication system. This dissertation investigates three distinct aspects of wireless-powered communications to get insights on the system operation. First, leveraging concepts from finite-length information theory, an analytical framework is developed for examining wireless-powered communications with short packets, i.e., in the finite blocklength regime. This is relevant as remotely-powered communications may entail short packets due to small payloads, low-latency requirements, or limited energy to support a longer transmission. Second, using a stochastic

geometry framework, an analytical model is developed for characterizing the performance of wireless-powered communications in the millimeter wave (mmWave) band. The proposed model incorporates the key features of mmWave systems such as directional beamforming and sensitivity to building blockages. Finally, the power transfer efficiency and the energy efficiency of a wireless-powered communication system aided by massive MIMO is characterized. The broad goal of this dissertation is to better understand wireless-powered communications in the context of the emerging technologies for 5G.

Table of Contents

List of Tables

List of Figures

Chapter 1

Introduction

In this chapter, I provide a general introduction to my research on wireless-powered communications. Section 1.1 highlights some of the challenges in the design and analysis of wireless-powered communication systems. Section 1.2 overviews and motivates the research problems investigated in this dissertation. Section 1.3 presents a brief summary of the research contributions, while Section 1.4 concludes this chapter with an organization of the rest of the dissertation.

1.1 Background

With wireless devices getting smaller and more energy-efficient, energy harvesting is emerging as a potential technology for powering such miniature devices [1–7]. This is attractive for future paradigms such as the Internet of Things (IoT), where powering a massive number of devices will be a major challenge [1, 8]. This is because it eliminates the need of battery replacement which may be practically infeasible due to physical (e.g., remote location) or economic (e.g., labor cost) reasons. Many IoT applications will entail sensors with sporadic sensing and communication activity, resulting in an *average* power requirement on the order of microwatts to milliwatts. Depending on the specific application, the sensor may harvest energy

Table 1.1: Power output for energy harvesting sources

Source	Approximate power per cm^2
Solar	μW (indoor lighting), mW (direct sunlight) [2]
Kinetic	μW (human activity), mW (industrial machinery) [2, 9]
Thermal	μW (humans), mW (industrial) [2]
RF	μW [1, 3–5, 10]

from ambient sources such as solar, thermal, kinetic, or RF (radio frequency) waves, ensuring a perpetual operation [1, 2]. The suitability of a particular harvesting technology for a specific application depends on various factors such as cost, size, power output, and the operating environment (see Table 1.1 for a brief summary). For example, solar energy harvesting requires direct sunlight, kinetic energy harvesting relies on high-frequency vibrations [9], whereas thermal energy harvesting requires a high temperature gradient, which may not be available in many IoT applications [2]. Of interest to this dissertation is RF or wireless energy harvesting, where a harvesting node extracts energy from the incident RF signals [1, 10–14]. This is a suitable option for ultra low-power applications because i) wireless signals are available anywhere and anytime, ii) the harvesting operation relies on a simple circuit consisting of a rectifying antenna which can be integrated with the communication circuitry, allowing for small form factors [11], and iii) the energy delivered to the harvester can be controlled by leveraging the existing infrastructure and the emerging wireless technologies [5, 11]. This brings us to what is commonly known as wireless-powered communications where a communicating node exploits wireless energy harvesting to power its operation [1, 11, 15–18].

Wireless energy harvesting poses many new design challenges to the existing

communication systems. In a stark contrast to a traditionally-powered node, the energy availability at a wirelessly powered node fluctuates with time/frequency due to the inherent randomness in the wireless link. This uncertain energy availability brings additional energy constraints to the communication link. For example, a wireless-powered information transmitter needs to adapt its transmit power relative to the harvested energy. Similarly, there is an inherent trade-off between the channel resources allocated for energy harvesting versus that for information transmission. This means that the existing communication protocols need to be revisited for wireless-powered communication systems.

The analysis of a wireless-powered communication system is fundamentally different from a traditional communication system. For example, though interference is usually harmful for a communication link, it may be beneficial for a wireless-powered communication link. This is because the harvester may exploit the interference signals to boost the harvested energy. Another distinguishing feature of a wireless-powered communication link is the concept of energy outages. A communication link could be in outage either due to a decoding error at the receiver or the lack of sufficient energy at the transmitter. This means that new metrics are needed to characterize the performance of a wireless-powered communication system. For these reasons, the existing literature on traditionally-powered communication systems is not applicable to wireless-powered communications.

Wireless-powered communications has been an active area of research over the last decade. The characterization of fundamental performance limits is a recurring theme in existing work. Various scenarios have been considered featuring

single-antenna/multi-antenna nodes, single-user/multi-user systems, as well as cooperative/opportunistic architectures [17, 19–32]. Optimal policies for resource allocation, energy beamforming, signal/waveform design, and user scheduling have also received considerable attention [12, 33–43]. A detailed discussion about related work is presented in chapters 2-4 of this dissertation.

1.2 Motivation

In this dissertation, I investigate three distinct aspects of wireless-powered communication systems. The presented research provides useful design guidelines for wireless-powered communications, especially in the context of emerging technologies for next-generation wireless systems featuring IoTs, millimeter wave (mmWave), and massive MIMO. I briefly overview the proposed research as follows.

The first part of this dissertation deals with the analysis and design of wireless-powered communication systems in the finite blocklength regime. This is motivated by the fact that wireless-powered communications will typically entail short data packets due to naturally small payloads, and/or insufficient energy resources to support longer transmissions. I, therefore, investigate a wireless-powered communication system where an energy harvesting transmitter, charged by one or more power beacons via wireless energy transfer, attempts to communicate with a receiver over a noisy channel using short packets. Leveraging the frameworks of finite-length information theory and stochastic geometry, I characterize the system performance using metrics such as the energy supply probability at the energy harvester, and the achievable rate at information receiver for the case of short packets. This research provides useful

insights on the system operation in terms of key design parameters such as the energy harvesting duration, the information transmission duration, the harvested power and the transmit power.

The second part of this dissertation deals with the millimeter wave (mmWave) band, which is a prime candidate for 5G cellular networks. It seems attractive for wireless information and energy transfer because it will feature large antenna arrays and extremely dense base station (BS) deployments. The viability of mmWave for wireless-powered communications though is unclear, due to the differences in propagation characteristics (versus lower-frequency counterparts) such as extreme sensitivity to building blockages. With this motivation, I investigate the performance of wireless-powered communication in the mmWave band. Leveraging tools from stochastic geometry, I characterize the system-level performance using metrics such as the energy coverage probability and the overall (energy-and-information) coverage probability at a typical wireless-powered node which extracts energy and/or information from the incident mmWave singals. The developed analytical model incorporates the key features of mmWave systems such as the use of directional antenna arrays and the sensitivity to building blockages. This research provides useful system-level design guidelines in terms of key parameters such as the BS density, the antenna geometry parameters, and the channel parameters.

The final part of this dissertation explores the potential of another emerging technology - massive MIMO - for wireless-powered communications. Because of its ability to focus energy towards desired spatial locations, massive MIMO is attractive for wireless energy transfer. While deploying more antennas at the BS is beneficial

for wireless energy transfer, the additional antenna circuitry leads to increased power consumption at the BS. This motivates the need for an energy efficient system design. I analytically characterize the system-level power transfer efficiency and the energy efficiency (often defined as the ratio of the achievable data rate (bits/sec) and the total power consumption (Watt)) of a massive MIMO wireless-powered communication system where a massive MIMO BS charges energy harvesting nodes in the downlink, and the energy harvesting nodes exploit the harvested energy to transmit information to the BS on the uplink. This analysis provides useful design guidelines for an energy-efficient system operation in terms of the key parameters such as the number of antennas, the number of users, the BS transmit power, and the energy harvesting parameters.

1.3 Overview of Contributions

The main research contributions of this dissertation are summarized as follows.

1. Performance characterization of wireless-powered communications in the finite blocklength regime

    - Proposed an analytical model to characterize the performance of a short packet wireless-powered system using metrics such as the energy supply probability and the achievable rate.
    - Derived scaling laws to expose the interplay between key system parameters such as the harvest blocklength, the transmit blocklength, the harvested power, and the transmit power.

- Extended the analysis to a large-scale network with Poisson-distributed power beacons.

2. Performance characterization of wireless-powered communications in the millimeter wave band

    - Derived tractable analytical expressions for metrics such as the energy coverage probability and the average harvested power for energy harvesting mmWave receivers.
    - Derived analytical expressions for the overall energy-and-information coverage probability for the general case where receivers extract both energy and information from the mmWave signals.
    - Proposed low-power receiver architecture for mmWave simultaneous information and energy transfer.

3. Performance characterization of wireless-powered communications with massive MIMO

    - Investigated the system-level power transfer efficiency of a massive MIMO wireless energy transfer system while using realistic models for energy harvesting and power consumption.
    - Analytically characterized the optimal values for system parameters such as the number of BS antennas and users.

- Extended the analysis to characterize the system-level energy efficiency of a massive MIMO wireless energy and information transfer system.
- Analytically characterized the optimal values for system parameters such as the transmit power that maximizes the energy efficiency.

1.4 Organization

This rest of the dissertation is organized as follows. The contributions of the dissertation are discussed in chapters 2 through 4 in order of completion. The dissertation is concluded in Chapter 5.

Chapter 2

Wireless-powered Communications with Short Packets

In this chapter[1], I propose an analytical framework for characterizing the performance of a wireless-powered communication system in the finite blocklength regime. This is applicable to practical energy harvesting communication systems which usually use short data packets. The proposed framework provides useful design guidelines on optimizing the date rate and reliability of wireless-powered communications.

2.1 Prior Work and Motivation

Energy harvesting is a potential technology for powering miniature devices [1–3, 5–7, 18]. This is attractive for future paradigms such as the Internet of Things (IoT), where powering a massive number of devices will be a major challenge [8]. Many IoT applications will entail sensors with sporadic sensing and communication activity, resulting in an average power requirement on the order of microwatts to milliwatts. Depending on the application, the sensor may harvest energy from ambient sources

[1]This chapter is based on my published work in [44] and [45]. This research was supervised by Prof. Robert W. Heath, Jr. The useful feedback from Prof. Petar Popovski helped improve the quality of this research.

such as solar, thermal, kinetic, or RF (radio frequency) waves [1–3, 5, 6]. Of interest to this chapter is RF or wireless energy harvesting, where a harvesting node extracts energy from the incident RF signals. This is a suitable option for ultra low-power applications because i) wireless signals are available anywhere and anytime, ii) the harvesting operation relies on a simple circuit consisting of a rectifying antenna which can be integrated with the communication circuitry in small form factors [11], and iii) the energy delivered to the harvester can be controlled by leveraging the wireless infrastructure [5,11]. In contrast to most wireless systems designed for Internet access, the energy harvesting communication systems used in IoT applications will likely feature short packets. This is due to intrinsically small data payloads, low-latency requirements, and/or lack of energy resources to support longer transmissions [1, 46–48].

For an energy harvesting system with short packets, the capacity analysis conducted in the asymptotic blocklength regime could be misleading. This has spurred research characterizing the performance of an energy harvesting communication system in the non-asymptotic or finite blocklength regime [47–53]. This line of research leverages the finite-blocklength information theoretic framework proposed in [49] (see [54] for an overview). The work in [47] was first to investigate energy harvesting channels in the finite blocklength regime. In [47], the non-asymptotic achievable rate was characterized for a noiseless binary communications channel with an energy harvesting transmitter. This work was extended to the case of an additive white Gaussian noise (AWGN) channel and to more general discrete memoryless channels in [48]. For an energy harvesting transmitter operating under a save-then-transmit protocol (first

proposed in [55]), a lower bound on the achievable rate at the receiver was derived in the finite blocklength regime [48]. For the setup considered in [48], the work in [50] provided tighter bounds on the non-asymptotic achievable rate for an AWGN energy harvesting channel. The authors in [51] investigated the mean delay of an energy harvesting channel in the finite blocklength regime. In [52], the outage probability of a delay-constrained wireless energy and information transfer system with retransmission protocols was analyzed. Unlike the work in [47, 48, 50, 51] which assume an infinite battery at the energy harvester, [53] conducted a finite-blocklength analysis for a battery-less energy harvesting channel.

The capacity analysis of energy harvesting channels in the asymptotic blocklength regime has received considerable attention [55–60]. The capacity of an energy harvesting AWGN channel under stochastic energy arrivals was derived in [55] assuming an infinite battery at the energy harvester. For a similar setup, the capacity analysis for a battery-less energy harvester was conducted in [56]. An energy harvesting transmitter with a finite battery was considered in [57], and the capacity was analyzed using Shannon strategies for discrete memoryless channels. The capacity of an energy harvesting AWGN channel with a finite battery was considered in [58] for the case of deterministic energy arrivals. Also assuming a finite battery, the approximate capacity of an energy harvesting AWGN channel with Bernoulli energy arrivals was derived in [59]. A comprehensive review of the capacity of energy harvesting channels is provided in [60].

2.2 Contributions

In this chapter, I investigate the performance of a wireless-powered communication system where an RF energy harvesting node, charged by wireless power beacons via wireless energy transfer, attempts to communicate with a receiver over an AWGN channel. I conduct the analysis for two cases. I first provide an analytical treatment for the case of a single power beacon. I then extend the analysis to a large-scale Poisson network with multiple power beacons. Using the framework of finite-length information theory [49], I characterize the energy supply probability and the achievable rate of the considered system with short packets, i.e., in the non-asymptotic or finite blocklength regime. Leveraging the analytical results, I expose the interplay between key system parameters such as the harvest and transmit blocklengths, the average harvested power, and the transmit power. I analytically characterize the scaling laws for the harvest and transmit blocklengths in terms of the transmit-to-harvested power ratio and the target error probability. I also provide closed-form analytical expressions for the asymptotically optimal transmit power. Numerical results reveal that the asymptotically optimal transmit power yields nearly optimal performance in the finite blocklength regime. I also examine how the power beacon transmit power and density impacts the overall performance.

This work in this chapter differs from the existing literature on several accounts. The prior work [47, 48, 50, 51, 53] on energy harvesting systems in the finite blocklength regime falls short of characterizing the performance for the case of wireless energy harvesting. Moreover, most prior work [47, 48, 50, 51, 53, 55] implicitly assumes concurrent harvest and transmit operation, which may be infeasible in prac-

tice. For example, a power beacon may remain silent during the communication phase to avoid interfering with the communication link [11]. Furthermore, none of these finite-blocklength analyses treats the case of multiple power beacons.

The rest of this chapter is organized as follows. The system model is described in Section 2.3. The analytical characterization of the energy supply probability and the achievable rate for the case of a single power beacon is presented in Section 2.4. Section 2.5 extends the analysis to include multiple power beacons. Simulation results are provided in Section 2.6, and Section 2.7 concludes this chapter.

Notation: I let $F_X(x) = \Pr[X \leq x]$ denote the cumulative distribution function (CDF) of a random variable X. I use $X \sim \mathrm{Exp}(\varrho)$ to indicate that X is an Exponential random variable with mean $\mathbb{E}[X] = \varrho^{-1}$. Similarly, $X \sim \mathrm{Ga}(\varrho_1, \varrho_2)$ means that X is a Gamma random variable with shape ϱ_1 and scale ϱ_2. I define $\mathcal{L}_X(s) \triangleq \mathbb{E}\left[e^{-sX}\right]$ as the Laplace transform of a random variable X. I define $\gamma(K, \varrho) = \int_0^{\varrho} t^{K-1}e^{-t}\mathrm{d}t$ as the lower incomplete Gamma function, $\Gamma(K, \varrho) = \int_{\varrho}^{\infty} t^{K-1}e^{-t}\mathrm{d}t$ as the upper incomplete Gamma function, $\Gamma(K) = \int_0^{\infty} t^{K-1}e^{-t}\mathrm{d}t$ as the (complete) Gamma function, $\mathcal{P}(K, \varrho) = \frac{\gamma(K,\varrho)}{\Gamma(K)}$ as the regularized lower incomplete Gamma function, and $\mathcal{Q}(K, \varrho) = \frac{\Gamma(K,\varrho)}{\Gamma(K)}$ as the regularized upper incomplete Gamma function. I use $\log(x)$ to denote the natural logarithm of x.

2.3 System Model

I consider a wireless-powered communication system where one or more wireless power beacons (PBs) use wireless energy transfer to charge an energy harvesting (EH) node, which then attempts to communicate with another receiver (RX) using

the harvested energy (see Fig. 2.1). The nodes are assumed to be equipped with a single antenna each. I present an analytical treatment for two cases: i) the energy harvesting node is powered by a single power beacon, and ii) the energy harvesting node is powered by a large-scale network consisting of multiple power beacons. I now describe the system model for the case of a single power beacon. Any additional description for the case of multiple power beacons will be provided in Section 2.5. I assume that the energy harvester uses a *save-then-transmit* protocol [55] to enable wireless-powered communications. The considered protocol divides the communication frame consisting of S channel uses (or slots) into an energy harvesting phase having m channel uses, and an information transmission phase having n channel uses. The first m channel uses are used for harvesting energy from the RF signals transmitted by the power beacon. This is followed by an information transmission phase consisting of n channel uses, where the transmitter uses the harvested energy to transmit information to the receiver. I assume that any left-over energy at the end of the transmission is stored in a dedicated battery for system-level energy supply. For example, this dedicated battery may support other functions like sensing and computation, which an EH node often needs to perform. This implies that the energy accumulated in a harvesting phase is independent of the previous harvesting phases. I leave the case where left-over energy supports subsequent transmissions for future work. I call m the *harvest* blocklength, n the *transmit* blocklength, and $S = m + n$ the *total* blocklength or frame size. I will conduct the subsequent analysis for the non-asymptotic blocklength regime, i.e., for the practical case of *short packets* where the total blocklength is finite.

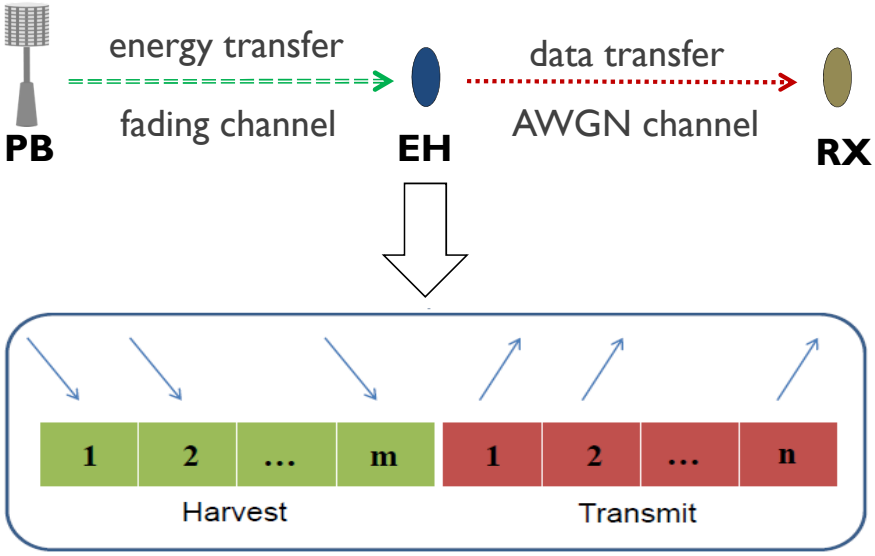

Figure 2.1: A single power beacon charges an energy harvesting node, which operates under a save-then-transmit protocol to communicate with its desired receiver.

2.3.1 Energy Harvesting Phase

The signal transmitted by a power beacon experiences distance-dependent path loss and channel fading before reaching the energy harvesting node. The harvested energy is, therefore, a random quantity due to the underlying randomness of the wireless link. I let random variable $Z_i = \frac{\mu P_{\rm PB} H_i}{\ell(r,\eta)}$ model the power (or energy) harvested in slot i ($i = 1, \cdots, m$), where $\mu \in (0, 1]$ denotes the EH conversion efficiency, $P_{\rm PB}$ is the PB transmit power (i.e., energy per PB symbol), $\ell(r, \eta)$ gives the average large-scale path loss given a PB-EH link distance r and a path loss exponent $\eta > 2$, while the random variable H_i denotes the small-scale channel gain. I let $Z_{\rm tot} = \sum_{i=1}^{m} Z_i$ denote the total harvested energy during a harvesting phase. Note that I have ignored the energy due to noise since it is negligibly small. I assume the

PB-EH link undergoes IID Rayleigh fading such that H_i is exponentially distributed with unit mean, i.e., $H_i \sim \text{Exp}(1)$ and $Z_i \sim \text{Exp}(P_{\text{H}}^{-1})$ where $P_{\text{H}} \triangleq \mathbb{E}[Z_i] = \frac{\mu}{\ell(r,\eta)} P_{\text{PB}}$. I consider two fading scenarios for the PB-EH link: i) quasi-static block flat fading where the channel remains constant over (the harvesting phase of) a frame, and randomly changes to a new value for the next frame, and ii) IID fading where the link sees an independent channel realization in each slot of the harvesting phase. For the former, the energy arrivals within a harvesting phase are fully correlated, i.e., $Z_i = Z_1 \triangleq Z, \forall\, i = 1, 2, \cdots, m$ such that $Z_{\text{tot}} \sim \text{Ga}(1, mP_{\text{H}})$. This is motivated by the observation that the harvest blocklength in a *short-packet* communication system may be smaller than the channel coherence time. For the latter, the energy arrivals are uncorrelated such that $Z_{\text{tot}} \sim \text{Ga}(m, P_{\text{H}})$. This caters to the other extreme where the link is subjected to fast fading.

2.3.2 Information Transmission Phase

The energy harvesting phase is followed by an information transmission phase where the EH node attempts to communicate with a destination RX node over an unreliable AWGN channel. The AWGN channel abstracts a scenario where the EH-RX channel remains fairly static, for example, due to a small link distance. Contrary to the harvesting operation, here noise plays a significant role. I assume that the EH node uses a Gaussian codebook for signal transmission (see Section 2.3.3). I let X_ℓ be the signal intended for transmission in slot ℓ with an average power P_{EH}, where $\ell = 1, \cdots, n$, and n is fixed. In the ensuing analysis, I assume P_{EH} to be fixed before evaluating the considered metrics. The resulting (intended) sequence

$X^n = (X_1, \cdots, X_n)$ consists of independent and identically distributed (IID) Gaussian random variables such that $X_\ell \sim \mathcal{N}(0, P_{\text{EH}})$. To transmit the intended sequence X^n over the transmit block, the EH node needs to satisfy the following energy constraints.

$$\sum_{\ell=1}^{k} X_\ell^2 \leq \sum_{i=1}^{m} Z_i \qquad k = 1, 2, \cdots, n. \tag{2.1}$$

The following lemma simplifies the multiple energy constraints into a single constraint.

Lemma 1 For a random sequence $\{X_\ell\}_{\ell=1}^n$ for the transmit phase, and a random energy sequence $\{Z_i\}_{i=1}^m$ for the harvest phase, the probability of violating the energy constraints in (2.1) is given by

$$\Pr\left[\bigcup_{k=1}^{n}\left\{\sum_{\ell=1}^{k} X_\ell^2 > \sum_{i=1}^{m} Z_i\right\}\right] = 1 - \Pr\left[\sum_{\ell=1}^{n} X_\ell^2 \leq \sum_{i=1}^{m} Z_i\right]. \tag{2.2}$$

Proof: The result follows by noting that

$$\Pr\left[\bigcap_{k=1}^{n}\left\{\sum_{\ell=1}^{k} X_\ell^2 \leq \sum_{i=1}^{m} Z_i\right\}\right] = \Pr\left[\left\{\sum_{\ell=1}^{n} X_\ell^2 \leq \sum_{i=1}^{m} Z_i\right\}\right] \underbrace{\times \Pr\left[\bigcap_{k=1}^{n-1}\left\{\sum_{\ell=1}^{k} X_\ell^2 \leq \sum_{i=1}^{m} Z_i\right\} \Big| \sum_{\ell=1}^{n} X_\ell^2 \leq \sum_{i=1}^{m} Z_i\right]}_{1}$$

□

The constraints in (2.1), which need to be satisfied to transmit the intended codeword, simplify to $\sum_{\ell=1}^{n} X_\ell^2 \leq Z_{\text{tot}}$ due to Lemma 1. I let $\tilde{X}^n = \left(\tilde{X}_1, \cdots, \tilde{X}_n\right)$ be the transmitted sequence. Note that $\tilde{X}^n \neq X^n$ when the energy constraints are violated as the EH node lacks sufficient energy to put the intended symbols on the channel.

The signal received at the destination node in slot ℓ is given by $Y_\ell = \tilde{X}_\ell + V_\ell$, where $V^n = (V_1, \cdots, V_n)$ is an IID sequence modeling the receiver noise such that $V_\ell \sim \mathcal{N}(0, \sigma^2)$ is a zero-mean Gaussian random variable with variance σ^2. I note that any deterministic channel gain (attenuation) $\zeta \in (0, 1]$ for the EH-RX link can be equivalently tackled by scaling the noise variance by a factor ζ (as the equivalent channel is still AWGN). Similarly, I define $Y^n = (Y_1, \cdots, Y_n)$ as the received sequence.

2.3.3 Information Theoretic Preliminaries

I now describe the information theoretic preliminaries for the EH-RX link. Let us assume that the EH node transmits a message $W \in \mathcal{W}$ over n channel uses. Assuming W is drawn uniformly from $\mathcal{W} \triangleq \{1, 2, \cdots, M\}$, I define an (n, M)-code having the following features: It uses a set of encoding functions $\{\mathcal{F}_\ell\}_{\ell=1}^n$ for encoding the source message $W \in \mathcal{W}$ given the energy harvesting constraints, i.e., the source node uses $\mathcal{F}_\ell : \mathcal{W} \times \mathbb{R}_+ \to \mathbb{R}$ for transmission slot ℓ, where $\mathcal{F}_\ell(W, Z_{\text{tot}}) = \tilde{X}_\ell$ given Z_{tot} such that the energy harvesting constraints in (2.1) are satisfied. Specifically, $\tilde{X}_\ell = X_\ell$ where $X_\ell \sim \mathcal{N}(0, P_{\text{EH}})$ is drawn IID from a Gaussian codebook when (2.1) is satisfied, and $\tilde{X}_\ell = 0$ otherwise. It uses a decoding function $\mathcal{G} : \mathbb{R}^n \to \mathcal{W}$ that produces the output $\mathcal{G}(Y^n) = \hat{W}$, where $Y^n = (Y_1, \cdots, Y_n)$ is the sequence received at the destination node.

I let $\epsilon \in [0, 1)$ denote the target error probability for the noisy communication link. For $\epsilon \in [0, 1)$, an (n, M, ϵ)-code for an AWGN EH channel is defined as the (n, M)-code for an AWGN channel such that the average probability of decoding error $\Pr\{\hat{W} \neq W\}$ does not exceed ϵ. A rate R is ϵ-*achievable* for an AWGN EH

channel if there exists a sequence of (n, M_n, ϵ_n)-codes such that $\liminf_{n\to\infty} \frac{1}{n}\log(M_n) \geq R$ and $\limsup_{n\to\infty} \epsilon_n \leq \epsilon$. The ϵ-*capacity* C_ϵ for an AWGN EH channel is defined as $C_\epsilon = \sup\{R : R \text{ is } \epsilon\text{-}achievable\}$.

2.3.4 Performance Metrics

I now introduce the metrics used for characterizing the performance of the considered *short-packet* wireless-powered communications system. Note that the overall performance is marred by two key events. First, due to lack of sufficient energy, the EH node may not be able to transmit the intended codewords during the information transmission phase, possibly causing a decoding error at the receiver. Second, due to a noisy EH-RX channel, the received signal may not be correctly decoded. For the former, I define a metric called the *energy supply probability*, namely, the probability $\Pr\left[\sum_{i=1}^{n} X_i^2 \leq Z_{\text{tot}}\right]$ that an EH node can support the intended transmission. For the latter, I define and characterize the ϵ-*achievable rate* in the finite blocklength regime.

2.4 Single Power Beacon

In this section, I characterize the energy supply probability and the achievable rate in the finite blocklength regime for an energy harvester powered by a single power beacon. I also provide closed-form analytical expressions for the optimal transmit power.

2.4.1 Energy Supply Probability

I define the *energy supply probability* $P_{\text{es}}(m, n, a)$ as the probability that an EH node has sufficient energy to transmit the intended codeword, namely,

$$P_{\text{es}}(m, n, a) = \Pr\left[\sum_{i=1}^{n} X_i^2 \leq Z_{\text{tot}}\right] \tag{2.3}$$

for a harvest blocklength m, a transmit blocklength n, and a power ratio $a = \frac{P_{\text{EH}}}{P_{\text{H}}}$. Similarly, I define $P_{\text{eo}}(m, n, a) = 1 - P_{\text{es}}(m, n, a)$ as the *energy outage probability* at the EH node.

2.4.1.1 Correlated Energy Arrivals

In this subsection, I treat the energy supply probability for the case of correlated energy arrivals.

Proposition 2 Assuming the intended transmit symbols $\{X_i\}_{i=1}^{n}$ are drawn IID from $\mathcal{N}(0, P_{\text{EH}})$, the energy sequence $\{Z_i\}_{i=1}^{m} = Z$ is fully correlated, and Z follows an exponential law with mean P_{H}, the energy supply probability is given by

$$P_{\text{es}}(m, n, a) = \frac{1}{\left(1 + \frac{2a}{m}\right)^{\frac{n}{2}}} \tag{2.4}$$

for $m > 2a$ where $a = \frac{P_{\text{EH}}}{P_{\text{H}}}$, while m and n denote the blocklengths for the harvest and the transmit phase.

Proof: The proof follows by leveraging the statistical properties of the random variables. Consider

$$P_{\text{es}}\left(m, n, a\right) = \Pr\left[\sum_{i=1}^{n} X_i^2 \leq mZ\right] \overset{(a)}{=} \Pr\left[\varphi \leq \frac{mZ}{P_{\text{EH}}}\right]$$

$$\overset{(b)}{=} \mathbb{E}_{\varphi}\left[e^{-\frac{P_{\mathrm{EH}}}{P_{\mathrm{H}}m}\varphi}\right] = \frac{1}{\left(1+\frac{2a}{m}\right)^{\frac{n}{2}}} \tag{2.5}$$

where (a) follows from the substitution $\varphi = \frac{\sum_{i=1}^{n} X_i^2}{P_{\mathrm{EH}}}$ where φ is a Chi-squared random variable with n degrees of freedom. Equality (b) is obtained by conditioning on the random variable φ, and by further noting that $Z \sim \mathrm{Exp}\left({P_{\mathrm{H}}}^{-1}\right)$. Assuming $m > 2a$, the last equation follows from the definition of the moment generating function of a Chi-squared random variable. When $m \leq 2a$, I can evaluate the energy supply probability using the form in (b). □

While the representation in (2.4) is valid for $m > 2a$, I note that this is the case of practical interest since it is desirable to operate at $a < 1$, as evident from Section 2.6. Further, the expression in (2.4) makes intuitive sense as the energy outages would increase with the transmit blocklength n for a given m, and decrease with the harvest blocklength m for a given n. Let us fix P_{EH} and P_{H}. For a given m, I may improve the reliability of the EH-RX communication link by increasing the blocklength n, albeit at the expense of the energy supply probability. With a smaller transmit power P_{EH}, the energy harvester is less likely to run out of energy during an ongoing transmission. Therefore, when $m+n$ is fixed, I may reduce P_{EH} to meet the energy supply constraint, but this would reduce the channel signal-to-noise ratio (SNR). This underlying tension between the energy availability and the communication reliability will be highlighted throughout the rest of this chapter. The following discussion relates the transmit power to the harvest and transmit blocklengths, illustrating some of the key tradeoffs.

Remark 3 The energy supply probability is more sensitive to the length of the transmit phase compared to that of the harvest phase. This observation also manifests

itself in terms of the energy requirements at the transmitter. For instance, to maintain an energy supply probability p, it follows from (2.4) that the power ratio satisfies $a \leq \frac{m}{2}\left(p^{-\frac{2}{n}} - 1\right)$. Note that the power ratio varies only linearly with the harvest blocklength m, but superlinearly with the transmit blocklength n. This further implies that for a fixed n, doubling the harvest blocklength relaxes the transmit power budget by the same amount. That is, the energy harvester can double its transmit power P_{EH} (and therefore the channel SNR) without violating the required energy constraints. In contrast, reducing the transmit blocklength for a given m brings about an exponential increase in the transmit power budget at the energy harvester.

The following corollary treats the scaling behavior of the energy supply probability as the blocklength becomes large.

Corollary 4 When the harvest blocklength m scales in proportion to the transmit blocklength n such that $m = cn$ for some constant $c > 0$, the energy supply probability $P_{\text{es}}(m, n, a)$ converges to a limit as m and n become asymptotically large. In other words, $\lim_{m,n\to\infty} P_{\text{es}}(m, n, a) = e^{-\frac{a}{c}} < 1$ such that the limit only depends on the power ratio $a > 0$ and the proportionality constant $c > 0$. Further, under proportional blocklength scaling, this limit also serves as an upper bound on the energy supply probability for finite blocklengths, i.e., $P_{\text{es}}(m, n, a) \leq e^{-\frac{a}{c}} < 1$.

The previous corollary also shows that energy outage is a fundamental bottleneck regardless of the blocklength, assuming at best linear scaling.

2.4.1.2 IID Energy Arrivals

I now characterize the energy supply probability for the case of IID energy arrivals.

Proposition 5 Assuming the intended transmit symbols $\{X_i\}_{i=1}^n$ and the energy arrivals $\{Z_i\}_{i=1}^m$ are drawn IID from $\mathcal{N}(0, P_{\text{EH}})$ and $\text{Exp}\left(P_{\text{H}}^{-1}\right)$ respectively, the energy supply probability is given by

$$P_{\text{es}}(m, n, a) = \int_0^\infty \frac{t^{m-1}e^{-t}}{(m-1)!} \mathcal{P}\left(\frac{n}{2}, 2at\right) \text{d}t, \tag{2.6}$$

where $\mathcal{P}(\cdot, \cdot)$ is the regularized lower incomplete Gamma function.

Proof: Consider $P_{\text{es}}(m, n, a) = \Pr\left[\sum_{i=1}^n X_i^2 \leq Z_{\text{tot}}\right] = \Pr\left[\varphi - \frac{Z_{\text{tot}}}{P_{\text{EH}}} \leq 0\right]$, where $\varphi = \sum_{i=1}^{n} \frac{X_i^2}{P_{\text{EH}}}$ such that $\varphi \sim \text{Ga}\left(\frac{n}{2}, 2\right)$, while $\frac{Z_{\text{tot}}}{P_{\text{EH}}} \sim \text{Ga}\left(m, \frac{1}{a}\right)$. This means that $U \triangleq \varphi - \frac{Z_{\text{tot}}}{P_{\text{EH}}}$ follows a Gamma difference distribution [61]. The final result follows by evaluating $\Pr[U \leq 0]$. □

Compared to (2.4), the analytical expression in (2.6) is more involved as it requires integration over mathematical functions. To simplify the analysis, I propose the following approximation for the energy supply probability.

Corollary 6 The energy supply probability for IID energy arrivals can be tightly approximated as $P_{\text{es}}(m, n, a) \approx \mathcal{Q}(m, an)$, where $\mathcal{Q}(\cdot, \cdot)$ is the regularized upper incomplete Gamma function.

Proof: The proposed expression follows by plugging $\varphi \approx \mathbb{E}[\varphi] = n$ in the proof of Proposition 5. □

I note that the proposed approximation results in only a minor loss in accuracy for the parameter range considered in this chapter.

2.4.2 Achievable Rate

In this section, I characterizes the ϵ-achievable rate of the considered wireless-powered communication system in the finite blocklength regime.

2.4.2.1 Correlated Energy Arrivals

I first consider the case of correlated energy arrivals.

Theorem 7 Given a target error probability $\epsilon \in [0, 1)$ for the noisy channel, the ϵ-achievable rate $R_{\text{EH}}(\epsilon, m, n, a, \gamma)$ of the considered system with harvest blocklength m, transmit blocklength n, power ratio a (where $2a < m$), and the SNR $\gamma = \frac{P_{\text{EH}}}{\sigma^2}$ is given by

$$R_{\text{EH}}(\epsilon, m, n, a, \gamma) = \frac{\frac{n\log(1+\gamma)}{2} - \sqrt{\frac{2+\epsilon}{\epsilon}\frac{\gamma}{\gamma+1}n} - (n)^{\frac{1}{4}} - 1}{n+m} \tag{2.7}$$

for all tuples (m, n) satisfying

$$m \geq \frac{2a}{\exp\left(\frac{2\log(1+0.5\epsilon)}{\left(\log\left[\frac{2+\epsilon}{\epsilon^2}\right]\right)^4}\right) - 1} \tag{2.8}$$

and

$$n \leq 2\frac{\log(1+0.5\epsilon)}{\log\left(1+\frac{2a}{m}\right)}. \tag{2.9}$$

Proof: See Appendix A. □

For a given target error probability ϵ, a harvest blocklength m can support a transmit blocklength only as large as in (2.9). Moreover, a sufficiently large m, as given in (2.8), is required for a sufficiently large n to meet the target error probability ϵ. The constraints in (2.8) and (2.9) can be equivalently written as

$$n \geq \left[\log\left(\frac{2+\epsilon}{\epsilon^2}\right)\right]^4 \tag{2.10}$$

and

$$m \geq \frac{2a}{(1+0.5\epsilon)^{\frac{2}{n}}-1} \tag{2.11}$$

A sufficiently long transmit codeword is required to meet the reliability requirements of the communication link. Similarly, a sufficiently long harvest blocklength is required to replenish the energy supply. In latency-constrained systems where the total blocklength is fixed, this interplay between the transmit and harvest blocklength results in a trade-off between the energy supply probability and the communication reliability. For the rest of the analysis, I assume that minimum possible blocklengths are selected to satisfy the constraints in (2.10) and (2.11), i.e., I set $n = \left\lceil \left(\log\left(\frac{2+\epsilon}{\epsilon^2}\right)\right)^4 \right\rceil_{\text{ev}}$ and $m = \left\lceil \frac{2a}{(1+0.5\epsilon)^{\frac{2}{n}}-1} \right\rceil$, where $\lceil x \rceil$ (or $\lceil x \rceil_{\text{ev}}$) returns the smallest integer (or even integer) not smaller than x. I call it the *minimum latency approach*. The following remark illustrates the scaling behavior of the harvest and transmit blocklengths.

Remark 8 Under the minimum latency approach, the harvest blocklength scales almost linearly with the transmit blocklength according to the law $m \approx \frac{2a}{\epsilon}n$. This follows from the constraint in (2.9) where $m = \frac{2a}{[1+0.5\epsilon]^{\frac{2}{n}}-1} \approx \frac{2a}{\epsilon}n$ when ϵ is small. Further, the scaling rate $\frac{m}{n}$ is directly proportional to the power ratio a and inversely

proportional to the error ϵ. For example, fix n and a. A k-fold reduction in ϵ requires a k-fold increase in the harvest blocklength to attain the corresponding ϵ-achievable rate. This increase in reliability, however, comes at the expense of a reduced rate and an increased latency since the harvesting overhead is $1+\frac{2a}{\epsilon}$ and the total blocklength grows as $(1+\frac{2a}{\epsilon})n$. This further suggests that I may overcome the rate (and latency) loss by a k-fold increase in a, i.e., by increasing P_{H} for a fixed P_{EH}. This could be achieved by increasing the PB transmit power and/or improving the rectifier efficiency.

The following proposition provides an analytical expression for the achievable rate in the asymptotic blocklength regime. I note that the asymptotic results provide a useful analytical handle for the non-asymptotic case as well.

Proposition 9 Let $R^{\infty}_{\mathrm{EH}}(\epsilon, a, \gamma)$ denote the asymptotic achievable rate as the transmit blocklength $n \to \infty$ (and consequently the harvest blocklength $m \to \infty$ following (2.11)), i.e., $R^{\infty}_{\mathrm{EH}}(\epsilon, a, \gamma) = \lim_{n\to\infty} R_{\mathrm{EH}}(\epsilon, m, n, a, \gamma)$. It is given by

$$R^{\infty}_{\mathrm{EH}}(\epsilon, a, \gamma) = L(a, \epsilon) C^{\infty}_{\mathrm{AWGN}}(\gamma) \tag{2.12}$$

where

$$C^{\infty}_{\mathrm{AWGN}}(\gamma) = \frac{1}{2}\log(1+\gamma), \quad \gamma \geq 0 \tag{2.13}$$

denotes the capacity of an AWGN channel without the energy harvesting constraints, whereas

$$L(a, \epsilon) = \frac{1}{1+\frac{a}{\log(1+0.5\epsilon)}}, \quad a \geq 0,\ \epsilon \in [0, 1) \tag{2.14}$$

where $L(a, \epsilon) \in [0, 1]$ such that $1 - L(a, \epsilon)$ gives the (fractional) loss in capacity due to energy harvesting constraints.

Proof: Using (2.7), $R_{\text{EH}}^{\infty}(\epsilon, a, \gamma)$ can be expressed as

$$R_{\text{EH}}^{\infty}(\epsilon, a, \gamma) = \lim_{n\to\infty} \frac{\frac{n\log(1+\gamma)}{2} - \sqrt{\frac{2+\epsilon}{\epsilon}\frac{\gamma}{\gamma+1}n} - (n)^{\frac{1}{4}} - 1}{n+m} \tag{2.15}$$

$$\stackrel{(a)}{=} \lim_{n\to\infty} \frac{1}{1+\frac{m}{n}} \frac{\log(1+\gamma)}{2} \tag{2.16}$$

$$\stackrel{(b)}{=} \lim_{n\to\infty} \frac{1}{1+\frac{2a}{n[1+0.5\epsilon]^{\frac{2}{n}}-1}} \frac{\log(1+\gamma)}{2} \tag{2.17}$$

$$\stackrel{(c)}{=} \underbrace{\frac{1}{1+\frac{a}{\log(1+0.5\epsilon)}}}_{L(a,\epsilon)} \underbrace{\frac{\log(1+\gamma)}{2}}_{C_{\text{AWGN}}^{\infty}(\gamma)} \tag{2.18}$$

where (a) follows since the higher order terms in (2.7) vanish as $n \to \infty$. Note that for a given ϵ and a, m and n should satisfy (2.10) and (2.11). Equality (b) is obtained by substituting the minimum harvest blocklength $m = \frac{2a}{[1+0.5\epsilon]^{\frac{2}{n}}-1}$ from (2.11), and by further assuming that $n \geq \left(\log\left(\frac{2+\epsilon}{\epsilon^2}\right)\right)^4$. Finally, (c) follows by noting that $\lim_{n\to\infty} n\left((1+x)^{\frac{2}{n}} - 1\right) = 2\log(1+x)$. □

Remark 10 Proposition 9 reveals a fundamental communications limit of the considered wireless-powered system. To guarantee an ϵ-reliable communication over n channel uses, the node first needs to accumulate sufficient energy during the initial harvesting phase. A sufficiently large m helps improve the energy availability at the transmitter. This harvesting overhead, however, causes a rate loss (versus a non-energy harvesting system) as the first m channel uses are reserved for harvesting. Moreover, as the transmit blocklength n grows, so does the length of the initial harvesting phase m, resulting in an inescapable performance limit on the communication system. This limit depends on i) the power ratio a, and ii) the required reliability

ϵ, and is captured by the prelog term $L(a, \epsilon)$ in (2.14) for a given γ. Moreover, this behavior is more visible for latency-constrained systems where the total blocklength is fixed.

Remark 11 In the asymptotic blocklength regime, the harvest blocklength should be scaled proportionally to the transmit blocklength with a scaling rate $\frac{a}{\log(1+0.5\epsilon)}$ to attain the corresponding asymptotic ϵ-achievable rate. Note that this scaling rate approximately equals $\frac{2a}{\epsilon}$ (when ϵ is small), which is similar to the non-asymptotic scaling rate discussed in Remark 8. Moreover, this remark also justifies the linear blocklength scaling assumed in Corollary 4.

Remark 12 I note that the asymptotic achievable rate vanishes as $\epsilon \to 0$. This is because the wireless energy transfer link may fade completely, resulting in a transmission outage for the information transfer link.

Corollary 13 As the power ratio $a \to 0$ in (2.12), the asymptotic achievable rate converges to the capacity of a non-energy harvesting AWGN channel, i.e., $\lim_{a\to 0} R^{\infty}_{\mathrm{EH}}(\epsilon, a, \gamma) = C^{\infty}_{\mathrm{AWGN}}(\gamma)$.

Remark 14 With P_{EH} fixed, decreasing a (by increasing P_{H}) improves the energy availability at the EH node during the information transmission phase. As a is decreased, a smaller harvest blocklength is required to support a certain transmit blocklength and ϵ. As a result, in the limit $a \to 0$, the harvesting overhead as well as the energy outage probability vanish as the transmit blocklength goes to infinity. Therefore, the system effectively reduces to a traditionally-powered communication system.

Corollary 15 In the high-reliability regime (when $\epsilon \in [0,1)$ is small), the asymptotic achievable rate $R_{\mathrm{EH}}^{\infty}(\epsilon, a, \gamma)$ in (2.12) can be approximated as

$$R_{\mathrm{EH}}^{\infty}(\epsilon, a, \gamma) \approx \frac{1}{1+\frac{2a}{\epsilon}} C_{\mathrm{AWGN}}^{\infty}(\gamma) = \frac{1}{1+\frac{2P_{\mathrm{EH}}}{\epsilon P_{\mathrm{H}}}} C_{\mathrm{AWGN}}^{\infty}(\gamma), \tag{2.19}$$

which follows since $\log(1+x) \approx x$ when x is small.

Remark 16 The previous corollary illustrates an interesting interplay between the key design parameters. For a given target rate, the error probability ϵ scales inversely with the average harvested power P_{H} in the high-reliability regime. This implies that increasing P_{H} (e.g., by increasing the PB transmit power) reduces the communication unreliability by the same factor.

2.4.2.2 IID Energy Arrivals

I now provide the achievable rate for the case of IID energy arrivals.

Theorem 17 The ϵ-achievable rate of the considered system for the case of IID energy arrivals is given by (2.7) for all tuples (m, n) satisfying

$$n \geq \left\lceil \log\left(\frac{2+\epsilon}{\epsilon^2}\right) \right\rceil^4 \tag{2.20}$$

and

$$\int_0^{\infty} \frac{t^{m-1}e^{-t}}{(m-1)!} \mathcal{P}\left(\frac{n}{2}, 2at\right) \mathrm{d}t \geq \frac{2}{2+\epsilon}. \tag{2.21}$$

Proof: The proof is similar to the case of correlated energy arrivals. □

Theorem 17 differs from Theorem 7 in that it is governed by a different constraint (2.21) on the blocklength. This is because the energy supply proabability with IID energy arrivals is different from that achieved with correlated arrivals.

2.4.3 Transmit power optimization

For optimal performance, the energy harvesting node needs to use the *right* amount of transmit power. On the one hand, reducing P_{EH} helps improve the energy supply probability as a packet transmission is less likely to face an energy outage. On the other hand, it is detrimental for the communication link as it reduces the SNR. I now quantify the optimal transmit power that maximizes the asymptotic achievable rate for a given set of parameters. I note that many of the analytical insights obtained for the asymptotic regime are also useful for the non-asymptotic regime (see Remark 19). In this section, I focus on the case of correlated energy arrivals.

Corollary 18 For a given ϵ and P_{H}, there exists an optimal transmit power that maximizes the achievable rate. I let $P^*_{\mathrm{EH},\infty}$ be the rate-maximizing transmit power in the asymptotic blocklength regime. It follows that

$$P^*_{\mathrm{EH},\infty}(\epsilon, P_{\mathrm{H}}, \sigma^2) = \sigma^2 \left(\frac{\frac{P_{\mathrm{H}}}{\sigma^2} \log(1+0.5\epsilon) - 1}{\mathrm{W}\left[\left(\frac{P_{\mathrm{H}}}{\sigma^2} \log(1+0.5\epsilon) - 1\right) e^{-1}\right]} - 1 \right) \tag{2.22}$$

where $\mathrm{W}[\cdot]$ is the Lambert W-function [62].

Proof: See Appendix A. □

Note that $\mathrm{W}[x]$ is a real increasing function of x for $x \geq -\frac{1}{e}$ [62]. As $\frac{P_{\mathrm{H}}}{\sigma^2} \log\left(1+0.5\epsilon\right) > 0$ in practice, this ensures that the function $\mathrm{W}\left[\left(\frac{P_{\mathrm{H}}}{\sigma^2} \log(1+0.5\epsilon) - 1\right) e^{-1}\right]$ is real, resulting in a nonnegative transmit power. Also, plugging $P_{\mathrm{EH}} = P^*_{\mathrm{EH},\infty}$ in Proposition 9 gives the optimal achievable rate in the asymptotic blocklength regime. Furthermore, when P_{EH} is fixed, the achievable rate improves monotonically with P_{H} due to an increase in the energy supply probability.

Remark 19 The optimal transmit power for the asymptotic case serves as a conservative estimate for the optimal transmit power for the non-asymptotic case (Fig. 2.5). Moreover, the achievable rate in the non-asymptotic regime obtained using the asymptotically optimal transmit power, gives a tight lower bound for the optimal achievable rate in the non-asymptotic regime (Fig. 2.4). This suggests that Corollary 18 provides a useful analytical handle for transmit power selection even for the finite blocklength regime (despite the fact that the resulting rate for the non-asymptotic case could be much smaller than that for the asymptotic case).

Corollary 20 With ϵ and σ^2 fixed, the asymptotically optimal transmit power $P^*_{\mathrm{EH},\infty}(\epsilon, P_{\mathrm{H}}, \sigma^2)$ increases with P_{H} with a slope

$$\frac{\log(1+0.5\epsilon)}{1+\mathrm{W}\left[\left(\frac{P_{\mathrm{H}}}{\sigma^2}\log(1+0.5\epsilon)-1\right)e^{-1}\right]}. \tag{2.23}$$

The slope is a non-negative decreasing function of the P_{H}, suggesting that i) the optimal transmit power increases monotonically with P_{H}, and ii) it is more sensitive to P_{H} when P_{H} is small. In addition, the optimal transmit power scales sublinearly with P_{H}.

Proof: It follows by differentiating the optimal transmit power with respect to P_{H}. □

Though the transmit power increases with P_{H}, the optimal power ratio $a^* = \frac{P^*_{\mathrm{EH},\infty}}{P_{\mathrm{H}}}$ is a monotonically decreasing function of P_{H}. This is because $P^*_{\mathrm{EH},\infty}$ varies sublinearly with P_{H}.

2.5 Multiple Power Beacons

In this section, I extend the analysis to the case of a large-scale network consisting of power beacons, wireless-powered transmitters, and their dedicated receivers. I assume that the power beacons are distributed on a two-dimensional plane according to a homogeneous Poisson point process (PPP) $\Phi_{\mathrm{PB}} = \{x_k\}_{k=1}^{\infty}$ with density (intensity) λ_{PB}, where x_k denotes the location of a node k in Φ_{PB}. The energy harvesting transmitters are drawn from another homogeneous PPP $\Phi_{\mathrm{EH}} = \{y_k\}_{k=1}^{\infty}$ of density λ_{EH} independently of the power beacons. Similar to the case of a single power beacon, each energy harvesting transmitter is assumed to have a dedicated receiver located a fixed distance away. Leveraging Slivnyak's theorem [63], I consider a typical energy harvesting node located at the origin. It exploits the energy harvested from the transmissions of multiple power beacons to communicate with its dedicated receiver amid interference and noise. I let h_k model the small-scale fading coefficient for the PB-EH link originating at x_k. I assume IID Rayleigh fading for the PB-EH links such that $H_k = |h_k|^2 \sim \mathrm{Exp}\,(1)$. As defined previously, $\ell\left(\|x_k\|, \eta\right)$ models the distance-dependent path loss for the link from x_k. The energy harvested in an arbitrary channel use for the case of multiple power beacons is given by $Z = P_{\mathrm{PB}}\mu\tilde{Z}$, where $\tilde{Z} = \sum\limits_{x_k \in \Phi_{\mathrm{PB}}} \frac{H_k}{\ell(\|x_k\|,\eta)}$. In this section, I focus on the case of correlated energy arrivals. I derive tractable analytical expressions for the energy supply probability and the non-asymptotic achievable rate in a network setting.

2.5.1 Energy Supply Probability

I first characterize the energy supply probability in a general form. I then specialize it to the scenario considered in this chapter.

Proposition 21 For the case of multiple power beacons with PB density λ_{PB}, the energy supply probability at a typical EH node is given by

$$P_{\mathrm{es}}^{\mathrm{MP}}\left(m,n,a,\lambda_{\mathrm{PB}},\eta\right)=1-\sum_{i=0}^{\frac{n}{2}-1}(-1)^{i}\frac{m^{i}}{(2a)^{i}i!}\frac{\mathrm{d}^{i}}{\mathrm{d}s^{i}}\mathcal{L}_{\tilde{Z}}(s)|_{s=\frac{m}{2a}} \tag{2.24}$$

where the power ratio $a=\frac{P_{\mathrm{EH}}}{\mu P_{\mathrm{PB}}}$, η is the path loss exponent, while $\mathcal{L}_{\tilde{Z}}(s)=\mathbb{E}[e^{-s\tilde{Z}}]$ is the Laplace transform of $\tilde{Z}$, which is a function of λ_{PB} and η.

Proof: See Appendix B. □

Note that the power ratio a is defined here slightly differently from the case of a single power beacon (Proposition 2). Here, it is defined as the ratio of the transmit power at an energy harvester to that at a power beacon (scaled by the rectifier efficiency). Previously, it was defined as the ratio of the EH transmit power to the harvested power, i.e., the large-scale fading term, being deterministic, was absorbed in the power ratio. For generality, I have expressed Proposition 21 in terms of the Laplace transform of the harvested energy. Depending on the propagation and network model, this could be evaluated in closed form. For example, the following lemma analytically characterizes the Laplace transform for the scenario relevant to this chapter.

Lemma 22 Let us assume the PBs are drawn from a homogeneous PPP of density λ_{PB}, the PB-EH links are IID Rayleigh fading, and follow a bounded path loss model $\ell(r,\eta) = \max(1, r^{\eta})$ where $\eta > 2$ is the path loss exponent while r is the PB-EH link distance. The Laplace transform $\mathcal{L}_Z(s)$ of the per-slot harvested energy Z is analytically characterized by

$$\mathcal{L}_Z(s) = \exp\left(-\pi\lambda_{\mathrm{PB}}\frac{P_{\mathrm{PB}}\mu s}{1+P_{\mathrm{PB}}\mu s}\right)\exp\left(-\pi\lambda_{\mathrm{PB}}\,\mathcal{F}\left(P_{\mathrm{PB}}\mu s,\eta\right)\right), \tag{2.25}$$

where the function $\mathcal{F}(x_1,x_2)$ for $x_1 \geq 0, x_2 > 2$ is defined as

$$\mathcal{F}(x_1,x_2) = \frac{2x_1}{x_2-2}\,{}_2F_1\left(1,1-\frac{2}{x_2};2-\frac{2}{x_2};-x_1\right) \tag{2.26}$$

in terms of the Gauss's hypergeometric function ${}_2F_1\left(c_1,c_2\,;c_3\,;z\right)$ [64]. The Laplace transform $\mathcal{L}_{\tilde{Z}}(s)$ is a special case of (2.25), which is obtained by plugging $P_{\mathrm{PB}}\mu = 1$.

Proof: See Appendix B. □

I note that the Laplace transform is expressed in terms of tractable mathematical functions, which can be evaluated using most numerical toolboxes. I now characterize the mean harvested energy in terms of the network density and the path loss exponent.

Lemma 23 The average per-slot harvested energy for the case of multiple power beacons is given by $\mathbb{E}[Z] = \lambda_{\mathrm{PB}}\pi\frac{\eta}{\eta-2}\mu P_{\mathrm{PB}}$. This shows that the λ_{PB} and P_{PB} have the same effect on the mean harvested energy.

Proof: See Appendix B. □

The following lemmas treat the partial derivatives of the functions involved in the Laplace transform. I will apply them in the analytical characterization of the energy supply probability for the propagation model considered in this chapter.

Lemma 24 I let ${}_2F_1^{(k)}\left(1, 1-\frac{2}{x_2}; 2-\frac{2}{x_2}; -x_1\right)$ denote the kth-order partial derivative of the function ${}_2F_1\left(1, 1-\frac{2}{x_2}; 2-\frac{2}{x_2}; -x_1\right)$ with respect to the variable x_1, where $k = 0$ refers to the original function. Using the properties of the hypergeometric function [64], it follows that

$$
\begin{aligned}
{}_2F_1^{(k)}\left(1, 1-\frac{2}{x_2}; 2-\frac{2}{x_2}; -x_1\right) = \\
(-1)^k k! \frac{\left(1-\frac{2}{x_2}\right)_{(k)}}{\left(2-\frac{2}{x_2}\right)_{(k)}} \, {}_2F_1^{(0)}\left(k+1, k+1-\frac{2}{x_2}; k+2-\frac{2}{x_2}; -x_1\right)
\end{aligned}
\tag{2.27}
$$

where $(x)_{(k)} = \frac{\Gamma(x+k)}{\Gamma(x)}$ is the Pochhammer symbol, while $\Gamma(\cdot)$ is the Gamma function [64].

Lemma 25 I let $\mathcal{F}^{(k)}(x_1, x_2)$ denote the kth order partial derivative of the function $\mathcal{F}(x_1, x_2)$ with respect to the variable x_1. It follows that

$$
\begin{aligned}
\mathcal{F}^{(k)}(x_1, x_2) = \frac{2k}{x_2 - 2} \, {}_2F_1^{(k-1)}\left(1, 1-\frac{2}{x_2}, 2-\frac{2}{x_2}, -x_1\right) \\
+ \frac{2x_1}{x_2 - 2} \, {}_2F_1^{(k)}\left(1, 1-\frac{2}{x_2}, 2-\frac{2}{x_2}, -x_1\right)
\end{aligned}
\tag{2.28}
$$

where $\mathcal{F}^{(0)}(x_1, x_2) = \mathcal{F}(x_1, x_2)$.

Proof: The result follows by successive differentiation of (2.26) with respect to x_1, invoking Lemma 24, and (recursively) expressing the result in terms of the lower-order derivatives of the original function. □

Leveraging Lemma 22 and Faà di Bruno formula [65], I now specialize Proposition 21 to the scenario considered in this chapter.

Proposition 26 The energy supply probability for the bounded path loss model considered in Lemma 22 can be expressed in closed-form as

$$P_{\text{es}}^{\text{MP}}\left(m,n,a,\lambda_{\text{PB}},\eta\right)=e^{-\pi\lambda_{\text{PB}}\left(\frac{s}{1+s}+\mathcal{F}(s,\eta)\right)}\sum_{i=0}^{\frac{n}{2}-1}\frac{(-s)^{i}}{i!}\,B_{i}\left(g^{(1)}(s),\cdots,g^{(i)}(s)\right)\Big|_{s=\frac{m}{2a}} \tag{2.29}$$

where $B_i(u_1,\cdots,u_i)$ is the complete Bell polynomial of the second kind [65], and

$$g^{(i)}(s)=-\pi\lambda_{\text{PB}}\left(\left[-\frac{1}{1+s}\right]^{i+1}i!+\ \frac{i}{s}\Upsilon(i-1,\eta)\mathcal{F}^{(i-1)}(s,\eta)+\ \Upsilon(i,\eta)\mathcal{F}^{(i)}(s,\eta)\right), \tag{2.30}$$

where $\mathcal{F}^{(i)}\left(x_1,x_2\right)$ is given in Lemma 25 and $\Upsilon\left(i,x_2\right)=(-1)^{i}\,i!\,\frac{\left(1-\frac{2}{x_2}\right)_{(i)}}{\left(2-\frac{2}{x_2}\right)_{(i)}}$.

Proof: The proof follows by invoking Faà di Bruno formula [65] to calculate the partial derivatives of the Laplace transform in Lemma 22, and applying Lemma 24 and 25. □

The energy supply probability in Proposition 26 is expressed in terms of numerically tractable mathematical functions, which can be evaluated using numerical toolboxes. This analytical treatment is fairly general since Proposition 26 can be specialized to various scenarios. I further note that the exact characterization of the energy supply probability is rather unwieldy since it involves evaluating higher order derivatives of the Laplace transform. In the following proposition, I propose an approximate expression to simplify the computation of the energy supply probability.

Proposition 27 The energy supply probability for the case of multiple power beacons can be approximated as

$$P_{\text{es}}^{\text{MP}}\left(m,n,a,\lambda_{\text{PB}},\eta\right)\approx 1-F_{\tilde{Z}}\left(\frac{an}{m}\right), \tag{2.31}$$

where $F_{\tilde{Z}}(\cdot)$ can be evaluated using the numerical inversion technique of Lemma 28, aided by the Laplace transform characterization of Lemma 22.

Proof: The proof follows by substituting $\varphi = \mathbb{E}[\varphi] = n$ in the proof of Lemma 21. □

I now present an analytical expression to evaluate $F_{\tilde{Z}}(\cdot)$ using numerical inversion.

Lemma 28 Let us define positive constants A, B and C. I can evaluate $F_{\tilde{Z}}(x)$ using

$$F_{\tilde{Z}}(x) = \frac{2^{-B}e^{\frac{A}{2}}}{x} \sum_{b=0}^{B} \binom{B}{b} \sum_{c=0}^{C+b} \frac{(-1)^c}{D_c} \operatorname{Re}\left[\frac{\mathcal{L}_{\tilde{Z}}(s)}{s}\right], \tag{2.32}$$

where $s = \frac{A+j2\pi c}{2x}$, $D_c = 2$ when $c = 0$ and $D_c = 1$ when $c \in \{1, 2, \cdots, C+b\}$, Re[$\cdot$] denotes the real part, and $\mathcal{L}_{\tilde{Z}}(s)$ follows from Lemma 22.

Proof: See [66, 67] □

With parameters A, B and C chosen carefully, the finite summation in (2.32) yields stable numerical inversion with a bounded estimation error. To obtain a solution correct to $\varrho - 1$ decimal places, these parameters should satisfy $A \geq \varrho \log(10)$, $B \geq 1.243\varrho - 1$ and $C \geq 1.467\varrho$ [66–68].

2.5.2 Achievable Rate

I leverage the results from the previous sections to characterize the ergodic achievable rate for the case of multiple power beacons. I also account for the network interference due to other EH transmitters. Let us consider a typical receiver at

the origin, which receives useful signal from its dedicated EH transmitter over an AWGN channel, and interference from the other EH nodes over possibly fading links. This is a potential scenario as the dedicated EH-RX link distance could be much smaller than that from an interferer. For analytical simplicity, I assume that the interfering links undergo quasi-static fading such that the channels remain static over the entire codeword. I define g_k as the small-scale fading coefficient for the link originating from the EH transmitter at y_k. I assume IID Rayleigh fading for the interfering links such that $G_k = |g_k|^2 \sim \text{Exp}(1)$. Similar to the serving EH, an interfering EH transmits independent symbols from a Gaussian codebook with an average transmit power P_{EH} during the transmit phase. I define $I = \sum_{y_k \in \Phi_{\text{EH}}, k \neq 0} \frac{P_{\text{EH}} G_k}{\ell(\|y_k\|, \eta)}$ as the aggregate interference power and $\gamma_I = \frac{\zeta P_{\text{EH}}}{\sigma^2 + I}$ as the signal-to-interference-plus-noise ratio (SINR) at the typical receiver, where the constant $\zeta \in (0, 1]$ models any (deterministic) attenuation for the serving link, known to the transmitter and receiver. I further assume that interference is treated as noise for the purpose of decoding. I first characterize the Laplace transform of I, which is then used for evaluating the CDF $F_I(\cdot)$ using numerical inversion.

Lemma 29 The Laplace transform $\mathcal{L}_I(s)$ of the interference I is analytically characterized by

$$\mathcal{L}_I(s) = \exp\left(-\pi \lambda_{\text{EH}} \frac{P_{\text{EH}} s}{1 + P_{\text{EH}} s}\right) \exp\left(-\pi \lambda_{\text{EH}} \, \mathcal{F}\left(P_{\text{EH}} s, \eta\right)\right), \tag{2.33}$$

where $\mathcal{F}(\cdot, \cdot)$ follows from (2.26).

Proof: The proof is similar to that of Lemma 22. □

Theorem 30 In a large-scale network with PB density λ_{PB}, EH density λ_{EH}, PB transmit power P_{PB}, EH transmit power P_{EH}, the ergodic non-asymptotic ϵ-achievable rate at a typical receiver is characterized by

$$R_{\mathrm{EH}}^{\mathrm{MP}}\left(\epsilon, a, P_{\mathrm{PB}}, P_{\mathrm{EH}}, m, n, \lambda_{\mathrm{PB}}, \lambda_{\mathrm{EH}}\right) = \frac{\frac{n}{2}\mathbb{E}_I\left[\log(1+\gamma_I)\right] - \sqrt{\frac{2+\epsilon}{\epsilon}n}\mathbb{E}_I\left[\sqrt{\frac{\gamma_I}{\gamma_I+1}}\right] - (n)^{\frac{1}{4}} - 1}{n+m}, \tag{2.34}$$

where

$$\mathbb{E}_I\left[\log\left(1+\gamma_I\right)\right] = \int_0^{\tau} F_I\left(\frac{\zeta P_{\mathrm{EH}}}{e^t-1} - \sigma^2\right) \mathrm{d}t \tag{2.35}$$

for $\tau = \log\left(1+\zeta\gamma\right)$,

$$\mathbb{E}_I\left[\sqrt{\frac{\gamma_I}{\gamma_I+1}}\right] = \int_0^{\hat{\tau}} F_I\left(\zeta P_{\mathrm{EH}}\left(\frac{1}{t^2}-1\right) - \sigma^2\right) \mathrm{d}t \tag{2.36}$$

for $\hat{\tau} = \sqrt{\frac{1}{1+\frac{1}{\zeta\gamma}}}$, and $F_I(\cdot)$ can be evaluated using Lemma 28. The expression in (2.34) holds for all tuples (m, n) satisfying the constraints in (2.37) and (2.38), i.e.,

$$n \geq \left[\log\left(\frac{2+\epsilon}{\epsilon^2}\right)\right]^4 \tag{2.37}$$

and

$$\sum_{i=0}^{\frac{n}{2}-1}(-1)^i \frac{m^i}{(2a)^i i!}\frac{\mathrm{d}^i}{\mathrm{d}s^i}\mathcal{L}_{\tilde{Z}}(s)\Big|_{s=\frac{m}{2a}} \leq \frac{\epsilon}{2+\epsilon} \tag{2.38}$$

where $\mathcal{L}_{\tilde{Z}}\left(s\right)$ follows from Lemma 22.

Proof: See Appendix B. □

The achievable rate expression for the case of multiple power beacons can be interpreted similar to the case of a single power beacon. For example, (2.37) specifies

the minimum transmit blocklength required for the target ϵ. Similarly, given n and a, (2.38) ensures that the harvest blocklength is large enough such that the energy outage probability is bounded by $\frac{\epsilon}{2+\epsilon}$ (and the target error probability by ϵ). The impact of other parameters such as the PB density and the path loss exponent is captured by $\mathcal{L}_{\tilde{Z}}(s)$. Eq. (2.38), expressed in terms of the Laplace transform for generality, can be evaluated using Proposition 26. I note that the Poisson network of PBs impacts the energy outage probability, which is captured in (2.38). The Poisson network of EHs generates interference hurting the communication link, which is accounted for in (2.34). Further, the *ergodic* achievable rate in (2.34) is obtained by averaging over the aggregate interference, i.e., interferer locations and small-scale fading.

Remark 31 I note that Theorem 2 assumes all EH interferes to be active. This is pessimistic since a fraction $1 - P_{\text{es}}^{\text{MP}}(\cdot)$ of the EHs may be inactive due to insufficient energy. I ignore this distinction as $P_{\text{es}}^{\text{MP}}(\cdot)$ is at least $\frac{2}{2+\epsilon}$ due to (2.38), which is close to unity for various values of ϵ. A less pessimistic approach entails independently thinning the PPP Φ_{EH} with thinning probability $P_{\text{es}}^{\text{MP}}(\cdot)$. This means replacing the density λ_{EH} in Lemma 29 by a reduced density $P_{\text{es}}^{\text{MP}}(\cdot)\,\lambda_{\text{EH}}$.

2.6 Numerical Results

I now present the simulation results for the energy supply probability and the achievable rate based on the analyses in Section 2.4 and 2.5. I assume that the noise power $\sigma^2 = 1$, the rectifier efficiency $\mu = 1$, and path loss exponent $\eta = 3.6$. I assume the EH-RX distance is set to 1 m such that $\zeta = 1$. I do not specify the units of P_{EH}, P_{PB}, or P_{H} since the results are valid for any choice of the units (say Joules/symbol).

2.6.1 Single Power Beacon

I first present the results for the case of a single power beacon treated in Section 2.4. In the following plots, I adopt the minimum latency approach where the minimum possible blocklength is selected for the given set of parameters, based on the constraints in (2.10) and (2.11). That is, for a given ϵ, I select the minimum required n using $n = \left\lceil \left(\log\left(\frac{2+\epsilon}{\epsilon^2}\right)\right)^4 \right\rceil_{\text{ev}}$. I then choose the minimum required m using (2.11).

2.6.1.1 Energy Supply Probability: IID vs. Correlated Arrivals

In Fig. 2.2, I plot the energy supply probability versus the transmit blocklength for a fixed harvest blocklength m and power ratio a. I include the plots for IID as well as correlated energy arrivals. I observe that the energy supply probability for the IID case exhibits a sharp decay compared to the correlated case. With IID arrivals, the total harvested energy hardens to its mean mP_{H} when m is large, and has a variance that is m times smaller than the correlated case. This explains the sharp decay of the IID curve. Moreover, when n is small, IID energy arrivals yield a higher energy supply probability compared to correlated arrivals. As the blocklength is increased, the roles are reversed. I also obtain the energy supply probability using Monte Carlos simulations. The simulation (sim) results validate the analytical (anl) approximation proposed in Corollary 6 for IID arrivals. In the following subsections, I focus on the case of correlated energy arrivals.

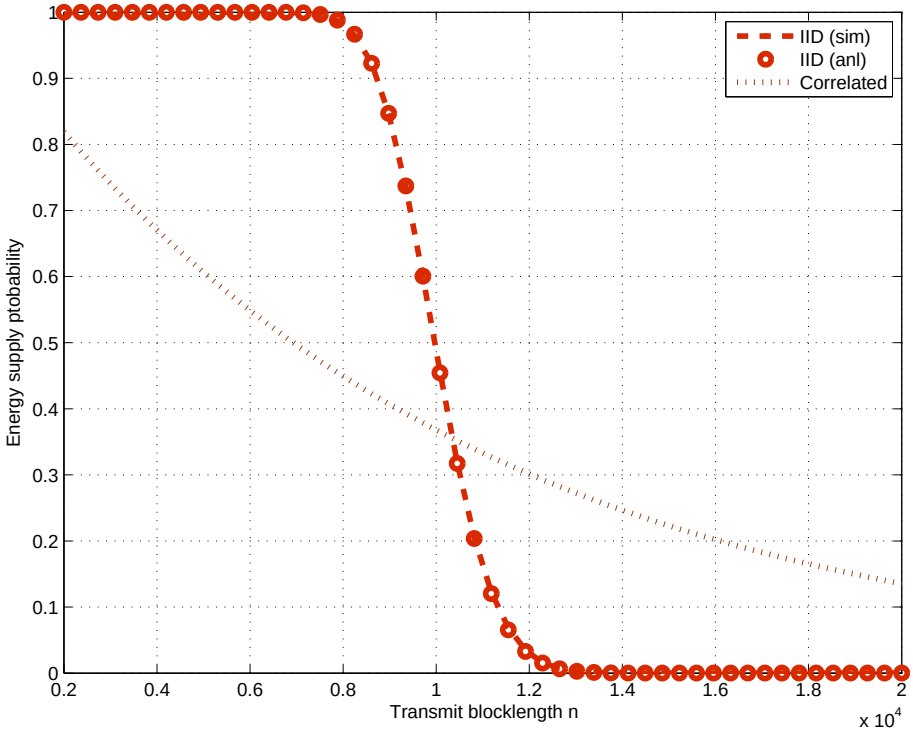

Figure 2.2: The energy supply probability vs. transmit blocklength for $m = 100$ and $a = 0.01$. IID arrivals yield a higher energy supply probability than correlated arrivals when n is small.

2.6.1.2 Achievable Rate vs. Power Ratio

In Fig. 2.3, I use Theorem 1 and Proposition 2 to plot the achievable rate versus the power ratio a for a given ϵ and P_{H}. The plot reflects the underlying tension between the energy supply probability and the channel SNR, resulting in an optimal transmit power (or power ratio) that maximizes the achievable rate. I also observe that the EH node can transmit at a higher rate as the target error probability is increased.

2.6.1.3 Achievable Rate vs. Target Error Probability

In Fig. 2.4, I plot the achievable rate versus the target error probability ϵ for a given power ratio a. I first consider the (fixed power) case where I fix the transmit power $P_{\mathrm{EH}} = 1.1554$ and the power ratio $a = 0.0012$ (these values are asymptotically optimal for $P_{\mathrm{H}} = 10^3$ and $\epsilon = 10^{-3}$). As ϵ increases, the achievable rate tends to increase until a limit, beyond which the rate tends to decrease. This is because as I allow for more error ($\epsilon \uparrow$), the required total blocklength decreases. This means a possible increase in the energy supply probability (as the power ratio is fixed), and a larger backoff from capacity due to a shorter transmit blocklength. Beyond a certain ϵ, further reduction in blocklength pronounces the higher order backoff terms, eventually reducing the rate. For a *fixed* total blocklength, however, the achievable rate indeed increases with ϵ. I note that these trends differ from the asymptotic case where the rate monotonically increases with ϵ. I then consider the case where I adapt the transmit power using Corollary 18. In Fig. 2.4, I observe a substantial increase in the rate by optimally adjusting the transmit power in terms of the system parameters. Moreover, using the *asymptotically* optimal transmit power $P^*_{\mathrm{EH},\infty}$ (from Corollary 18) in the finite blocklength regime results in only a minor loss in performance. As evident from Fig. 2.4, the optimal rate in the finite blocklength regime (obtained by numerically optimizing over P_{EH}) is almost indistinguishable from the lower bound obtained using the asymptotically optimal power $P^*_{\mathrm{EH},\infty}$.

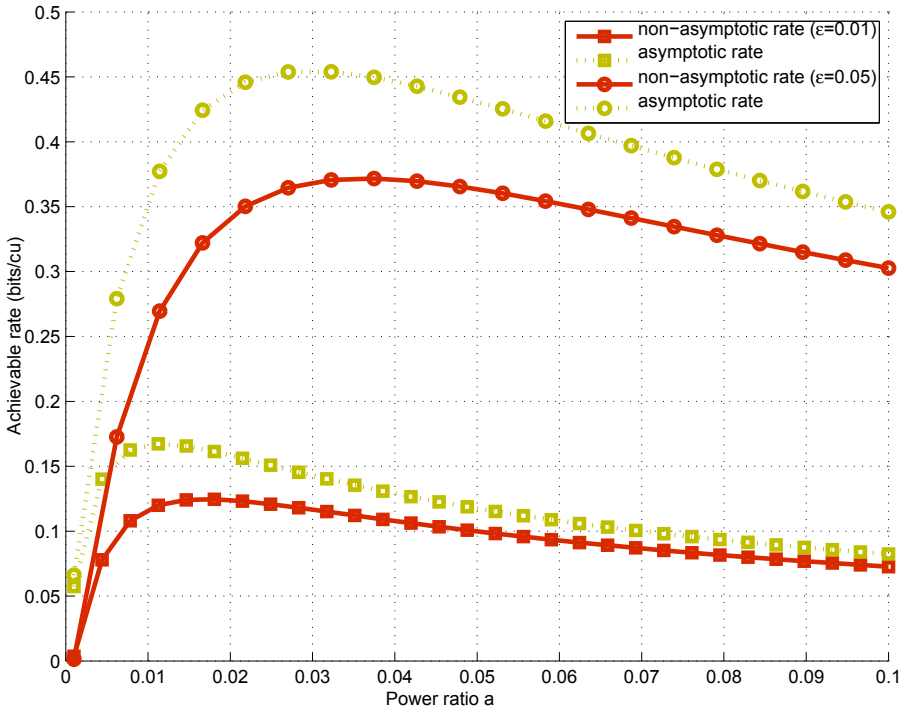

Figure 2.3: The achievable rate (bits/channel use) vs. the power ratio $a = \frac{P_{\mathrm{EH}}}{P_{\mathrm{H}}}$ for $P_{\mathrm{H}} = 10^2$. There is an optimal transmit power that maximizes the rate.

2.6.1.4 Optimal Transmit Power

In Fig. 2.5, I plot the optimal transmit power versus the average harvested power for $\epsilon = 0.05$ and the transmit blocklength $n = \lceil \log\left(\frac{2+\epsilon}{\epsilon^2}\right)^4 \rceil_{\mathrm{ev}} = 2026$. For each P_{H}, the harvest blocklength is selected to satisfy the constraint in (2.11). I observe that the asymptotically optimal transmit power is a conservative estimate of the optimal transmit power for the finite case (Remark 19). In Fig. 2.6, I plot the optimal power ratio against the average harvested power. Even though the optimal transmit power increases with P_{H}, I note that the optimal power ratio still decreases

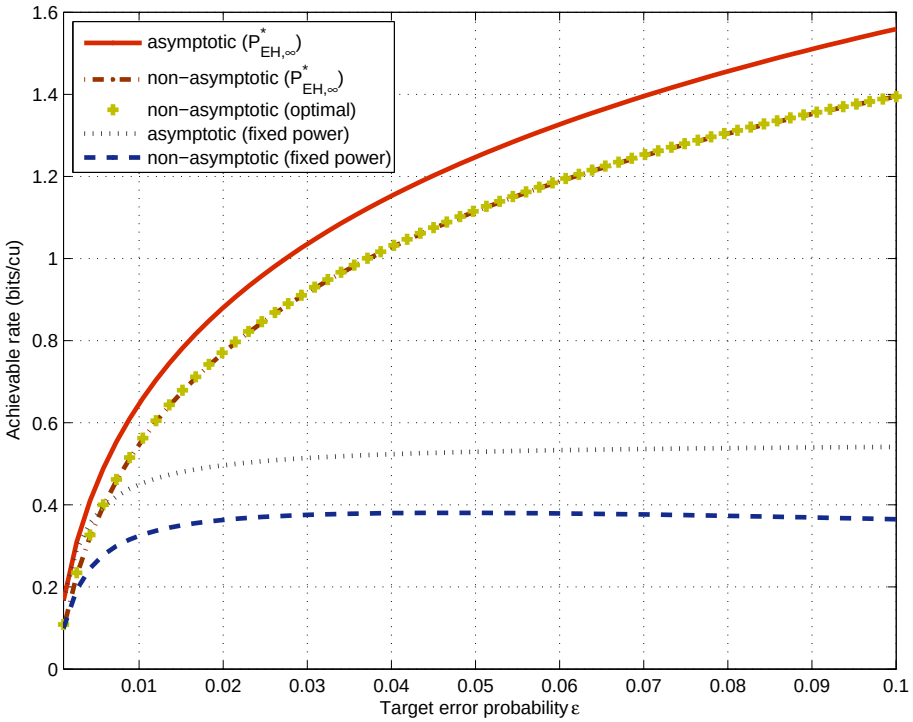

Figure 2.4: The achievable rate (bits/channel use) vs. the target error probability ϵ for a given power ratio $a = 0.0012$. While the asymptotic rate increases as I allow for more error, the non-asymptotic rate behaves differently. Moreover, power control is essential for improving the achievable rate.

as P_{H} is increased. In other words, while it is optimal to increase P_{EH} with P_{H}, the scaling is sublinear in P_{H} (Corollary 20).

2.6.2 Multiple Power Beacons

I now consider the case of multiple power beacons treated in Section 2.5. I plot results obtained via Monte Carlo simulation (sim) as well as the analytical (anl) expression. The simulations are conducted for 10^4 runs, where each run consists of generating PB and EH node locations according to the respective PPP intensities.

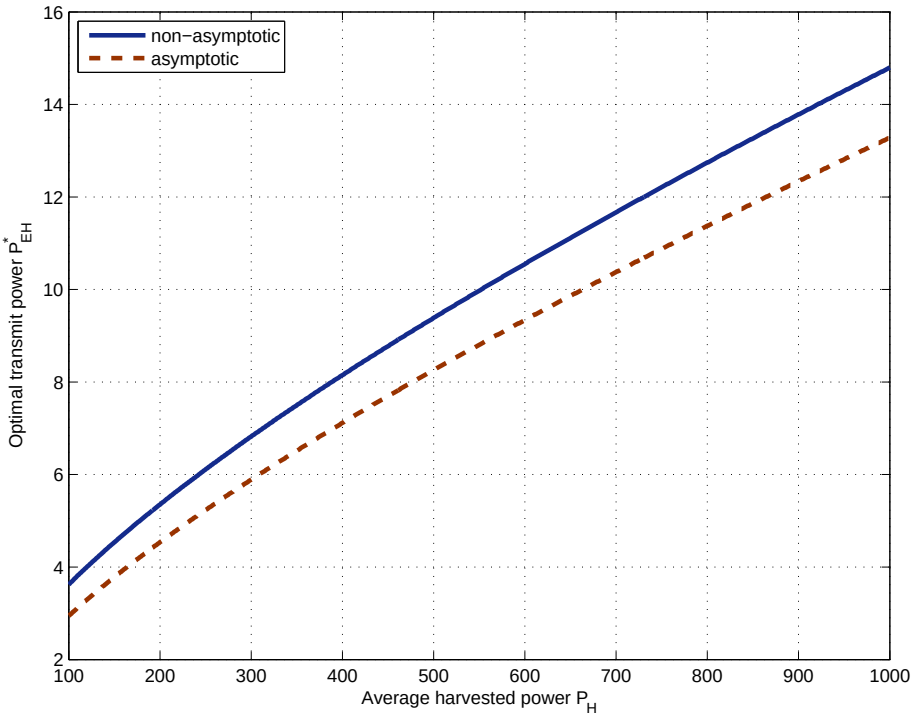

Figure 2.5: Optimal transmit power P_{EH} vs. average harvested power P_{H} in the asymptotic and non-asymptotic blocklength regimes. The asymptotically optimal transmit power is a conservative estimate of the non-asymptotic transmit power.

The fading coefficients are generated according to independent Rayleigh distribution for each link. The distance between an EH and its dedicated RX is set to 1 m such that $\zeta = 1$. While applying Lemma 28, I set $A = 8\log(10)$, $B = 11$, and C=14 to achieve a stable numerical inversion correct to 7 decimal places.

2.6.2.1 Energy Supply Probability

In Fig. 2.7, I plot the energy supply probability versus the mean harvested power for a fixed total blocklength and EH transmit power. The average harvested

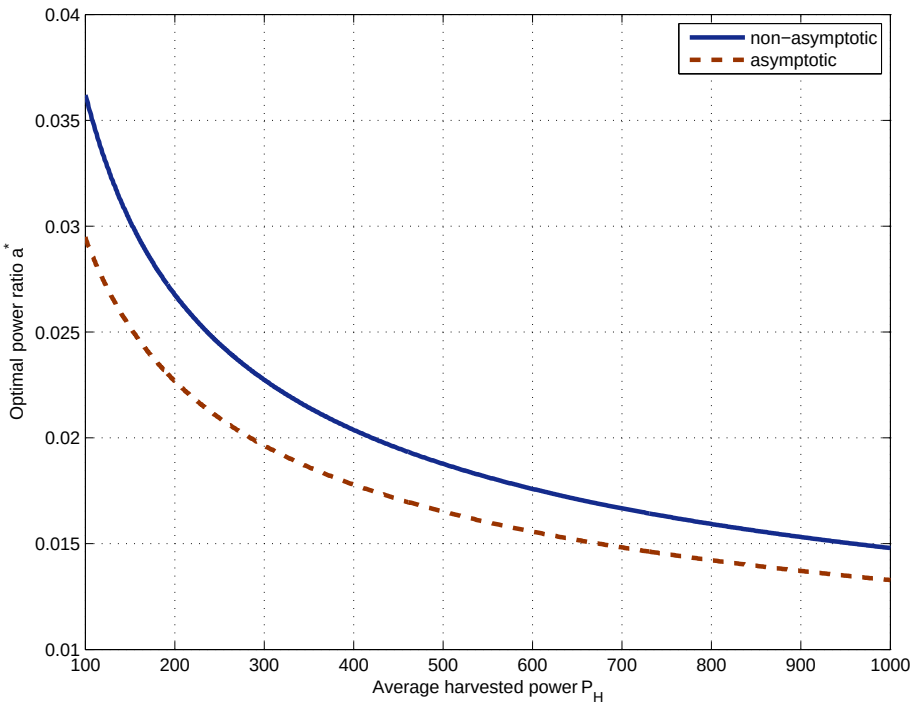

Figure 2.6: Optimal power ratio a^* vs. average harvested power P_{H} in asymptotic and non-asymptotic blocklength regimes. The optimal power ratio decays as the average harvested power is increased.

power is increased by increasing either the PB transmit power P_{PB} or the PB density λ_{PB}, according to Lemma 23. I consider two cases: i) λ_{PB} is fixed and P_{PB} is increased, and ii) P_{PB} is fixed and λ_{PB} is increased. For the former, I obtain the plot for P_{PB} ranging from 10^3 to 10^4 and $\lambda_{\mathrm{PB}} = 10^{-3}$ nodes per m^2. For the latter, I assume λ_{PB} ranges from 10^{-3} to 10^{-2} nodes per m^2 and $P_{\mathrm{PB}} = 10^3$. Keeping the average harvested power the same in both cases, I observe that increasing the PB density is more beneficial for the energy supply probability than increasing the PB transmit power. Furthermore, I also plot the results using Proposition 27. I find that the

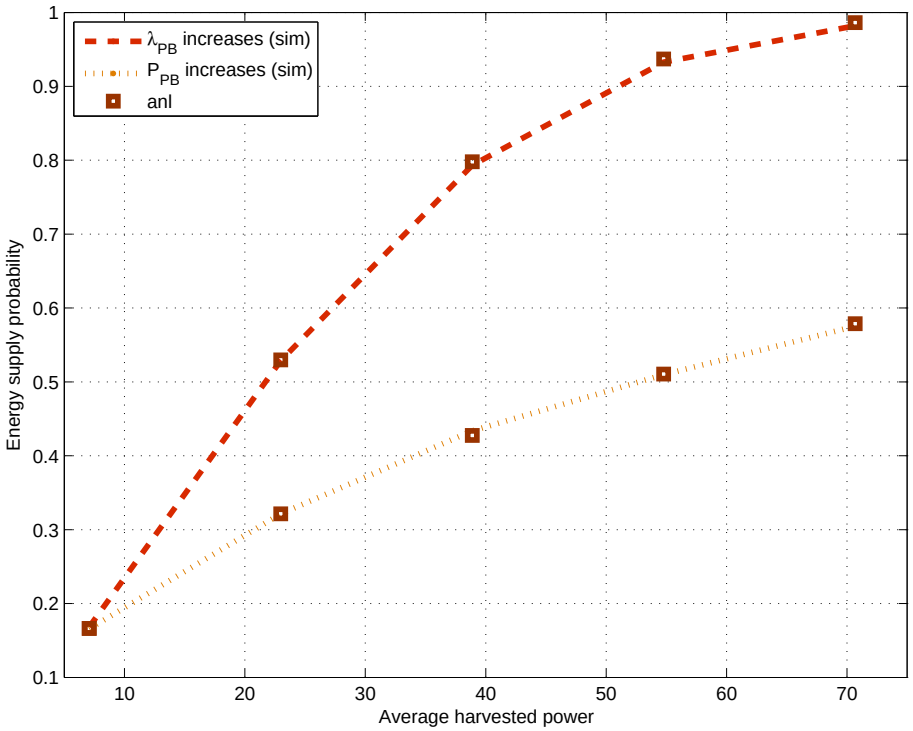

Figure 2.7: The energy supply probability $P_{\text{es}}(m, n, a, \lambda_{\text{PB}}, \eta)$ vs. the average harvested power for $m = 1500$, $n = 1000$, $P_{\text{EH}} = 1$. For the same *mean* harvested power, increasing the PB density is more beneficial than increasing the PB transmit power.

proposed analytical expression provides a tight approximation of the energy supply probability.

2.6.2.2 Achievable Rate

In Fig. 2.8, I invoke Theorem 30 to plot the ergodic achievable rate versus the transmit blocklength n for a fixed ϵ. The analytical results are based on Theorem 3 and the simulation results are obtained using Monte Carlo simulations. Also included is the plot for the AWGN only case, where I ignore the network interference. I set

$\epsilon = 0.05$, $P_{\text{PB}} = 10^4$, $\lambda_{\text{PB}} = 0.005$ nodes per m^2, $\lambda_{\text{EH}} = 0.01$ nodes per m^2, and $\zeta = 1$. I select n in the range that satisfies (2.10). For each n, I numerically optimize over m and P_{EH} to maximize the AWGN rate, while satisfying (2.11). I use the same values for evaluating the rate for the case with interference. I observe that network interference due to concurrently transmitting EHs degrades the ergodic achievable rate. Moreover, the simulation results validate the analytical results. Finally, I observe that the ergodic achievable rate is extremely sensitive to the blocklength, confirming that the asymptotic analyses fail to capture the behavior of a wirelessly powered system with short packets.

2.7 Conclusions

In this chapter, characterized the energy supply probability and the achievable rate of a wireless-powered communication system in the finite blocklength regime. Using analytical expressions as well as numerical simulations, I investigated the interplay between key system parameters such as the harvest blocklength, the transmit blocklength, the error probability, and the power ratio. For the case of a single power beacon, I showed that the harvest blocklength should be scaled proportionally to the transmit blocklength in order to maintain the ϵ-achievable rate. The rate of growth is characterized by the power ratio as well as the target error probability. Moreover, I derived closed-form expression for the optimal transmit power in the asymptotic blocklength regime. Numerical results show that using the asymptotically optimal transmit power can substantially improve the achievable rate even in the finite blocklength regime. I also extended the analysis to a large-scale network

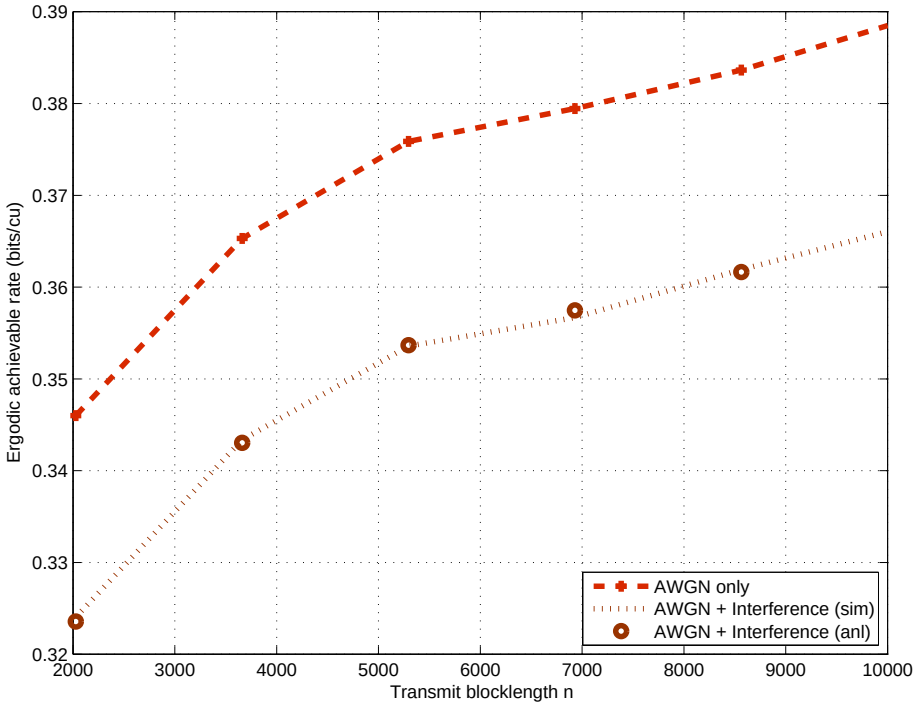

Figure 2.8: The ergodic ϵ-achievable rate versus transmit blocklength at a typical harvester powered by multiple power beacons ($\lambda_{\mathrm{PB}} = 0.005$ nodes per m^2, $\lambda_{\mathrm{EH}} = 0.01$ nodes per m^2). The achievable rate improves as the blocklength is increased, confirming that the non-asymptotic rate is substantially smaller than the asymptotic rate.

with Poisson-distributed power beacons. Numerical results reveal that the performance is sensitive to the blocklength, confirming that the asymptotic analyses of wireless-powered systems fail to capture the behavior in the short packet regime.

Appendix A: Single Power Beacon

The following proof is modified from the proof provided in [48]. The key steps are similar to [48], except for a different expression for the energy supply probability,

which leads to different blocklength constraints. The proof leverages the fact that the communication link failure mainly results from two events: energy outages at the transmitter or decoding error at the receiver. The first step of the proof involves bounding the decoding errors due to energy outages and channel noise in terms of the target error probability. The second step uses conventional information theoretic arguments to derive an expression for the non-asymptotic achievable rate for the considered wireless-powered channel. Let us first bound the energy outage probability as

$$\Pr\left[\bigcup_{k=1}^{n}\left\{\sum_{\ell=1}^{k}X_{\ell}^{2}>\sum_{i=1}^{m}Z_{i}\right\}\right]\leq 1-\frac{2}{2+\epsilon} \tag{2.39}$$

for $\epsilon\in[0,1)$. Using Lemma 1, the constraint in (2.39) can be equivalently expressed in terms of the energy supply probability as $\Pr\left[\sum_{\ell=1}^{n}X_{\ell}^{2}\leq\sum_{i=1}^{m}Z_{i}\right]\geq\frac{2}{2+\epsilon}$. I let $X^n(W)$ and Y^n denote the intended codeword sequence for a message $W\in\mathcal{W}$, and the received sequence. The decoder $\mathcal{G}(Y^n)$ employs the following threshold decoding rule [48] to decode the received signal: $\mathcal{G}(Y^n)=i$ if there exists a unique integer $i\in\mathcal{W}$ that satisfies

$$\log\left(\frac{p_{Y^n|X^n}\left(Y^n|X^n(i)\right)}{p_{Y^n}\left(Y^n\right)}\right)>\log(M)+n^{\frac{1}{4}}, \tag{2.40}$$

otherwise $\mathcal{G}(Y^n)=w$, where w is drawn uniformly at random from $\mathcal{W}$. Here, the notation $p_{Y^n|X^n}(\cdot)$ denotes the joint conditional distribution of random sequence Y^n given X^n. I express the probability of decoding error $\Pr\left[\mathcal{G}(Y^n)\neq W\right]$ in (2.41).

$$\begin{aligned}\Pr\left[\mathcal{G}(Y^n)\neq W\right]&=\Pr\left[\mathcal{G}(Y^n)\neq W,Y^n=X^n(W)+V^n\right]\\&\quad+\Pr\left[\mathcal{G}(Y^n)\neq W,Y^n\neq X^n(W)+V^n\right]\end{aligned}$$

$$\leq \Pr\left[\mathcal{G}(X^n(W)+V^n)\neq W\right]+\frac{\epsilon}{2+\epsilon}, \tag{2.41}$$

where the inequality results from (2.39), and because the term

$$\begin{aligned}
&\Pr\left[\mathcal{G}(Y^n)\neq W, Y^n = X^n(W)+V^n\right]\\
&\quad=\Pr\left[\mathcal{G}(X^n(W)+V^n)\neq W\right]\Pr\left[Y^n = X^n(W)+V^n)\right]\\
&\quad\leq \Pr\left[\mathcal{G}(X^n(W)+V^n)\neq W\right].
\end{aligned}$$

I note that it is possible to further tighten the inequality in (2.41) by using the exact expression for $\Pr\left[Y^n = X^n(W)+V^n)\right]$ (as outlined in [69]). Because this results in only a minor improvement in rate (especially when ϵ is small), I do not follow this approach to keep the analysis simple. Moreover, I assume the decoding error probability to be unity when a codeword is impacted by an energy outage. When an EH node finds the harvested energy insufficient to transmit the intended codeword, it may not transmit any symbol, and donate the harvested energy to the system-level battery. This is consistent with the assumption about the left-over energy in Section 3.3. To calculate $\Pr\left[\mathcal{G}(X^n(W)+V^n)\neq W\right]$, I define $\mathcal{A}_{i|j}$ as the event that $i\in\mathcal{W}$ satisfies the threshold decoding rule of (2.40) when $j\in\mathcal{W}$ is transmitted, i.e.,

$$\mathcal{A}_{i|j}=\left\{\log\left(\frac{p_{Y^n|X^n}\left(X^n(j)+V^n|X^n(i)\right)}{p_{Y^n}\left(X^n(j)+V^n\right)}\right)>\log(M)+n^{\frac{1}{4}}\right\}, \tag{2.42}$$

and $\mathcal{A}^c_{i|j}$ denotes its complement. As the message W is uniform on $\mathcal{W}$, it follows that the decoding error probability

$$\begin{aligned}
&\Pr\left[\mathcal{G}(X^n(W)+V^n)\neq W\right]\\
&\quad\overset{(a)}{=}\frac{1}{M}\sum_{w=1}^{M}\Pr\left[\mathcal{A}^c_{w|w}\bigcup\bigcup_{i\neq w, i\in\mathcal{W}}\mathcal{A}_{i|w}\Big|W=w\right]
\end{aligned}$$

$$\overset{(b)}{=} \Pr\left[\mathcal{A}_{1|1}^{c} \bigcup \bigcup_{i=2}^{M} \mathcal{A}_{i|1}\right] \overset{(c)}{\leq} \Pr\left[\mathcal{A}_{1|1}^{c}\right] + \Pr\left[\bigcup_{i=2}^{M} \mathcal{A}_{i|1}\right]$$
$$\overset{(d)}{\leq} \Pr\left[\mathcal{A}_{1|1}^{c}\right] + e^{-n^{\frac{1}{4}}} \overset{(e)}{\leq} \Pr\left[\mathcal{A}_{1|1}^{c}\right] + \frac{\epsilon^2}{2+\epsilon} \tag{2.43}$$

where (b) follows from the symmetry in random codebook construction, (c) results from applying the Union bound, and (d) is obtained by invoking Lemma 3 from [48]. Finally, (e) follows by assuming that $n \geq \left(\log\left(\frac{2+\epsilon}{\epsilon^2}\right)\right)^4$, which is the constraint in (2.10). Before proceeding further, let us assume that M is a unique integer that satisfies (2.44).

$$\log(M+1) \geq n\mathbb{E}\left[\log\left(\frac{p_{Y|X}(Y|X))}{p_Y(Y)}\right)\right]$$
$$-\left(\frac{2+\epsilon}{\epsilon} n \texttt{Var}\left[\log\left(\frac{p_{Y|X}(Y|X))}{p_Y(Y)}\right)\right]\right)^{\frac{1}{2}} - n^{\frac{1}{4}} > \log(M) \tag{2.44}$$

To find a bound for $\Pr\left[\mathcal{A}_{1|1}^{c}\right]$, consider the following set of inequalities in (2.45).

$$\Pr\left[\mathcal{A}_{1|1}^{c}\right] \overset{(a)}{=} \Pr\left[\log\left(\frac{p_{Y^n|X^n}(X^n(1)+V^n|X^n(1))}{p_{Y^n}(X^n(1)+V^n)}\right) \leq \log(M) + n^{\frac{1}{4}}\right]$$
$$= \Pr\left[\sum_{k=1}^{n} \log\left(\frac{p_{Y|X}(X_k(1)+V_k|X_k(1))}{p_Y(X_k(1)+V_k)}\right) \leq \log(M) + n^{\frac{1}{4}}\right]$$
$$\overset{(b)}{\leq} \Pr\left[\sum_{k=1}^{n} \log\left(\frac{p_{Y|X}(X_k(1)+V_k|X_k(1))}{p_Y(X_k(1)+V_k)}\right) \leq \right.$$
$$n\mathbb{E}\left[\log\left(\frac{p_{Y|X}(Y|X))}{p_Y(Y)}\right)\right]$$
$$\left. -\left(\frac{2+\epsilon}{\epsilon} n \text{Var}\left[\log\left(\frac{p_{Y|X}(Y|X))}{p_Y(Y)}\right)\right]\right)^{\frac{1}{2}}\right]$$
$$\leq \Pr\left[\left|\sum_{k=1}^{n} \log\left(\frac{p_{Y|X}(X_k(1)+V_k|X_k(1))}{p_Y(X_k(1)+V_k)}\right)\right.\right.$$
$$\left.\left. - n\mathbb{E}\left[\log\left(\frac{p_{Y|X}(Y|X))}{p_Y(Y)}\right)\right]\right| \geq$$

$$\left(\frac{2+\epsilon}{\epsilon} n\mathrm{Var}\left[\log\left(\frac{p_{Y|X}(Y|X))}{p_Y(Y)}\right)\right]\right)^{\frac{1}{2}}\Bigg]$$

$$\overset{(c)}{\leq} \frac{\epsilon}{2+\epsilon} \tag{2.45}$$

where (a) follows from the definition of $\mathcal{A}_{i|j}$ in (2.42), while the bound in (b) results from (2.44). Finally, (c) is obtained by applying Chebychev's inequality. From (2.42) and (2.45), it follows that $\Pr\left[\mathcal{G}(X^n(W)+V^n)\neq W\right]=\frac{\epsilon+\epsilon^2}{2+\epsilon}$; and further using (2.41), I conclude that $\Pr\left[\mathcal{G}(Y^n)\neq W\right]\leq\epsilon$, where W is the transmitted message. Therefore, I conclude that the constructed code is an $(n+m, M, \epsilon)$-code that satisfies the following equations (2.46)-(2.48).

$$\log(M+1)\geq n\mathbb{E}\left[\log\left(\frac{p_{Y|X}(Y|X))}{p_Y(Y)}\right)\right]-\left(\frac{2+\epsilon}{\epsilon}n\mathtt{Var}\left[\log\left(\frac{p_{Y|X}(Y|X))}{p_Y(Y)}\right)\right]\right)^{\frac{1}{2}}-n^{\frac{1}{4}} \tag{2.46}$$

$$\log(M+1)\geq\frac{n}{2}\log(1+\gamma)-\sqrt{\frac{2+\epsilon}{\epsilon}\frac{\gamma}{1+\gamma}n}-n^{\frac{1}{4}} \tag{2.47}$$

$$\log(M)\geq\frac{n}{2}\log(1+\gamma)-\sqrt{\frac{2+\epsilon}{\epsilon}\frac{\gamma}{1+\gamma}n}-n^{\frac{1}{4}}-1 \tag{2.48}$$

Here, (2.47) is obtained by noting that the mutual information $\mathbb{E}\left[\log\left(\frac{p_{Y|X}(Y|X))}{p_Y(Y)}\right)\right]=\frac{1}{2}\log\left(1+\gamma\right)$, while the variance $\mathtt{Var}\left[\log\left(\frac{p_{Y|X}(Y|X))}{p_Y(Y)}\right)\right]=\frac{\gamma}{1+\gamma}$. The last equation follows by noting that $\log\left(M+1\right)-\log\left(M\right)<1$. Using (2.48) with the constraints in (2.8) and (2.9) completes the proof.

Proof of Corollary 18

The proof follows by differentiating (2.12) with respect to P_{EH} and setting $\frac{\partial R^{\infty}_{\mathrm{EH}}}{\partial P_{\mathrm{EH}}}=0$. This leads to the following equation after simplification.

$$\left(P_{\mathrm{EH}}+\sigma^2\right)\log\left(P_{\mathrm{EH}}+\sigma^2\right)=$$

$$\left(1+\log\left(\sigma^2\right)\right)\left(P_{\mathrm{EH}}+\sigma^2\right)+P_{\mathrm{H}}\log\left(1+0.5\epsilon\right)-\sigma^2 \tag{2.49}$$

With the following change of variables $x=P_{\mathrm{EH}}+\sigma^2$, $c_1=P_{\mathrm{H}}\log\left(1+0.5\epsilon\right)-\sigma^2$, and $c_2=1+\log\left(\sigma^2\right)$, (2.49) can be written as $x\log(x)=c_1+c_2x$ which has the solution $x=\frac{c_1}{\mathrm{W}[c_1\exp(-c_2)]}$. Back substituting x, c_1, and c_2 in the solution yields (2.22).

Appendix B: Multiple Power Beacons

Energy Supply Probability

I now derive an exact expression for the energy supply probability in a Poisson network with multiple power beacons. Recall that the harvested energy in a given slot is $Z=\sum\limits_{x_k\in\Phi_{\mathrm{PB}}}\frac{P_{\mathrm{PB}}\mu H_k}{\ell(\|x_k\|,\eta)}$. From the definition of the energy supply probability, it follows that

$$\begin{aligned}
P_{\mathrm{es}}^{\mathrm{MP}}\left(m,n,a,\lambda_{\mathrm{PB}},\eta\right)&=\Pr\left[\sum_{i=1}^{n}X_i^2\leq mZ\right]\\
&\overset{(a)}{=}\Pr\left[\varphi\leq\frac{mZ}{P_{\mathrm{EH}}}\right]\\
&\overset{(b)}{=}1-\mathbb{E}\left[\sum_{\ell=0}^{\frac{n}{2}-1}\frac{\left(mZ\right)^{\ell}}{\left(2P_{\mathrm{EH}}\right)^{\ell}\ell!}e^{-\frac{m}{2P_{\mathrm{EH}}}Z}\right]\\
&\overset{(c)}{=}1-\sum_{\ell=0}^{\frac{n}{2}-1}(-1)^{\ell}\frac{m^{\ell}}{2^{\ell}a^{\ell}\ell!}\frac{\mathrm{d}^{\ell}}{\mathrm{d}s^{\ell}}\mathcal{L}_{\tilde{Z}}(s)|_{s=\frac{m}{2a}}
\end{aligned} \tag{2.50}$$

where (a) follows by the substitution $\varphi=\sum\limits_{i=1}^{n}\frac{X_i^2}{P_{\mathrm{EH}}}$ such that φ is a Chi-squared random variable with n degrees of freedom, i.e., $\varphi\sim\mathrm{Ga}\left(\frac{n}{2},2\right)$. Equality (b) is obtained by conditioning on the random variable Z, and by using the CDF of φ. Finally, (c) follows from the definition of a Laplace transform of a random variable X, namely,

$\mathcal{L}_X(s) = \mathbb{E}[e^{-sX}]$, and by invoking the property $\mathbb{E}[X^\ell e^{-sX}] = (-1)^\ell \frac{\mathrm{d}^\ell}{\mathrm{d}s^\ell}\mathcal{L}_X(s)$. Note that I substitute $Z = P_{\mathrm{PB}}\mu\tilde{Z}$ to obtain (c).

Proof of Lemma 22

I now derive the Laplace transform $\mathcal{L}_Z(s)$ for the bounded path loss model $\ell(r,\eta) = \max(1, r^\eta)$ considered in Lemma 22.

$$\begin{aligned}
\mathbb{E}\left[e^{-sZ}\right] &= \mathbb{E}\left[e^{-sP_{\mathrm{PB}}\mu \sum\limits_{x_k\in\Phi_{\mathrm{PB}}} \frac{H_k}{\ell(\|x_k\|,\eta)}}\right] \\
&= \mathbb{E}\left[\prod_{x_k\in\Phi_{\mathrm{PB}}} e^{-sP_{\mathrm{PB}}\mu\frac{H_k}{\ell(\|x_k\|,\eta)}}\right] \\
&= \mathbb{E}_{\Phi_{\mathrm{PB}}}\left[\prod_{x_k\in\Phi_{\mathrm{PB}}} \mathbb{E}_{H_k}\left[e^{-sP_{\mathrm{PB}}\mu\frac{H_k}{\ell(\|x_k\|,\eta)}}\right]\right] \\
&\overset{(a)}{=} \mathbb{E}_{\Phi_{\mathrm{PB}}}\left[\prod_{x_k\in\Phi_{\mathrm{PB}}} \frac{1}{1+sP_{\mathrm{PB}}\mu\ell\left(\|x_k\|,\eta\right)^{-1}}\right] \\
&\overset{(b)}{=} e^{-2\pi\lambda_{\mathrm{PB}}\int\limits_0^1\left[1-\frac{1}{1+sP_{\mathrm{PB}}\mu}\right]r\mathrm{d}r} e^{-2\pi\lambda_{\mathrm{PB}}\int\limits_1^\infty\left[1-\frac{1}{1+sP_{\mathrm{PB}}\mu r^{-\eta}}\right]r\mathrm{d}r} \\
&\overset{(c)}{=} e^{-\pi\lambda_{\mathrm{PB}}\frac{sP_{\mathrm{PB}}\mu}{1+sP_{\mathrm{PB}}\mu}} e^{-\pi\lambda_{\mathrm{PB}}\mathcal{F}(sP_{\mathrm{PB}}\mu,\eta)}
\end{aligned} \tag{2.51}$$

where (a) follows from the independence of the small-scale fading gain $\{H_k\}_k$ across the PB-EH links, and by further conditioning on the locations of the PB nodes. Equality (b) is obtained by accounting for the bounded path loss model while invoking the probability generating functional (PGFL) of the PPP Φ_{PB} [63]. Finally, (c) results by expressing the integrals in terms of the hypergeometric function as defined in (2.26).

Proof of Lemma 3

The proof follows by noting that $\mathbb{E}[H_k] = 1$, and by applying Campbell's theorem [63] to obtain $\mathbb{E}[Z] = P_{\text{PB}}\mu 2\pi\lambda_{\text{PB}}\left(\int_0^1 r\mathrm{d}r + \int_1^\infty r^{1-\eta}\mathrm{d}r\right) = P_{\text{PB}}\mu\lambda_{\text{PB}}\pi\frac{\eta}{\eta-2}$.

Achievable Rate

The ergodic achievable rate for the case of multiple power beacons can be derived following the procedure in Appendix A. I first adapt the upper bound on the energy outage probability in (2.39) to the case of multiple power beacons as

$$\Pr\left[\bigcup_{k=1}^{n}\left\{\sum_{\ell=1}^{k}X_\ell^2 \geq \sum_{i=1}^{m}Z_i\right\}\right] = \sum_{i=0}^{\frac{n}{2}-1}(-1)^i\frac{m^i}{(2a)^i i!}\frac{\mathrm{d}^i}{\mathrm{d}s^i}\mathcal{L}_Z(s)|_{s=\frac{m}{2a}} \leq \frac{\epsilon}{2+\epsilon}, \tag{2.52}$$

where I have used the expression (and the notation) from Proposition 21. I then condition on the interference I, and treat the communication link as an AWGN channel with SNR γ_I [70]. Following steps similar to (2.40)-(2.47), I can derive the achievable rate (conditioned on I) for the AWGN channel with SNR γ_I. The next step is to decondition with respect to I to recover the result in (2.34). To this end, I calculate $\mathbb{E}_I\left[\log\left(1+\gamma_I\right)\right]$ and $\mathbb{E}_I\left[\sqrt{\frac{\gamma_I}{1+\gamma_I}}\right]$ as follows.

$$\begin{aligned}\mathbb{E}_I\left[\log\left(1+\gamma_I\right)\right] &\overset{(a)}{=} \int_0^\tau \Pr\left[\log\left(1+\gamma_I\right) > t\right]\mathrm{d}t \\ &\overset{(b)}{=} \int_0^\tau \Pr\left[\gamma_I > e^t - 1\right]\mathrm{d}t \overset{(c)}{=} \int_0^\tau F_I\left(\frac{\zeta P_{\text{EH}}}{e^t-1} - \sigma^2\right)\mathrm{d}t\end{aligned} \tag{2.53}$$

where (a) follows by noting that $\log\left(1+\gamma_I\right)$ is a non-negative random variable with support in $[0,\tau]$, and $\tau = \log\left(1+\zeta\gamma\right)$ since the SINR $\gamma_I = \frac{\zeta P_{\text{EH}}}{\sigma^2+I}$ has support in

$[0, \zeta\gamma]$. By simple algebraic steps, I express the expectation in terms of the interference distribution as in (c). Similarly, I can express $\mathbb{E}_I\left[\sqrt{\frac{\gamma_I}{1+\gamma_I}}\right]$ in the form given in (2.36). This completes the proof of Theorem 30.

Chapter 3

Wireless-powered Communications with Millimeter Wave

In this chapter[1], I propose an analytical model for investigating the performance of wireless information and power transfer in the mmWave band. The proposed model incorporates the key features of mmWave systems such as directional antenna arrays and sensitivity to building blockages. The proposed research provides several system-level design guidelines.

3.1 Prior Work and Motivation

Millimeter wave communications is a key candidate technology for future 5G cellular networks. This is mainly due to the availability of large spectrum resources at higher frequencies, which leads to much higher data rates. Recent research suggests that mmWave systems will typically feature (i) large-dimensional antenna arrays with directional beamforming at the transmitter/receiver—which is motivated by the small wavelength that allows packing a large number of antenna elements into small form-factors; and (ii) a dense deployment of base stations (BSs) to ensure comparable cov-

[1]This chapter is based on my published work in [71] and [72]. This research was supervised by Prof. Robert W. Heath, Jr. The useful feedback from Dr. Ahmed Alkhateeb helped improve the quality of this research.

erage to ultra high frequency (UHF) networks [73,74]. These mmWave design features are also attractive for RF (radio frequency) energy harvesting where a harvesting device may extract energy from the incident RF signals [1,11,16]. This could potentially power the massive number of low-power wireless devices in future paradigms such as the Internet of Things [8]. The signal propagation at mmWave frequencies, however, suffers from poor penetration and diffraction characteristics, making it sensitive to blockage by buildings [74, 75]. It is, therefore, unclear if mmWave cellular networks will be more favorable for RF energy harvesting compared to the conventional (sub 6 GHz) frequencies. Further, the network level design principles for mmWave energy harvesting systems are not well understood. This motivates a network view of energy harvesting in a mmWave cellular network.

Stochastic geometry is a popular tool for analyzing a variety of setups ranging from ad hoc, to cognitive and cellular networks. It often leads to tractable analytical models that yield general performance insights, thus obviating the need of exhaustive simulations [63]. The performance of ad hoc networks has been characterized using metrics such as outage probability and transmission capacity [76–78]. Similar analysis has been applied to single and multi-tier cellular networks under different assumptions about cell association, scheduling and power control [78–80]. Multi-cell cooperation has been analyzed for different cooperation models in [81–84]. For example, random clustering with intercell interference nulling was considered in [81], and pairwise cooperation with limited channel knowledge was analyzed in [82]. Similarly, joint transmission without prior channel knowledge and/or tight synchronization has also been considered [83, 84].

I now briefly review the prior work investigating the performance of wireless information and power transfer in large-scale networks [26–32]. In [26], the performance of ambient RF energy harvesting was characterized using tools from stochastic geometry. Using a repulsive point process to model RF transmitters, it was shown that more repulsion helps improve the performance at an energy harvester for a given transmitter density. In [27, 28], cognitive radio networks were considered, and opportunistic wireless energy harvesting was proposed and analyzed. In [30], a hybrid cellular network architecture was proposed to enable wireless power transfer for mobiles. In particular, an uplink cellular network was overlaid with power beacons and trade-offs between transmit power and deployment densities were investigated under an outage constraint on the data links. A broadband wireless network with transmit beamforming was considered in [31], where optimal power control algorithms were devised for improving the throughput and power transfer efficiency. Simultaneous information and energy transfer in a relay-aided network was considered in [32]. Under a random relay selection strategy, the network-level performance was characterized in terms of the relay density and the relay selection area. In [29], relay selection in a wireless-powered cooperative network with energy storage was considered. None of the prior work, however, has investigated wireless information and power transfer in the mmWave band. Parallel to this contribution, wireless energy and information transfer in a mmWave network was also studied in [85]. With energy transfer in the downlink and data transfer in the uplink, [85] derived the average harvested power and the average achievable rate for the considered system.

In other related work, stochastic geometry has also been used for analyzing

general energy harvesting networks. Large-scale self-powered ad hoc networks were analyzed in [86] and [87]. In [86], the network model consisted of a large number of energy harvesting transmitters, where each transmitter has a dedicated receiver located a fixed distance away. Leveraging tools from stochastic geometry and random walk theory, spatial throughput was derived by optimizing over the transmission power. For a similar setup, the author in [87] derived the transmission capacity for a random access network by optimizing over the medium access probability. Self-powered heterogeneous cellular networks were treated in [88]. In [88], base-station availability (i.e., the fraction of the time it can remain ON) was analytically characterized using tools from random walk theory and stochastic geometry. In [89], a power-availability aware user association policy was proposed for a cellular network with energy harvesting base-stations (see [90] and references therein for a stochastic geometry-based analysis of wireless information and power transfer in heterogeneous cellular networks). The work in [86–88], however, does not consider any node cooperation or joint transmission at the physical layer. In [91, 92], the performance of a large-scale wireless network with energy harvesting transmitters was characterized while assuming cooperative transmission. It was shown that node cooperation helps improve the system performance in certain scenarios.

3.2 Contributions

I propose a stochastic-geometry based framework to characterize the performance of wireless energy and/or information transfer aided by a large-scale mmWave cellular network. The developed model helps evaluate the performance for practi-

cal scenarios where the energy harvesters may or may not be visible to the cellular network. It also captures the key features of mmWave systems such as directional antenna arrays and sensitivity to building blockages. The main contributions are summarized as follows.

- Tractable analytical expressions are derived for metrics such as the energy coverage probability and the average harvested power at mmWave energy harvesting receivers.
- The analysis is extended to characterize the overall energy-and-information coverage probability for the general case where receivers extract both energy and information from the mmWave signals.
- A switch-based low-power receiver architecture is proposed for mmWave simultaneous information and energy transfer.

The work in this chapter differs from the prior work in that I investigate wireless energy and information transfer in a large-scale *mmWave* cellular network. Due to different physical characteristics and design features at mmWave, prior work on energy/information transfer in lower frequency networks does not directly apply to mmWave networks. In another line of work, the performance of mmWave cellular networks in terms of signal-to-interference-and-noise ratio (SINR) coverage and rate has also been analyzed using stochastic geometry [93, 94]. None of this work on mmWave networks, however, provides a performance characterization from the perspective of wireless energy and information transfer.

The rest of the chapter is organized as follows. In Section 3.3, I introduce the system model. Section 3.4 presents the analytical results for mmWave energy transfer. The case with simultaneous information and energy transfer is treated in Section 3.5. I conclude the paper in Section 3.6.

3.3 System Model

In this section, I introduce the network and channel models, followed by a description of the antenna model. The parameters defined in this section are summarized in Table 3.1.

3.3.1 Network Model

I consider a large-scale cellular network consisting of mmWave BSs and a population of wireless-powered devices (or users) that operate by extracting energy and/or information in the mmWave band. The mmWave BSs are located according to a homogeneous Poisson point process (PPP) $\Phi(\lambda)$ of density λ. The user population is drawn from another homogeneous PPP $\Phi_u(\lambda_u)$ of density λ_u, independently of Φ. In general, mmWave BSs and users may be located outdoors or indoors. Empirical evidence suggests that mmWave signals exhibit high penetration losses for many common building materials [75, 93]. Assuming the building blockages to be impenetrable, I focus on the case where the BSs and users are located outdoors. A BS-user link is line-of-sight (LOS) or non-line-of-sight (NLOS) depending on whether or not it is intersected by a building blockage. Channel measurement campaigns have reported markedly different propagation characteristics for LOS/NLOS links [73, 75]. To model

blockage due to buildings, I leverage the results in [95] where the buildings are drawn from a boolean stochastic point process. I define a line-of-sight (LOS) probability function $p(r) = e^{-\beta r}$ for a link of length r, where β is a constant that depends on the geometry and density of the building blockage process: a BS-receiver link of length r is declared LOS with a probability $p(r)$, independently of other links. While conducting stochastic geometry analysis, I will apply this result to split the BS PPP into two independent but non-homogeneous PPPs consisting of LOS and NLOS BSs.

I allow the user population to consist of two types of users, namely *connected* and *nonconnected*. A connected user is assumed to be tagged with the BS, either LOS or NLOS, that maximizes the average received power at that user. Moreover, for the connected case, I assume perfect beam alignment between a BS and its tagged user, i.e., the BS and user point their beams so as to have the maximum directivity gain. Further, I assume that a BS serves only one connected user at a given time. For a nonconnected user, I do not assume any prior beam alignment with a BS, i.e., it is not tagged with any BS. This allows us to model a wide range of scenarios. For instance, due to limited resources, the mmWave network may (directly) serve only a fraction of the user population as connected users, leaving the rest in the nonconnected mode. Another interpretation could be that due to the challenges associated with channel acquisition, not all the users could be simultaneously served in the connected mode. I let ϵ be the probability that a randomly selected node is a connected user, independently of other nodes. With this assumption, I can thin the user PPP Φ_u into two independent PPPs $\Phi_{u,\text{con}}$ and $\Phi_{u,\text{ncon}}$, with respective densities $\epsilon\lambda_u$ and $(1-\epsilon)\lambda_u$. Note that an arbitrary user, either connected or nonconnected, may

experience an energy outage if the received power falls short of a required threshold ψ. This threshold would depend on the power consumption requirements of the receiver. To capture the sensitivity requirements of the harvesting circuit, I define $\psi_{\min}$ to be the harvester activation threshold, i.e., the minimum received energy needed to activate the harvesting circuit (the energy outage threshold ψ would typically be greater than $\psi_{\min}$). I use ξ to denote the rectifier efficiency. I define $\mathrm{P}_{\mathrm{con}}(\lambda, \psi_{\mathrm{con}})$ to be the energy coverage probability given an outage threshold ψ_{con} for a connected user, while $\mathrm{P}_{\mathrm{ncon}}(\lambda, \psi_{\mathrm{ncon}})$ denotes the same for the nonconnected case. With these definitions, I can define the overall energy coverage probability $\Lambda(\epsilon, \lambda, \psi_{\mathrm{con}}, \psi_{\mathrm{ncon}})$ of the network as

$$\Lambda(\epsilon, \lambda, \psi_{\mathrm{con}}, \psi_{\mathrm{ncon}}) = \epsilon \mathrm{P}_{\mathrm{con}}(\lambda, \psi_{\mathrm{con}}) + (1-\epsilon)\mathrm{P}_{\mathrm{ncon}}(\lambda, \psi_{\mathrm{ncon}}) \tag{3.1}$$

where the energy coverage probability is a function of several parameters such as the BS density, the channel propagation parameters, as well as the antenna beam patterns at the transmitter/receiver. For cleaner exposition, I drop the subscript in ψ_{con} or ψ_{ncon}, using the notation $\Lambda(\epsilon, \lambda, \psi)$ when the context is clear. In Section 3.4.1, I provide analytical expressions to compute the energy coverage probability in a mmWave network.

3.3.2 Channel Model

I now describe the channel model for an arbitrary user without losing generality. Empirical evidence suggests that mmWave frequencies exhibit different propagation characteristics for the LOS/NLOS links [75]. While the LOS mmWave signals propagate as if in free space, the NLOS mmWave signals typically exhibit a higher

path loss exponent (and additional shadowing) [75]. I let α_{L} and α_{N} be the path loss exponents for the LOS and NLOS links respectively. I define the distance-dependent path loss for a user located a distance r_ℓ from the ℓ-th BS: $g_\ell(r_\ell) = C_{\mathrm{L}} r_\ell^{-\alpha_{\mathrm{L}}}$ when the link is LOS, where the constant C_{L} is the path loss intercept; and $g_\ell(r_\ell) = C_{\mathrm{N}} r_\ell^{-\alpha_{\mathrm{N}}}$ for the NLOS case. Note that by including blockages in the network model (Section 3.3.1), I capture the distance-dependent signal attenuation due to buildings. To simplify the analysis, I do not include additional forms of shadowing in the considered model. I further define h_ℓ to be the small-scale fading coefficient corresponding to a BS $\ell \in \Phi$. Assuming independent Nakagami fading for each link, the small-scale fading power $H_\ell = |h_\ell|^2$ can be modeled as a normalized Gamma random variable, i.e., $H_\ell \sim \Gamma(N_{\mathrm{L}}, 1/N_{\mathrm{L}})$ when the link is LOS and $H_\ell \sim \Gamma(N_{\mathrm{N}}, 1/N_{\mathrm{N}})$ for the NLOS case, where the fading parameters N_{L} and N_{N} are assumed to be integers for simplicity.

3.3.3 Antenna Model

To compensate for higher propagation losses, mmWave BSs will use large directional antennas arrays. I assume that the BSs and users are equipped with N_{t} and N_{r} antenna elements each. To simplify the analysis while capturing the key antenna characteristics, I use the sectored antenna model of Fig. 3.1 (except for Section IV), similar to the one considered in [93, 96]. I use $A_{M,m,\theta,\bar{\theta}}(\phi)$ to characterize the antenna beam pattern, where ϕ gives the angle from the boresight direction, M denotes the directivity gain and θ the half power beamwidth for the main lobe, while m and $\bar{\theta}$ give the corresponding parameters for the side lobe. With this notation, $A_{M_{\mathrm{t}},m_{\mathrm{t}},\theta_{\mathrm{t}},\bar{\theta}_{\mathrm{t}}}(\cdot)$ denotes the antenna beam pattern at an arbitrary BS in Φ, and

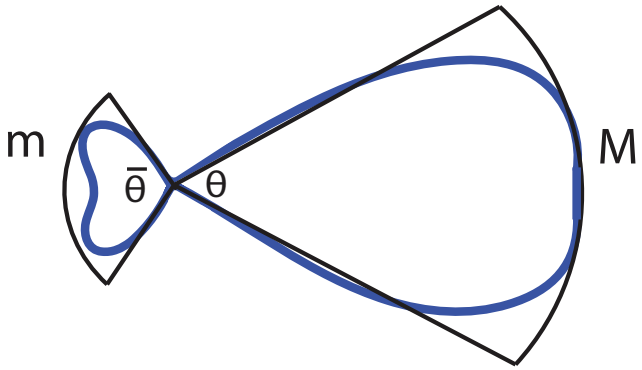

Figure 3.1: Sectored antenna model. The antenna beam pattern is parameterized by the directivity gains for the main lobe (M) and side lobe (m), and the half power beamwidths for the main lobe (θ) and side lobe ($\bar{\theta}$).

$A_{M_\mathrm{r},m_\mathrm{r},\theta_\mathrm{r},\bar{\theta}_\mathrm{r}}(\cdot)$ denotes the same for an energy harvesting user in Φ_u. I further define $\delta_\ell = A_{M_\mathrm{t},m_\mathrm{t},\theta_\mathrm{t},\bar{\theta}_\mathrm{t}}(\phi_\mathrm{t}^\ell)A_{M_\mathrm{r},m_\mathrm{r},\theta_\mathrm{r},\bar{\theta}_\mathrm{r}}(\phi_\mathrm{r}^\ell)$, the total directivity gain for the link between the ℓ-th BS and the typical user; ϕ_t^ℓ and ϕ_r^ℓ give the angle-of-arrival and angle-of-departure of the signal.

Without any further assumptions about the beam alignment between a user and its BS, I model the directivity gain δ_ℓ as a random variable. I assume the angles ϕ_t^ℓ and ϕ_r^ℓ are uniformly distributed in $[0, 2\pi)$. Due to the sectored antenna model, the random variable $\delta_\ell = D_i$ with a probability p_i ($i \in \{1,2,3,4,5\}$), where $D_i \in \{M_\mathrm{t}M_\mathrm{r}, M_\mathrm{t}m_\mathrm{r}, m_\mathrm{t}M_\mathrm{r}, m_\mathrm{t}m_\mathrm{r}, 0\}$ with corresponding probabilities $p_i \in \{q_\mathrm{t}q_\mathrm{r}, q_\mathrm{t}\bar{q}_\mathrm{r}, \bar{q}_\mathrm{t}q_\mathrm{r}, \bar{q}_\mathrm{t}\bar{q}_\mathrm{r}, q_o\}$; the constants $q_\mathrm{t} = \frac{\theta_t}{2\pi}$, $\bar{q}_\mathrm{t} = \frac{\bar{\theta}_t}{2\pi}$, $q_\mathrm{r} = \frac{\theta_r}{2\pi}$, $\bar{q}_\mathrm{r} = \frac{\bar{\theta}_r}{2\pi}$, and $q_o = 2 - q_\mathrm{t} - \bar{q}_\mathrm{t} - q_\mathrm{r} - \bar{q}_\mathrm{r}$. Note that $D_5 = 0$ models the extreme case where the BS and user beams have no alignment at all. Note that for the connected mode, since I assume perfect beam alignment between the typical user and its serving BS (hereby denoted by subscript

0), the directivity gain $\delta_0 = M_{\mathrm{t}} M_{\mathrm{r}}$ due to the sectored antenna model.

3.4 MmWave with Energy Harvesting

In this section, I assume that each user is equipped with an energy harvesting circuit, and attempts to extract energy from the incident mmWave signals. No decoding of information is considered in this section. The case with simultaneous information and power transfer is treated in Section 3.5. I first provide analytical expressions to evaluate the energy coverage probabilities for both connected and non-connected users. I then validate the analytical model, and conclude the section by providing network level design insights.

3.4.1 Stochastic Geometry Analysis

I first provide some lemmas before stating the main analytical results for this section.

Lemma 32 (Modified from [95, Theorem 8]) The probability density function (PDF) of the distance from an energy harvesting user to its nearest LOS BS, given that the user observes at least one LOS BS, is given by $\tau_{\mathrm{L}}(x) = 2\pi\lambda {B_{\mathrm{L}}}^{-1} x p(x) e^{-2\pi\lambda \int_0^x v p(v) \mathrm{d}v}$, where $x > 0$ and $B_{\mathrm{L}} = 1 - e^{-2\pi\lambda \int_0^\infty v p(v) \mathrm{d}v}$ is the probability that the receiver observes at least one LOS BS. Similarly, the distance distribution of the link between the user and its nearest NLOS BS, given that the user observes at least one NLOS BS, is given by $\tau_{\mathrm{N}}(x) = 2\pi\lambda {B_{\mathrm{N}}}^{-1} x (1 - p(x)) e^{-2\pi\lambda \int_0^x v(1-p(v)) \mathrm{d}v}$, where $x > 0$ and $B_{\mathrm{N}} = 1 - e^{-2\pi\lambda \int_0^\infty v(1-p(v)) \mathrm{d}v}$ is the probability that the user observes at least one NLOS BS.

Table 3.1: Model Parameters

Notation	**Description**
N_{t}, N_{r}	Antenna array size at the transmitter (t) and receiver (r)
M_{t}, M_{r}	Main lobe directivity gain
m_{t}, m_{r}	Side lobe directivity gain
θ_{t}, θ_{r}	Main lobe half power beamwidth
$\bar{\theta}_{\mathrm{t}}$, $\bar{\theta}_{\mathrm{r}}$	Side lobe half power beamwidth
$\Phi(\lambda)$	BS PPP with density λ
$\Phi_u(\lambda_u)$	User PPP with density λ_u
ϵ	Fraction of connected users
ψ	Energy outage threshold
$\psi_{\min}$	Harvester activation threshold
ξ	Rectifier efficiency
$\Lambda(\epsilon, \lambda, \psi)$	Energy coverage probability
$p(r)$	LOS probability function
β	Building blockage parameter
α_{L}, α_{N}	LOS/NLOS path loss exponents
C_{L}, C_{N}	LOS/NLOS path loss intercepts
N_{L}, N_{N}	LOS/NLOS fading parameters
P_{t}	Transmit power of BSs in Φ

Lemma 33 (Modified from [93, Lemma 2]) Let ϱ_{L} and ϱ_{N} denote the probability that the energy harvesting user is connected to a LOS and a NLOS BS respectively, then ϱ_{L} is given by $\varrho_{\mathrm{L}} = B_{\mathrm{L}} \int_0^{\infty} e^{-2\pi\lambda \int_0^{\rho_{\mathrm{L}}(x)} (1-p(v))v\mathrm{d}v} \tau_{\mathrm{L}}(x)\,\mathrm{d}x$, where $\rho_{\mathrm{L}}(x) = \left(\frac{C_{\mathrm{N}}}{C_{\mathrm{L}}}\right)^{\frac{1}{\alpha_{\mathrm{N}}}} x^{\frac{\alpha_{\mathrm{L}}}{\alpha_{\mathrm{N}}}}$ and $\varrho_{\mathrm{N}} = 1 - \varrho_{\mathrm{L}}$.

Lemma 34 (Modified from [93, Lemma 3]) Given that the energy harvesting user is connected to a LOS mmWave BS, the PDF of the link distance is given by the expression $\tilde{\tau}_{\mathrm{L}}(x) = \frac{B_{\mathrm{L}}\tau_{\mathrm{L}}(x)}{\varrho_{\mathrm{L}}} e^{-2\pi\lambda \int_0^{\rho_{\mathrm{L}}(x)} (1-p(v))v\mathrm{d}v}$, where $x > 0$. Given that the user is connected to a NLOS mmWave BS, the PDF of the link distance is given by $\tilde{\tau}_{\mathrm{N}}(x) = \frac{B_{\mathrm{N}}\tau_{\mathrm{N}}(x)}{\varrho_{\mathrm{N}}} e^{-2\pi\lambda \int_0^{\rho_{\mathrm{N}}(x)} p(v)v\mathrm{d}v}$ for $x > 0$ and $\rho_{\mathrm{N}}(x) = \left(\frac{C_{\mathrm{L}}}{C_{\mathrm{N}}}\right)^{\frac{1}{\alpha_{\mathrm{L}}}} x^{\frac{\alpha_{\mathrm{N}}}{\alpha_{\mathrm{L}}}}$.

Leveraging Slivnyak's theorem [63], I conduct the analysis at a typical energy harvesting user located at the origin without losing generality. I let P_{t} be the BS transmit power, and $Y = \sum_{\ell \in \Phi(\lambda)} P_{\mathrm{t}} \delta_\ell H_\ell g_\ell(r_\ell)$ be the power received at the user. Recall that $\psi_{\min}$ denotes the harvester activation threshold defined in Section 3.3.1. The energy harvested at a typical receiver (in unit time) can be expressed as

$$\gamma = \xi Y \mathbb{1}_{\{Y > \psi_{\min}\}} \tag{3.2}$$

where $\xi \in (0, 1]$ is the rectifier efficiency. Note that I have neglected the noise term since it is extremely small relative to the aggregate received signal. The remaining parameters follow from Section 3.3. Recall that given a BS $\ell \in \Phi(\lambda)$, the corresponding fading parameters will be distinct depending on whether the link is LOS or NLOS, which in turn depends on the LOS probability function (Section 3.3.1). Further note that for the connected case, it follows from Section 3.3.3 that $\delta_0 = M_{\mathrm{t}} M_{\mathrm{r}}$ for the link from the serving BS (denoted by subscript 0).

Connected case

The following theorem provides an analytical expression for the energy coverage probability $\mathrm{P}_{\mathrm{con}}(\lambda, \psi) = \Pr\{\gamma > \psi\}$ at a connected user, where the random variable γ is given in (3.2), and ψ is the energy outage threshold. Note that $\mathrm{P}_{\mathrm{con}}(\lambda, \psi)$ can also be interpreted as the complementary cumulative distribution function (CCDF) of the harvested energy.

Theorem 35 In a mmWave network with density λ, the energy coverage probability $\mathrm{P}_{\mathrm{con}}(\lambda, \psi)$ for the connected case given an energy outage threshold ψ, can be evaluated as

$$\mathrm{P}_{\mathrm{con}}(\lambda, \psi) = \mathrm{P}_{\mathrm{con,L}}\left(\lambda, \hat{\psi}\right) \varrho_{\mathrm{L}} + \mathrm{P}_{\mathrm{con,N}}\left(\lambda, \hat{\psi}\right) \varrho_{\mathrm{N}}, \tag{3.3}$$

where $\hat{\psi} = \max\left(\frac{\psi}{\xi}, \psi_{\min}\right)$, $\varrho_{\mathrm{L}} = 1 - \varrho_{\mathrm{N}}$ is given in Lemma 2, while $\mathrm{P}_{\mathrm{con,L}}(\cdot)$ and $\mathrm{P}_{\mathrm{con,N}}(\cdot)$ are the conditional energy coverage probabilities given the serving BS is LOS or NLOS. These terms can be tightly approximated as

$$\mathrm{P}_{\mathrm{con,L}}(\lambda, \psi) \approx \sum_{k=0}^{N} (-1)^k \binom{N}{k} \times \int_{r_g}^{\infty} \zeta_k^{\mathrm{L}}(r) e^{-\Upsilon_{k,1}(\lambda,\psi,r) - \Upsilon_{k,2}(\lambda,\psi,\rho_{\mathrm{L}}(r))} \tilde{\tau}_{\mathrm{L}}(r)\, \mathrm{d}r, \tag{3.4}$$

where $\zeta_k^{\mathrm{L}}(x) = \left(1 + \frac{akP_{\mathrm{t}}M_{\mathrm{t}}M_{\mathrm{r}}C_{\mathrm{L}}}{\psi N_{\mathrm{L}} x^{\alpha_{\mathrm{L}}}}\right)^{-N_{\mathrm{L}}}$, the approximation constant $a = N(N!)^{-\frac{1}{N}}$ where N denotes the number of terms in the approximation, while r_g defines the minimum link distance and is included to avoid unbounded path loss at the receiver. Similarly,

$$\mathrm{P}_{\mathrm{con,N}}(\lambda, \psi) \approx \sum_{k=0}^{N} (-1)^k \binom{N}{k} \times$$

$$\int_{r_g}^{\infty} \zeta_k^{\mathrm{N}}(r) e^{-\Upsilon_{k,1}(\lambda,\psi,\rho_{\mathrm{N}}(r))-\Upsilon_{k,2}(\lambda,\psi,r)} \tilde{\tau}_{\mathrm{N}}(r)\,\mathrm{d}r, \tag{3.5}$$

where $\zeta_k^{\mathrm{N}}(x) = \left(1+\frac{akP_{\mathrm{t}}M_{\mathrm{t}}M_{\mathrm{r}}C_{\mathrm{N}}}{\psi N_{\mathrm{N}} x^{\alpha_{\mathrm{N}}}}\right)^{-N_{\mathrm{N}}}$,

$$\Upsilon_{k,1}(\lambda,\psi,x) = 2\pi\lambda \sum_{i=1}^{4} p_i \int_{x}^{\infty} \left(1-\left[1+\frac{aP_{\mathrm{t}}kD_iC_{\mathrm{L}}}{\psi N_{\mathrm{L}} t^{\alpha_{\mathrm{L}}}}\right]^{-N_{\mathrm{L}}}\right) \times p(t) t \mathrm{d}t, \tag{3.6}$$

$$\Upsilon_{k,2}(\lambda,\psi,x) = 2\pi\lambda \sum_{i=1}^{4} p_i \int_{x}^{\infty} \left(1-\left[1+\frac{aP_{\mathrm{t}}kD_iC_{\mathrm{N}}}{\psi N_{\mathrm{N}} t^{\alpha_{\mathrm{N}}}}\right]^{-N_{\mathrm{N}}}\right) \times (1-p(t))\, t \mathrm{d}t, \tag{3.7}$$

and the distance distributions $\tilde{\tau}_{\mathrm{L}}(\cdot)$ and $\tilde{\tau}_{\mathrm{N}}(\cdot)$ follow from Lemma 3.

Proof: See Appendix A. □

Recall that $p(t) = e^{-\beta t}$ is the LOS probability function defined in Section 3.3.1, and captures the effect of building blockages. In (3.4), the term $\zeta_k^{\mathrm{L}}(\cdot)$ models the contribution from the LOS serving link, $\Upsilon_{k,1}(\cdot)$ accounts for the other LOS links, and $\Upsilon_{k,2}(\cdot)$ captures the effect of the NLOS links. Note that the ith term in (3.6), (3.7) corresponds to the contributions from the BS-user links having directivity gain D_i. Similarly, $\zeta_k^{\mathrm{N}}(\cdot)$ in (3.5) models the case where the serving BS is NLOS. Note that these terms further depend on the channel propagation conditions (α_{L}, α_{N}, N_{L}, N_{N}, C_{L}, C_{N}), the network density λ as well as the antenna geometry parameters (via D_i, p_i), which are summarized in Table 3.1. Furthermore, the outage threshold ψ

will depend on the power requirements at a particular user, and would typically be greater than the sensitivity of the harvesting circuit (i.e., $\psi \geq \psi_{\min}$ such that $\hat{\psi} = \frac{\psi}{\xi}$). Though the expressions in Theorem 1 can be evaluated using numerical tools, this could be tedious due to the presence of multiple integrals. To address this, I simplify the analysis by approximating the LOS probability function with a step function, and by further ignoring the small-scale fading. This result in a much simpler expression for the energy coverage probability.

Proposition 36 Let $R_B = \left(\frac{-\ln(1-\varrho_{\mathrm{L}})}{\lambda\pi}\right)^{0.5}$, $\tilde{a} = \lambda\pi R_B^2 e^{-\lambda\pi R_B^2}$, and $W_{ik} = \frac{akD_i P_{\mathrm{t}} C_{\mathrm{L}}}{\hat{\psi}}$ for $i \in \{1,2,3,4\}$, $k \in \{0,1,\cdots,N\}$. The energy coverage probability can be further approximated as

$$P_{\mathrm{con}}(\lambda,\psi) \approx \tilde{a}\sum_{k=0}^{N}(-1)^k\binom{N}{k}\int_{\left(\frac{r_g}{R_B}\right)^2}^{1}\zeta_k^{\mathrm{L}}\left(t^{\frac{1}{2}}R_B\right)\times$$
$$\prod_{i=1}^{4}e^{-\frac{2\pi\lambda}{\alpha_{\mathrm{L}}}p_i W_{ik}^{\frac{2}{\alpha_{\mathrm{L}}}}\Gamma\left(-\frac{2}{\alpha_{\mathrm{L}}};W_{ik}\left(t^{\frac{1}{2}}R_B\right)^{-\alpha_{\mathrm{L}}},W_{ik}R_B^{-\alpha_{\mathrm{L}}}\right)}\mathrm{d}t, \tag{3.8}$$

where $\Gamma(h;u,v) = \int_u^v x^{h-1}e^{-x}\mathrm{d}x$ is the generalized incomplete Gamma function.

Proof: See Appendix B. □

I note that Proposition 1 is relatively efficient to compute as it involves integration over a finite interval only, and because Gamma function can be readily evaluated using most numerical tools. I also observe that the coverage is mainly influenced by the LOS BSs. For example, a key term in (3.8) is $\lambda\pi R_B^2$ which represents the average number of LOS BSs seen by the user. I now provide analytical expressions for the average harvested power at a connected user.

Proposition 37 The average harvested power for the connected case $\bar{P}_{\text{con}}(\lambda, \psi)$ for an energy outage threshold $\psi \in [\psi_{\min}, \infty)$ is given by $\bar{P}_{\text{con}}(\lambda, \psi) = \int_{\psi}^{\infty} P_{\text{con}}(\lambda, x)\, \mathrm{d}x + \psi P_{\text{con}}(\lambda, \psi)$.

Proof: The proof follows by noting that γ has nonnegative support, and by treating $P_{\text{con}}(\cdot, \cdot)$ as the CCDF of γ. □

Here, $P_{\text{con}}(\cdot, \cdot)$ follows from Theorem 1 or Proposition 1. $\bar{P}_{\text{con}}(\lambda, \psi)$ can be interpreted as the *useful* average harvested power. This is because only those incident signals that meet the activation threshold can be harvested. To get further insights, I now analyze the limiting case $\psi \to 0$ of Proposition 2. This provides an upper bound on the average harvested power.

Corollary 38 The average harvested power for the limiting case $\lim_{\psi \to 0} \bar{P}_{\text{con}}(\lambda, \psi) = \bar{P}_{\text{con}}(\lambda, 0) = \xi \left(\varrho_{\text{L}} \bar{P}_{\text{L}} + \varrho_{\text{N}} \bar{P}_{\text{N}} \right)$, where

$$\bar{P}_{\text{L}} = \int_{r_g}^{\infty} \left(P_{\text{t}} M_{\text{t}} M_{\text{r}} C_{\text{L}} r^{-\alpha_{\text{L}}} + \Psi_{\text{L}}(r) + \Psi_{\text{N}}(\rho_{\text{L}}(r)) \right) \tilde{\tau}_{\text{L}}(r)\, \mathrm{d}r, \tag{3.9}$$

$$\bar{P}_{\text{N}} = \int_{r_g}^{\infty} \left(P_{\text{t}} M_{\text{t}} M_{\text{r}} C_{\text{N}} r^{-\alpha_{\text{N}}} + \Psi_{\text{L}}(\rho_{\text{N}}(r)) + \Psi_{\text{N}}(r) \right) \tilde{\tau}_{\text{N}}(r)\, \mathrm{d}r, \tag{3.10}$$

$$\Psi_{\text{L}}(x) = \kappa C_{\text{L}} \sum_{i=1}^{4} D_i p_i \int_{x}^{\infty} t^{-(\alpha_{\text{L}}-1)} p(t) \mathrm{d}t, \tag{3.11}$$

$$\Psi_{\mathrm{N}}(x) = \kappa C_{\mathrm{N}} \sum_{i=1}^{4} D_i p_i \left(\frac{x^{-(\alpha_{\mathrm{N}}-2)}}{\alpha_{\mathrm{N}}-2} - \int_x^{\infty} t^{-(\alpha_{\mathrm{N}}-1)} p(t) \mathrm{d}t \right), \tag{3.12}$$

and $\kappa = 2\pi\lambda P_{\mathrm{t}}$.

Proof: See Appendix C. □

$\bar{P}_{\mathrm{L}}$ and $\bar{P}_{\mathrm{N}}$ denote the average harvested power given the user is tagged to an LOS or an NLOS BS. Note that the average harvested power is independent of the small-scale fading parameters. To reveal further insights, I provide the following approximation for the average harvested power (which is validated in Section 3.4.2).

Corollary 39 The average harvested power for the limiting case, $\bar{P}_{\mathrm{con}}(\lambda, 0)$, can be further approximated as

$$\begin{aligned} \bar{P}_{\mathrm{con}}(\lambda, 0) &\overset{(a)}{\approx} \kappa M_{\mathrm{t}} M_{\mathrm{r}} C_L \int_{r_g}^{R_B} \frac{e^{-\lambda\pi t^2}}{t^{\alpha_{\mathrm{L}}-1}} \mathrm{d}t \\ &= \frac{\Gamma\left(1-0.5\alpha_{\mathrm{L}}; \lambda\pi r_g^2, \infty\right) - \Gamma\left(1-0.5\alpha_{\mathrm{L}}; \lambda\pi R_B^2, \infty\right)}{2\left(\kappa M_{\mathrm{t}} M_{\mathrm{r}} C_L\right)^{-1} (\lambda\pi)^{1-0.5\alpha_{\mathrm{L}}}}. \end{aligned} \tag{3.13}$$

Proof: The proof follows by using the simplifying assumptions of Appendix B, and by further ignoring the contributions from all but the serving LOS BS. □

This approximation suggests that the average harvested power is mainly determined by the LOS serving link. Note that $\bar{P}_{\mathrm{con}}(\cdot,\cdot)$ grows linearly with the transmit power P_{t} since $\kappa = 2\pi\lambda P_{\mathrm{t}}$. Depending on the path loss exponent α_{L}, it may exhibit a sublinear to approximately-linear scaling with the BS density λ. When α_{L} is large,

the denominator $t^{\alpha_{\mathrm{L}}-1}$ in (a) overshadows the impact of λ on the numerator $e^{-\pi\lambda t^2}$. Therefore, the scaling behavior is essentially determined by $\kappa = 2\pi\lambda P_{\mathrm{t}}$, which is linear in λ. This suggests that increasing the transmit power or BS density has almost the same effect on the average harvested power when α_{L} is large (e.g., when $\alpha_{\mathrm{L}} = 3$). Also note that (3.13) is relatively simple as it is expressed in terms of the incomplete Gamma function only.

Nonconnected case

Having discussed the connected case, I now consider the case where a user operates in the nonconnected mode. The following theorem characterizes the energy coverage probability at a typical user for the nonconnected case.

Theorem 40 In a mmWave network of density λ, the energy coverage probability for the nonconnected case $\mathrm{P}_{\mathrm{ncon}}(\lambda, \psi)$ given an outage threshold ψ can be evaluated using

$$\mathrm{P}_{\mathrm{ncon}}(\lambda, \psi) \approx \sum_{k=0}^{N} (-1)^k \binom{N}{k} e^{-\Upsilon_{k,1}\left(\lambda,\hat{\psi},r_g\right)-\Upsilon_{k,2}\left(\lambda,\hat{\psi},r_g\right)}, \tag{3.14}$$

where $\Upsilon_{k,1}(\cdot)$ and $\Upsilon_{k,2}(\cdot)$ are given by (3.6) and (3.7) respectively, $\hat{\psi} = \max\left(\frac{\psi}{\xi}, \psi_{\min}\right)$, and r_g is the minimum link distance.

Proof: The proof follows from that of Theorem 35. □

Similar to the connected case, the energy coverage probability for this case is also a function of the propagation conditions, the network density and the antenna geometry parameters. I note that the expressions in Theorem 2 are efficient to compute,

obviating the need for further simplification. I now consider the average harvested power for the nonconnected case.

Proposition 41 The average harvested power for the nonconnected case $\bar{P}_{\text{ncon}}(\lambda, \psi)$ for an energy outage threshold $\psi \in [\psi_{\min}, \infty)$ is given by $\bar{P}_{\text{ncon}}(\lambda, \psi) = \int_{\psi}^{\infty} P_{\text{ncon}}(\lambda, x)\, \mathrm{d}x + \psi P_{\text{ncon}}(\lambda, \psi)$.

Proof: The proof follows from that of Proposition 37. □

Corollary 42 The average harvested power for the limiting case $\lim_{\psi \to 0} \bar{P}_{\text{ncon}}(\lambda, \psi) = \bar{P}_{\text{ncon}}(\lambda, 0)$ is given by

$$\bar{P}_{\text{ncon}}(\lambda, 0) = \xi \left(\Psi_{\text{L}}(r_g) + \Psi_{\text{N}}(r_g) \right), \tag{3.15}$$

where $\Psi_{\text{L}}(\cdot)$ and $\Psi_{\text{N}}(\cdot)$ are given in (3.11) and (3.12) respectively.

Proof: The proof follows from that of Corollary 39. □

The average harvested power for the nonconnected case scales *linearly* with the transmit power and the BS density. This follows from (3.15) as both $\Psi_{\text{L}}(\cdot)$ and $\Psi_{\text{N}}(\cdot)$ relate linearly with the transmit power and density via the term $\kappa = 2\pi\lambda P_{\text{t}}$. This also suggests that increasing the transmit power or density has the same effect on the average harvested power. Note that this is different from the connected case where the path loss exponent affects how average harvested power scales with the BS density.

3.4.2 Results and Design Insights

I first verify the accuracy of the analytical expressions presented in Section 3.4.1 using simulations. I then study how key design parameters such as the antenna

beam pattern affects the energy coverage probability in purely connected ($\epsilon \to 1$) and nonconnected ($\epsilon \to 0$) networks. I also compare the performance of mmWave energy harvesting with lower frequency solutions. After developing key insights for purely connected/nonconnected scenarios, I provide energy coverage results for the general case ($0 < \epsilon < 1$), where the network serves both types of users.

Validation

In the following plots, the users are assumed to be equipped with a single omnidirectional receive antenna, the mmWave carrier frequency is set to 28 GHz, the blockage constant $\beta = 0.0071$ [93], and $\psi > \psi_{\min}$. In other words, for a given ψ, the plots are valid for any $\psi_{\min} < \psi$. Note that for the less relevant case when $\psi < \psi_{\min}$, the energy coverage probability flattens out, and is specified by $\mathrm{P}_{\mathrm{con}}(\lambda, \psi_{\min})$ or $\mathrm{P}_{\mathrm{ncon}}(\lambda, \psi_{\min})$. Without loss of generality, I set the rectifier efficiency $\xi = 1$ since this parameter does not impact the shape of the results, i.e., setting $\xi < 1$ results in shifting all the curves to the left by the same amount. I assume the rectifier efficiency to be the same when comparing mmWave and UHF. Note that there are no standard values for ξ since prior work has reported widely varying values [4, 97] depending on the device technology, operating frequency, etc. For example, [97, 98] suggest that a mmWave energy harvesting circuit may have better overall performance than its lower frequency counterparts. Fig. 3.4.2 and 3.4.2 plot the energy coverage probability for the connected case using different model parameters. The analytical results based on Theorem 1 are obtained using $N = 5$ terms in the approximation. The simulation results are generated using Monte Carlo simulations with 10,000 runs. Similarly,

using Theorem 2, Fig. 3.4.2 and 3.4.2 plot the energy coverage probability for the nonconnected case. There is a nice agreement between analytical and simulation results.

Connected case ($\epsilon \to 1$)

In Fig. 3.4.2, I plot the energy coverage probability with three distinct transmit beam patterns for a given network density. I observe that the energy harvesting performance improves with narrower beams, i.e., smaller beamwidths and larger directivity gains. As the beamwidth decreases, relatively fewer beams from the neighboring BSs would be incident on a typical user. But the beams that do reach, will have larger directivity gains, resulting in an overall performance improvement. This is possible due to the use of potentially large antenna arrays at the mmWave BSs. Note that this performance boost will possibly be limited due to the ensuing EIRP (equivalent isotropically radiated power) or other safety regulations on future mmWave systems [99].

For the purpose of comparison, I also plot the energy coverage probability for UHF energy harvesting under realistic assumptions. Given the current state-of-the-art [73, 100], the UHF BSs are assumed to have 8 transmit antennas each. Further, they are assumed to employ maximal ratio transmit beamforming to serve a connected user. For the channel model, I assume an IID Rayleigh fading environment and a path loss exponent of 3.6 (no blockage is considered). The network density is set to 25 nodes/km^2, which corresponds to an *average* distance of about 113 m to the closest UHF BS. The carrier frequency is set to 2.1 GHz and the transmission

bandwidth is 100 MHz. As can be seen from Fig. 3.4.2, mmWave energy harvesting could provide considerable performance gain over its lower frequency counterpart. Moreover, the anticipated dense deployments of mmWave networks would further widen this gap. This effect is illustrated in Fig. 3.4.2, where I plot the energy coverage probability for different mmWave network densities for a given transmit antenna beam pattern. In Fig. 3.4.2, I use Proposition 2 to plot the average harvested power at a typical mmWave user against the transmit array size. The plots based on Corollary 1 are also included. I note that the limiting case $\psi \to 0$ treated in Corollary 1 closely approximates the average harvested power obtained using Proposition 2. This figure also confirms the intuition that mmWave energy harvesting can benefit from (i) potentially large antenna arrays at the BSs, and (ii) high BS density, which would be the key ingredients of future mmWave cellular systems. Fig. 3.4.2 shows how the path loss exponent impacts the scaling behavior of the average harvested power with BS density, corroborating the discussion following Corollary 2.

Nonconnected case ($\epsilon \to 0$)

I now analyze the energy harvesting performance when the harvesting devices operate in the nonconnected mode. In a stark contrast to the connected case, Fig. 3.4.2 shows that for the nonconnected case, mmWave energy harvesting could benefit from using wider beams. This is because BS connectivity (alignment) is critical for the nonconnected case. With wider beams, it is more likely that a mmWave BS gets aligned with a receiver, albeit at the expense of the beamforming gain. Furthermore, a comparison with UHF energy harvesting shows that mmWave energy harvesting

gives a comparable performance to its UHF counterpart. Similarly, Fig. 3.4.2 plots the energy coverage probability for different deployment densities. I note that performance can be substantially improved with denser deployments, which would be a key feature of future mmWave cellular systems.

General case ($0 < \epsilon < 1$)

Having presented the energy coverage trends for the two extreme network scenarios, I now consider the general case where the user population consists of both connected and nonconnected users. I expect this to be the likely scenario for reasons explained in the network model (Section 3.3.1). As described in Section 3.3.3, an antenna beam pattern can be characterized by the half power beamwidth and directivity gain for both the main and side lobes. By tuning these parameters, the beam pattern can be particularized to a given antenna array. As an example, I assume that uniform linear arrays (ULA) are deployed at the mmWave BSs. I use the following relations to approximate the main and side lobe beamwidths as a function of the transmit array size: $\theta_{\mathrm{t}} \approx \frac{360}{\pi} \arcsin\left(\frac{0.892}{N_{\mathrm{t}}}\right)$ and $\bar{\theta}_{\mathrm{t}} \approx \frac{720}{\pi} \left|\arcsin\left(\frac{2}{N_{\mathrm{t}}}\right)\right|$ [101]. I use $M_{\mathrm{t}} = 10V \log\left(N_{\mathrm{t}}\right)$ and $m_{\mathrm{t}} = V\left(M_{\mathrm{t}} - 12\right)$ for the directivity gains of the main and side lobes [101]. To ensure the power normalization, the constant V is chosen to satisfy $\frac{\theta_{\mathrm{t}}}{2\pi} M_{\mathrm{t}} + \frac{\bar{\theta}_{\mathrm{t}}}{2\pi} m_{\mathrm{t}} = 1$.

In Fig. 3.5, I plot the overall energy coverage probability $\Lambda(\epsilon, \psi, \lambda)$ against transmit array size N_{t} for different values of parameter ϵ. I find that the optimal transmit array size depends on the statistics of the user population. For example, when ϵ is large, it is desirable to use large antenna arrays at the BSs. When ϵ is small, it is favorable to use small antenna arrays to improve the overall energy coverage

probability. Depending on the network load (or the user population *mix*) captured via ϵ, the energy coverage probability can be substantially improved by intelligent antenna switching schemes. Since the parameter ϵ would typically vary over large time-scales, such schemes would be practically feasible.

Having presented the energy coverage trends for mmWave energy harvesting, I now consider the scenario where the user attempts to extract both energy and information from the incident mmWave signals.

3.5 MmWave Simultaneous Information and Power Transfer

In this section, I consider the case where the energy harvesting device also attempts to decode information from the received signals, in what is known as simultaneous wireless information and power transfer (SWIPT) [1, 15]. I now assume that the energy harvesting receiver is also equipped with an information decoding circuit. I focus on the case where a given user is already aligned with its serving BS, i.e., $\epsilon = 1$ for this section. Further, I consider a power splitting receiver architecture [15] where the received signal is split using factors $\sqrt{\nu}$ and $\sqrt{1-\nu}$, $\nu \in [0, 1]$. A fraction $\sqrt{1-\nu}$ of received signal is available for energy harvesting, while the remaining signal is used for information decoding. With this notation, the signal-to-interference-plus-noise ratio (SINR) at a typical receiver can be expressed as $\text{SINR} = \frac{\nu S}{\nu(I+\sigma^2)+\sigma_c^2}$, where $S = P_{\text{t}} M_{\text{t}} M_{\text{r}} H_0 g_0(r_0)$ denotes the useful signal power and $I = \sum_{\ell>0, \ell \in \Phi(\lambda) \setminus \mathbb{B}(r_g)} P_{\text{t}} \delta_\ell H_\ell g_\ell(r_\ell)$ gives the aggregate interference power from the neighboring BSs. σ^2 is the thermal noise power before splitting, while σ_c^2 captures possible signal degradation after power splitting. Similarly,

$\gamma = (1-\nu)\,\xi\,(S+I+\sigma^2)\,\mathbb{1}_{\{S+I+\sigma^2>\psi_{\min}\}}$ denotes the received signal power fed to the energy harvester. Note that a user will be in outage if the harvested energy and/or the SINR fall below their respective thresholds. I now define $P_{\text{suc}}(\lambda, T, \psi, \nu) = \Pr[\text{SINR} > T, \gamma > \psi]$ to be the probability of successful reception given the SINR outage threshold T, the energy outage threshold ψ, and the power splitting ratio ν. Extending the results from the previous sections, I now provide an analytical expression to characterize the system performance with SWIPT.

3.5.1 Stochastic Geometry Analysis

Before stating the main result of this section, I first provide a lemma for the SINR coverage probability at a mmWave receiver [93].

Lemma 43 (Modified from [93, Theorem 1]) In a mmWave network of density λ, the SINR coverage probability $\mathrm{P}_{\text{cov}}(\lambda, T, \nu)$ at a SWIPT device, given an SINR outage threshold T and a power splitting ratio ν, is given by

$$\mathrm{P}_{\text{cov}}(\lambda, T, \nu) = \mathrm{P}_{\text{cov,L}}(\lambda, T, \nu)\,\varrho_{\text{L}} + \mathrm{P}_{\text{cov,N}}(\lambda, T, \nu)\,\varrho_{\text{N}}, \tag{3.16}$$

where $\varrho_{\text{L}} = 1 - \varrho_{\text{N}}$ is defined in Lemma 2, and $\mathrm{P}_{\text{cov,L}}(\cdot)$ gives the conditional SINR coverage probability given the device is served by a LOS BS, and can be approximated as

$$\begin{aligned}\mathrm{P}_{\text{cov,L}}(\lambda, T, \nu) \approx \sum_{k=1}^{N_{\text{L}}} (-1)^{k+1} \binom{N_{\text{L}}}{k} \int_{r_g}^{\infty} e^{-\frac{k c_{\text{L}} r^{\alpha_{\text{L}}} T\left(\sigma^2 + \nu^{-1}\sigma_c^2\right)}{P C_{\text{L}} M_{\text{t}} M_{\text{r}}}} \\ \times \quad e^{-\Delta_{k,1}(T,r) - \Delta_{k,2}(T,r)} \tilde{\tau}_{\text{L}}(r)\,\mathrm{d}r.\end{aligned} \tag{3.17}$$

Similarly, the conditional SINR coverage probability for the NLOS case $\mathrm{P}_{\mathrm{cov,N}}(\cdot)$ is given by

$$\mathrm{P}_{\mathrm{cov,N}}\left(\lambda,T,\nu\right)\approx\sum_{k=1}^{N_{\mathrm{N}}}\left(-1\right)^{k+1}\binom{N_{\mathrm{N}}}{k}\int_{r_g}^{\infty}e^{-\frac{kc_{\mathrm{N}}r^{\alpha_{\mathrm{N}}}T\left(\sigma^2+\nu^{-1}\sigma_c^2\right)}{PC_{\mathrm{N}}M_{\mathrm{t}}M_{\mathrm{r}}}}$$
$$\times\quad e^{-\Delta_{k,3}(T,r)-\Delta_{k,4}(T,r)}\tilde{\tau}_{\mathrm{N}}\left(r\right)\mathrm{d}r, \tag{3.18}$$

where

$$\Delta_{k,1}\left(T,x\right)=2\pi\lambda\sum_{i=1}^{4}p_i\int_{x}^{\infty}\left(1-\left[1+\frac{c_{\mathrm{L}}k\tilde{D}_iTx^{\alpha_{\mathrm{L}}}}{N_{\mathrm{L}}t^{\alpha_{\mathrm{L}}}}\right]^{-N_{\mathrm{L}}}\right)$$
$$\times\,p(t)t\mathrm{d}t, \tag{3.19}$$

$$\Delta_{k,2}\left(T,x\right)=2\pi\lambda\sum_{i=1}^{4}p_i\int_{\rho_{\mathrm{L}}(x)}^{\infty}\left(1-\left[1+\frac{c_{\mathrm{L}}k\tilde{D}_iC_{\mathrm{N}}Tx^{\alpha_{\mathrm{L}}}}{N_{\mathrm{N}}C_{\mathrm{L}}t^{\alpha_{\mathrm{N}}}}\right]^{-N_{\mathrm{N}}}\right)$$
$$\times\left(1-p(t)\right)t\mathrm{d}t, \tag{3.20}$$

$$\Delta_{k,3}\left(T,x\right)=2\pi\lambda\sum_{i=1}^{4}p_i\int_{\rho_{\mathrm{N}}(x)}^{\infty}\left(1-\left[1+\frac{c_{\mathrm{N}}k\tilde{D}_iC_{\mathrm{L}}Tx^{\alpha_{\mathrm{N}}}}{N_{\mathrm{L}}C_{\mathrm{N}}t^{\alpha_{\mathrm{L}}}}\right]^{-N_{\mathrm{L}}}\right)$$
$$\times\,p(t)t\mathrm{d}t, \tag{3.21}$$

$$\Delta_{k,4}\left(T,x\right)=2\pi\lambda\sum_{i=1}^{4}p_i\int_{x}^{\infty}\left(1-\left[1+\frac{c_{\mathrm{N}}k\tilde{D}_iTx^{\alpha_{\mathrm{N}}}}{N_{\mathrm{N}}t^{\alpha_{\mathrm{N}}}}\right]^{-N_{\mathrm{N}}}\right)$$
$$\times\left(1-p(t)\right)t\mathrm{d}t, \tag{3.22}$$

$\tilde{D}_i=\frac{D_i}{M_{\mathrm{t}}M_{\mathrm{r}}}$ for $i\in\{1,2,3,4,5\}$, $c_{\mathrm{L}}=N_{\mathrm{L}}\left(N_{\mathrm{L}}!\right)^{-\frac{1}{N_{\mathrm{L}}}}$ and $c_{\mathrm{N}}=N_{\mathrm{N}}\left(N_{\mathrm{N}}!\right)^{-\frac{1}{N_{\mathrm{N}}}}$.

The following theorem provides the main analytical result of this section.

Theorem 44 In a mmWave network of density λ, the success probability $P_{\text{suc}}(\lambda, T, \psi, \nu)$ given the SINR outage threshold T, the energy outage threshold ψ, and the power splitting ratio ν is given by

$$P_{\text{suc}}(\lambda, T, \psi, \nu) \approx P_{\text{cov}}(\lambda, T, \nu)\, \tilde{P}_{\text{con}}(\lambda, \mu) + P_{\text{con}}(\lambda, \varphi) \left[1 - \tilde{P}_{\text{con}}(\lambda, \mu)\right], \tag{3.23}$$

where the SINR coverage probability $P_{\text{cov}}(\cdot)$ can be evaluated using the expressions in Lemma 43, while the energy coverage probability $P_{\text{con}}(\cdot)$ follows from Theorem 1. I further define $\tilde{P}_{\text{con}}(\lambda, \mu) = \tilde{P}_{\text{con,L}}(\lambda, \mu)\varrho_{\text{L}} + \tilde{P}_{\text{con,N}}(\lambda, \mu)\varrho_{\text{N}}$, where $\tilde{P}_{\text{con,L}}(\cdot)$ and $\tilde{P}_{\text{ncon,N}}(\cdot)$ are specified by (3.4) and (3.5) respectively, by setting $\zeta_k^{\text{L}}(\cdot) = \zeta_k^{\text{N}}(\cdot) = 1$. Moreover, μ and φ depend on several parameters including the power splitting ratio ν, the SINR outage threshold T, the energy outage threshold ψ, the harvester activation threshold $\psi_{\min}$, the rectifier efficiency ξ, and the noise parameters. Further, $\mu = \frac{\hat{\psi}}{(1-\nu)(1+T)} - \sigma^2 - \frac{\sigma_c^2}{\nu(1+\frac{1}{T})}$, $\varphi = \frac{\hat{\psi}}{(1-\nu)}$, and $\hat{\psi} = \max\left(\frac{\psi}{\xi}, \psi_{\min}\right)$.

Proof: See Appendix D. □

Note that $\tilde{P}_{\text{con}}(\lambda, \mu)$ in (3.23) is the interference CCDF evaluated at parameter μ. It plays a key role in determining the operating mode of the system. Though the interference is harmful for information decoding, it can be beneficial for energy harvesting. When the interference is high, the SINR coverage probability will typically limit the success probability. In the other extreme, the energy coverage probability will play

the limiting role. Also note that the success probability can be optimized over the design paramter ν, given other parameters. Moreover, I can recover Theorem 1 and Lemma 4 from (3.23) by letting $\psi \to 0$ and $T \to 0$, respectively.

Note that, in principle, the success probability at a connected mmWave energy harvesting or SWIPT device can be further improved by leveraging large antenna arrays at the receiver, thanks to smaller wavelengths. Though the considered analytical model allows the users to have receive antenna arrays, it implicitly assumes the presence of ideal RF combining circuitry consisting of power-hungry components such as phase shifters, multiple RF chains, etc. When large antenna arrays are used at the receiver, the power consumption due to additional antenna circuitry may get prohibitively high, overshadowing the array gains. As SWIPT typically targets low-power devices, I present a simple low-power receiver architecture in the next section. Note that the analytical results based on Theorem 3 can be interpreted as an upper bound on performance when the receiver consists of suboptimal components (as is the case in the following section).

3.5.2 Low-power Receiver Architecture

I now propose a novel architecture for a mmWave SWIPT receiver with multi-antenna array, as depicted in Fig. 3.6. In this architecture, I assume per-antenna power splitting with parameter ν (as defined earlier). After power splitting, the input signal at each antenna passes through a rectifier, followed by a DC combiner that yields the harvested energy. For the information path, after passing through power splitters, the received signals are first combined in the RF domain using a combining

vector $\mathbf{w}$. The resulting signal is then decoded in the baseband. Because they require extremely small power, the combining vector is assumed to be implemented using switches [102, 103], i.e., $\mathbf{w} = [\mathrm{w}_1, \cdots, \mathrm{w}_{N_\mathrm{r}}]^* \in [0,1]^{N_\mathrm{r}}$. Note that both the signals for information decoding and energy harvesting are in the order of μW (Fig. 3.7). It is worth mentioning that recent results have shown that mmWave energy harvesting circuits can run with only a few μW [97, 98].

I now derive the combining gain expression for the proposed SWIPT receiver architecture in Fig. 3.6. Let y be the signal output at the RF combiner. If a BS applies a beamforming vector $\mathbf{f} \in \mathbb{C}^{N_\mathrm{t} \times 1}$ to send data symbol s (where $\mathbb{E}\left[|s|^2\right] = P_\mathrm{t}$) to a target user, it follows that

$$y = \sqrt{\nu}\left[\mathbf{w}^* \mathbf{H}_\mathrm{d} \mathbf{f} s + \mathbf{w}^* \mathbf{r}_\mathrm{int} + \mathbf{w}^* \mathbf{n}\right], \tag{3.24}$$

where $\mathbf{H}_\mathrm{d} \in \mathbb{C}^{N_\mathrm{r} \times N_\mathrm{t}}$ is the channel between the user and its serving BS, and $\mathbf{r}_\mathrm{int}$ is the received signal due to the interfering BSs. Since the channel between each user and its BS is assumed to be single-path, the channel matrix $\mathbf{H}_\mathrm{d} = h_0 \sqrt{g_0(r_0)} \mathbf{a}_\mathrm{r}\left(\phi_\mathrm{r}\right) \mathbf{a}_\mathrm{t}^*\left(\phi_\mathrm{t}\right)$, where $\mathbf{a}_\mathrm{t}\left(\phi_\mathrm{t}\right)$ and $\mathbf{a}_\mathrm{r}\left(\phi_\mathrm{r}\right)$ are the array response vectors at the BS and user, respectively. Recall that $g_0(r_0)$ denotes the path gain from the serving BS, while ϕ_r and ϕ_t respectively denote the channel angle-of-arrival and angle-of-departure at the user and BS. If the channel is known at the BS, and given the antenna model in Section 3.3.3, the BS will design the beamforming vector $\mathbf{f}$ to maximize the beamforming gain, i.e., to have $\left|\mathbf{a}_\mathrm{t}^*\left(\phi_\mathrm{t}\right)\mathbf{f}\right|^2 = N_\mathrm{t}$. Denoting $\bar{\alpha} = h_0 \sqrt{g_0(r_0)} \mathbf{a}_\mathrm{t}^*\left(\phi_\mathrm{t}\right)\mathbf{f}$, the received signal in (3.24) can be written as

$$y = \sqrt{\nu}\left(\bar{\alpha} \mathbf{w}^* \mathbf{a}_\mathrm{r}\left(\phi_\mathrm{r}\right) s + \mathbf{w}^* \mathbf{r}_\mathrm{int} + \mathbf{w}^* \mathbf{n}\right). \tag{3.25}$$

The post-combining SINR can then be expressed as

$$\text{SINR} = \frac{\nu P_{\text{t}} \left|\alpha\right|^2 N_t \left|\mathbf{w}^* \mathbf{a}_{\text{r}} \left(\phi_{\text{r}}\right)\right|^2}{I + \nu \mathbf{w}^* \mathbf{w} \sigma^2}, \tag{3.26}$$

where $\left|\mathbf{w}^* \mathbf{a}_{\text{r}} \left(\phi_{\text{r}}\right)\right|^2$ represents the combining gain at the receiver, and I denotes the aggregate interference power. The SINR in (3.26) can be maximized if the receiver designs the optimum combining vector, which can be implemented by activating certain antennas on or off. This requires the receiver to have global channel knowledge, which is often challenging in practice. I relax this condition by assuming that the receiver has the angle-of-arrival information for the serving BS only. Ignoring the interference, I propose to design the combining vector by maximizing the SNR $= \frac{P_{\text{t}} |\bar{\alpha}|^2 N_t \left|\mathbf{w}^* \mathbf{a}_{\text{r}} \left(\phi_{\phi_{\text{r}}}\right)\right|^2}{\mathbf{w}^* \mathbf{w} \sigma^2}$ instead, i.e., the receiver designs its combining vector $\mathbf{w}$ such that

$$\mathbf{w}^\star = \arg \max_{\mathbf{w} \in [0,1]^{N_{\text{r}}}} \frac{\left|\mathbf{w}^* \mathbf{a}_{\text{r}} \left(\phi_{\text{r}}\right)\right|^2}{\mathbf{w}^* \mathbf{w}}. \tag{3.27}$$

The optimal solution to (3.27) can be found by an exhaustive search over all possible combinations of $\mathbf{w}$. For large receive antenna arrays, this could entail high computational costs, which would further increase the power consumption. Therefore, it is important to consider computationally efficient approaches for designing the combining vector. As outlined in Algorithm 1, I propose a greedy solution for designing $\mathbf{w}$ by (step-wise) activating only those antennas that boost the received SNR. With $\hat{\mathbf{w}}$ denoting the combining vector designed using Algorithm 1, the combining gain for the switch-based architecture can be defined as $M_c = \frac{\left|\sum_{i=1}^{N_r} \hat{\text{w}}_i e^{\text{j}kd(i-1)\cos(\phi_{\text{r}})}\right|^2}{|\hat{\mathbf{w}}|^2}$ where k denotes the wavenumber and d is the antenna element spacing. Despite its low-complexity, numerical simulations in the next section reveal that the proposed low-

Algorithm 1 Greedy Switch Combining Design

Input N_{r}, ϕ_{r}
Initialization $\mathbf{w} = \mathbf{0}$, $\mathrm{w}_1 = 1$
for $i = 2, \cdots, N_{\mathrm{r}}$ **do**
  if $\frac{1}{i}\left|\sum_{n=1}^{i-1} \mathrm{w}_n e^{\mathrm{j}kd(n-1)\cos(\phi_{\mathrm{r}})} + e^{\mathrm{j}kd(i-1)\cos(\phi_{\mathrm{r}})}\right|^2 > \frac{1}{i-1}\left|\sum_{n=1}^{i-1} \mathrm{w}_n e^{\mathrm{j}kd(n-1)\cos(\phi_{\mathrm{r}})}\right|^2$ **then**
    $\mathrm{w}_i = 1$

power greedy approach could give a good combining gain, without losing substantial performance compared to more advanced but power-hungry solutions.

3.5.3 Results

Fig. 3.7 plots the overall success probability for a given transmit antenna beam pattern. The users are equipped with a single-antenna receiver, similar to the one in Fig. 3.6 with $N_{\mathrm{r}} = 1$. First, Fig. 3.7 shows that a reasonable success probability can be obtained with mmWave SWIPT system for typical mmWave propagation and system parameters. Further, this plot illustrates that the power splitting ratio ν needs to be optimized for a given SINR outage threshold to maximize the overall success probability. Matching the intuition, the figure shows that in the low SINR outage regime (when T is large), it is desirable to divert more power to the information decoding module, while a larger fraction of power needs to be portioned for the energy harvesting system in the high SINR outage regime (when T is small). This trend is consistent with prior studies on SWIPT architectures [15].

I now evaluate the performance of the proposed low-power receiver architecture for different number of receive antennas. In Fig. 3.8, the success probability

$P_{\text{suc}}(\lambda, T, \psi, \nu)$ is plotted for a fixed transmit antenna beam pattern. For the proposed architecture, the combining vector is obtained using Algorithm 1, and the curves are averaged over the angle-of-arrival parameter. For comparison, I also plot the success probability for (fully digital) maximal ratio combining (MRC) receivers. I observe that the success probability improves with the receive antenna array size. Further, when the SINR outage threshold T is small, the success probability is mainly limited by the energy outage. This also explains why the success probability converges to a limit (determined by the energy outage threshold) as T decreases. Moreover, there are diminishing returns as the number of antennas are increased. A comparison with power-hungry MRC receivers shows that the proposed switch-based architecture performs reasonably well. This is particularly desirable for future mmWave SWIPT devices.

3.6 Conclusions

In this chapter, I analyzed the energy harvesting performance at low-power devices powered by a mmWave cellular network. Using a stochastic geometry framework, I derived analytical expressions characterizing the performance of mmWave energy and information transfer in terms of system, channel and network parameters. Simulations results were used to validate the accuracy of the derived expressions. Leveraging the analytical framework, I also provided useful network and device level design insights. For the connected case when the transmitter and receiver beams are aligned, results show that the energy coverage improves with narrower beams. In contrast, wider beams provide better energy coverage when the receivers are not aligned

with a particular transmitter. This trade-off is evident in the more general scenario having both types of receivers, where there typically exists an optimal beamforming beamwidth that maximizes the network-wide energy coverage. Moreover, I found that several device-related parameters can significantly impact the system performance. For example, the performance can be substantially improved by optimizing over the power splitting ratio and by leveraging large antenna arrays. To allow using multiple antennas at the mmWave receivers while keeping the power consumption low, I proposed a low-power receiver architecture for mmWave energy and information transfer using antenna switches. Simulation results show that the proposed architecture can provide good gains for the overall mmWave energy harvesting performance. Simulation results also reveal that mmWave cellular networks could potentially provide better energy coverage than lower frequency solutions.

Appendix A: Theorem 1

The following inequality approximates the tail probability of a normalized Gamma distribution.

Lemma 45 (From [104]) For a normalized Gamma random variable u with parameter N, the probability $\Pr(u < x)$ can be tightly upper-bounded by $\Pr(u < x) < (1 - e^{-ax})^N$, where the constant $x > 0$ and $a = N(N!)^{-\frac{1}{N}}$.

I write $\mathrm{P_{con}}(\lambda, \psi) = \Pr\left[Y > \max\left(\frac{\psi}{\xi}, \psi_{\min}\right)\right] = \Pr\left[S + I > \hat{\psi}\right]$, where

$$S = P_{\mathrm{t}} M_{\mathrm{t}} M_{\mathrm{r}} H_0 g_0(r_0)$$

is the received signal power from the serving BS, and $I = \sum_{\ell>0, \ell\in\Phi(\lambda)\setminus\mathbb{B}(r_g)} P_{\mathrm{t}}\delta_\ell H_\ell g_\ell(r_\ell)$ is the received signal power from all the other BSs. I can derive the result in Theorem 35 by finding the conditional distributions $\mathrm{P}_{\mathrm{con,L}}(\lambda,\psi)$ and $\mathrm{P}_{\mathrm{con,N}}(\lambda,\psi)$. To proceed, first consider the conditional distribution $\mathrm{P}_{\mathrm{con,L}}(\lambda,\psi) = \Pr(S+I>\psi|\mathrm{L})$ given the receiver is aligned with a LOS BS (which is indicated by the subscript L in the following notation).

$$\begin{aligned}
\mathrm{P}_{\mathrm{con,L}}(\lambda,\psi) &= \mathbb{E}_{S,I|\mathrm{L}}\left[\Pr\left(u < \frac{S+I}{\psi}\right)\right] \\
&\overset{(a)}{\approx} \mathbb{E}_{S,I|\mathrm{L}}\left[\left(1-e^{-a\frac{S+I}{\psi}}\right)^N\right] \\
&= \mathbb{E}_{S,I|\mathrm{L}}\left[\sum_{k=0}^{N}(-1)^k\binom{N}{k}e^{-ak\frac{S+I}{\psi}}\right] \\
&= \sum_{k=0}^{N}(-1)^k\binom{N}{k}\mathbb{E}_{S,I|\mathrm{L}}\left[e^{-\hat{a}(S+I)}\right] \qquad (3.28)
\end{aligned}$$

where I have included a dummy random variable $u\sim\Gamma\left(N,\frac{1}{N}\right)$ in the first equation. Note that u converges to 1 as $N\to\infty$. Therefore, this substitution is in fact an approximation when N is finite. The introduction of u allows leveraging the inequality in Lemma 5, which leads to (a), where the constant $a = N(N!)^{-\frac{1}{N}}$. The last equation follows from the Binomial series expansion of (b), and by further substituting $\hat{a} = \frac{ak}{\psi}$. To evaluate the expectation in (3.28), consider

$$\mathbb{E}_{S,I|\mathrm{L}}\left[e^{-\hat{a}(S+I)}\right] = \mathbb{E}_{S|\mathrm{L}}\left[e^{-\hat{a}S}\mathbb{E}_{I|S,\mathrm{L}}\left[e^{-\hat{a}I}\right]\right]. \qquad (3.29)$$

The inner expectation in (3.29) can be simplified by applying the thinning theorem for a PPP [63]. Note that Φ can be independently thinned into two PPPs Φ_{L} and

Φ_{N}, where the former comprises the LOS BSs whereas the latter consists of NLOS BSs. Therefore, I can interpret Φ_{L} and Φ_{N} as two independent tiers of BSs. The user will be tagged with either the closest BS in Φ_{L} or in Φ_{N}, whichever maximizes the average received power at the user. I can further thin Φ_{L} into four independent PPPs $\{\Phi_{\mathrm{L}}^i\}_{i=1}^4$, where each resulting PPP Φ_{L}^i contains BSs that correspond to a nonzero directivity gain D_i with p_i being the thinning probability. This follows because the beam orientations are assumed to be independent across links. Thus, a link can have a directivity gain of D_i with probability p_i independently of other links. I let the received power due to the transmission from the BSs in Φ_{L}^i be I_{L}^i. Likewise, Φ_{N} can be split into $\{\Phi_{\mathrm{N}}^i\}_{i=1}^4$ with the corresponding received powers denoted by $\{I_{\mathrm{N}}^i\}_{i=1}^4$. Since the resulting PPPs are independent, (3.29) can be simplified as

$$\mathbb{E}_{I|S,\mathrm{L}}\left[e^{-\hat{a}I}\right] = \prod_{i=1}^{4}\mathbb{E}_{I|S,\mathrm{L}}\left[e^{-\hat{a}I_{\mathrm{L}}^i}\right]\prod_{j=1}^{4}\mathbb{E}_{I|S,\mathrm{L}}\left[e^{-\hat{a}I_{\mathrm{N}}^j}\right] \tag{3.30}$$

where

$$\begin{aligned}
\mathbb{E}_{I|S,\mathrm{L}}\left[e^{-\hat{a}I_{\mathrm{L}}^i}\right] &\overset{(a)}{=} \mathbb{E}_{\Phi_{\mathrm{L}}^i|r_o}\left[\prod_{\ell\in\Phi_{\mathrm{L}}^i\setminus\mathbb{B}(r_o)}\mathbb{E}_{H_\ell}\left[e^{-\hat{a}P_{\mathrm{t}}H_\ell D_i C_{\mathrm{L}} r_\ell{}^{-\alpha_{\mathrm{L}}}}\right]\right] \\
&\overset{(b)}{=} \mathbb{E}_{\Phi_{\mathrm{L}}^i|r_o}\left[\prod_{\ell\in\Phi_{\mathrm{L}}^i\setminus\mathbb{B}(r_o)}\left(\frac{1}{1+\hat{a}P_{\mathrm{t}}D_i C_{\mathrm{L}} r_\ell{}^{-\alpha_{\mathrm{L}}} N_{\mathrm{L}}{}^{-1}}\right)^{N_{\mathrm{L}}}\right] \\
&= e^{-2\pi\lambda p_i\int_{r_o}^{\infty}\left(1-\left(\frac{1}{1+\hat{a}P_{\mathrm{t}}D_i C_{\mathrm{L}} t^{-\alpha_{\mathrm{L}}} N_{\mathrm{L}}{}^{-1}}\right)^{N_{\mathrm{L}}}\right)p(t)t\mathrm{d}t}
\end{aligned} \tag{3.31}$$

where (a) follows by conditioning on the length r_o of the serving LOS link, and by further noting that small-scale fading is independent across links. Here, $\mathbb{B}\left(r_o\right)$ denotes

a circular disc of radius r_o centered at the typical user. (b) is obtained by using the moment generating function of a normalized Gamma random variable, while the last equation follows by invoking the probability generating functional [63] of the PPP Φ_L^i. Substituting (3.31) in the first (left) product term of (3.30) yields (3.6). Similarly, $\mathbb{E}_{I|S,\mathrm{L}}\left[e^{-\hat{a}I_{\mathrm{N}}^i}\right]$ is given by

$$\begin{aligned}&\mathbb{E}_{\Phi_{\mathrm{L}}^i,H|r_o}\left[e^{-\hat{a}\sum\limits_{\ell\in\Phi_{\mathrm{N}}^i\setminus\mathbb{B}(\rho_{\mathrm{L}}(r_o))}P_{\mathrm{t}}H_\ell D_i C_{\mathrm{N}} r_\ell^{-\alpha_{\mathrm{N}}}}\right]\\&=e^{-2\pi\lambda p_i\int\limits_{\rho_{\mathrm{L}}(r_o)}^{\infty}\left(1-\left(\frac{1}{1+\hat{a}P_{\mathrm{t}}D_iC_{\mathrm{N}}x^{-\alpha_{\mathrm{N}}}N_{\mathrm{N}}{}^{-1}}\right)^{N_{\mathrm{N}}}\right)(1-p(t))t\mathrm{d}t}.\end{aligned}\tag{3.32}$$

By substituting (3.32) in the second (right) product term of (3.30) yields (3.7). Using the expressions in (3.30)–(3.32) in (3.29), and by further evaluating the expectation of the resulting expression with respect to S, I obtain

$$\begin{aligned}&\int\limits_{r_g}^{\infty}\left(\frac{1}{1+\hat{a}P_{\mathrm{t}}M_{\mathrm{t}}M_{\mathrm{r}}C_{\mathrm{L}}r^{-\alpha_{\mathrm{L}}}N_{\mathrm{L}}{}^{-1}}\right)^{N_{\mathrm{L}}}\\&\qquad\times e^{-\Upsilon_{k,1}(\lambda,\psi,r)-\Upsilon_{k,2}(\lambda,\psi,\rho_{\mathrm{L}}(r))}\tilde{\tau}_{\mathrm{L}}(r)\mathrm{d}r\end{aligned}\tag{3.33}$$

where I have again used definition of the moment generating function of a normalized Gamma distribution. $\Upsilon_{k,1}(\cdot)$ and $\Upsilon_{k,2}(\cdot)$ are given in (3.6) and (3.7) respectively, r_g denotes the minimum link distance, while the distance distribution is provided in Lemma 3. Using (3.28) and (3.29), I can thus retrieve the expression in (3.4). I can similarly derive the conditional distribution $\mathrm{P}_{\mathrm{con,N}}(\lambda,\psi)=\Pr(S+I>\psi|\mathrm{N})$ in (3.5) for the NLOS case.

Appendix B: Proposition 1

To simplify the analysis, I approximate the LOS probability function $p(r)$ by a step function $p(r) = \mathbb{1}_{\{0<r<R_B\}}$, i.e., the BSs within a LOS ball of radius R_B are marked LOS with probability 1, while the rest as NLOS [93]. The radius R_B is chosen such that the LOS association probability ϱ_{L} remains the same (as in the original model). Using a step function for $p(r)$, it follows from Lemma 2 that $\varrho_{\mathrm{L}} = 1 - e^{-\lambda\pi R_B^2}$ and $R_B = \left(\frac{\ln(1-\varrho_{\mathrm{L}})}{\lambda\pi}\right)^{0.5}$. Moreover, I neglect small scale fading for all the links except for the serving BS. I also ignore the NLOS signals in the analysis. This effectively leads to a scenario where the user receives signals from the BSs within the LOS ball only. Intuitively, this would be the likely scenario in sufficiently dense networks. I only list the key steps since the rest of the proof follows from Appendix A. Ignoring the NLOS signals, I approximate (3.30) as $\mathbb{E}_{I|S,\mathrm{L}}\left[e^{-\hat{a}I}\right] \approx \prod_{i=1}^{4} \mathbb{E}_{I|S,\mathrm{L}}\left[e^{-\hat{a}I_{\mathrm{L}}^i}\right]$ where

$$\begin{aligned}
\mathbb{E}_{I|S,\mathrm{L}}\left[e^{-\hat{a}I_{\mathrm{L}}^i}\right] &= \mathbb{E}_{\Phi_{\mathrm{L}}^i|r_o}\left[\prod_{\ell\in\Phi_{\mathrm{L}}^i\cap[\mathbb{B}(R_B)\setminus\mathbb{B}(r_o)]} e^{-\hat{a}P_{\mathrm{t}}D_iC_{\mathrm{L}}r_\ell^{-\alpha_{\mathrm{L}}}}\right] \\
&\overset{(a)}{=} e^{-2\pi\lambda p_i \int_{r_o}^{R_B}\left(1-e^{-\hat{a}P_{\mathrm{t}}D_iC_{\mathrm{L}}t^{-\alpha_{\mathrm{L}}}}\right)t\mathrm{d}t} \\
&\overset{(b)}{=} e^{-\frac{2\pi\lambda p_i}{\alpha_{\mathrm{L}}}\int_{W_{ik}r_o^{-\alpha_{\mathrm{L}}}}^{W_{ik}R_B^{-\alpha_{\mathrm{L}}}} \frac{1-e^{-v}}{v^{1+\frac{2}{\alpha_{\mathrm{L}}}}}\mathrm{d}v} \\
&\overset{(c)}{=} e^{-\frac{2\pi\lambda p_i W_{ik}^{\frac{2}{\alpha_{\mathrm{L}}}}}{\alpha_{\mathrm{L}}}\Gamma\left(\frac{-2}{\alpha_{\mathrm{L}}};W_{ik}r_o^{-\alpha_{\mathrm{L}}},W_{ik}R_B^{-\alpha_{\mathrm{L}}}\right)} \\
&\qquad \times e^{-\pi\lambda p_i\left(R_B^2-r_o^2\right)}. \qquad (3.34)
\end{aligned}$$

Here, (a) follows by ignoring the small scale fading and invoking the probability generating functional [63] of PPP, (b) by a change of variables, and (c) by the definition of the generalized incomplete Gamma function. The result in Proposition 1 is obtained

by assuming $p_5 = 0$, and by further noting that the distance distribution simplifies to $\tau_{\mathrm{L}}(x) = \frac{2\pi\lambda x}{\varrho_{\mathrm{L}}} e^{-\lambda\pi x^2}$ due to the LOS ball approximation.

Appendix C: Corollary 1

I derive Corollary 1 by finding the conditional means $\bar{P}_{\mathrm{L}} = \mathbb{E}\left[S + I|\mathrm{L}\right]$ and $\bar{P}_{\mathrm{N}} = \mathbb{E}\left[S + I|\mathrm{N}\right]$. $\bar{P}_{\mathrm{L}}$ can be evaluated by conditioning on the link distance r_0 from the serving BS as follows.

$$\begin{aligned}
&\mathbb{E}\left[S + I|r_0, \mathrm{L}\right] = \mathbb{E}\left[S|r_0, \mathrm{L}\right] + \sum_{i=1}^{4} \mathbb{E}\left[I_{\mathrm{L}}^i + I_{\mathrm{N}}^i|r_0, \mathrm{L}\right] \\
&\overset{(a)}{=} P_{\mathrm{t}} M_{\mathrm{t}} M_{\mathrm{r}} C_{\mathrm{L}} {r_0}^{-\alpha_{\mathrm{L}}} + \sum_{i=1}^{4} 2\pi\lambda P_{\mathrm{t}} p_i D_i C_{\mathrm{L}} \int_{r_0}^{\infty} t^{-(\alpha_{\mathrm{L}}-1)} p(t)\mathrm{d}t \\
&+ \sum_{i=1}^{4} 2\pi\lambda P_{\mathrm{t}} p_i D_i C_{\mathrm{N}} \left[\frac{\left(\rho_{\mathrm{L}}(r_0)\right)^{-(\alpha_{\mathrm{N}}-2)}}{\alpha_{\mathrm{N}} - 2} - \int_{\rho_{\mathrm{L}}(r_0)}^{\infty} t^{-(\alpha_{\mathrm{N}}-1)} p(t)\mathrm{d}t \right] \\
&= P_{\mathrm{t}} M_{\mathrm{t}} M_{\mathrm{r}} C_{\mathrm{L}} {r_0}^{-\alpha_{\mathrm{L}}} + \Psi_{\mathrm{L}}\left(r_0\right) + \Psi_{\mathrm{N}}\left(\rho_{\mathrm{L}}(r_0)\right) \qquad (3.35)
\end{aligned}$$

where (a) is obtained by averaging over the fading distribution, followed by invoking Campbell's theorem [63], while (3.35) follows from the definitions of Ψ_{L} and Ψ_{N} provided in (3.11) and (3.12) respectively. Taking expectation of $\mathbb{E}\left[S + I|r_0, \mathrm{L}\right]$ with respect to r_o using Lemma 3 yields (3.9). The expression for $\bar{P}_{\mathrm{N}}$ is (3.10) can be derived using similar steps.

Appendix D: Theorem 3

From (3.2), it follows that the harvested energy $\gamma = \xi Y \mathbb{1}_{\{Y > \psi_{\min}\}}$. Let $Y = (1-\nu)\left(S + I + \sigma^2\right)$, where $S = P_{\mathrm{t}} M_{\mathrm{t}} M_{\mathrm{r}} H_0 g_0(r_0)$ and $I = \sum_{\ell>0, \ell\in\Phi(\lambda)\setminus\mathbb{B}(r_g)} P_{\mathrm{t}} \delta_\ell H_\ell g_\ell(r_\ell)$

respectively denote the contributions from the serving and the interfering BSs. To find $P_{\text{suc}}(\lambda, T, \psi, \nu) = \Pr[\text{SINR} > T, \gamma > \psi]$, consider

$$\begin{aligned}
&\Pr\left[\frac{\nu S}{\nu(I+\sigma^2)+\sigma_c^2} > T, (1-\nu)\left(S+I+\sigma^2\right) > \hat{\psi}\right] \\
&\overset{(a)}{=} \mathbb{E}_I\left[\Pr\left[S > T\left(I+\sigma^2+\frac{\sigma_c^2}{\nu}\right), S > \frac{\hat{\psi}}{(1-\nu)} - I - \sigma^2\right]\right] \\
&\overset{(b)}{=} \mathbb{E}_I\left[\Pr\left[S > T\left(I+\sigma^2+\frac{\sigma_c^2}{\nu}\right)\right] \middle| I > \mu\right] \Pr[I > \mu] \\
&\qquad + \mathbb{E}_I\left[\Pr\left[S > \frac{\hat{\psi}}{(1-\nu)} - I - \sigma^2\right] \middle| I \leq \mu\right] \Pr[I \leq \mu] \\
&\overset{(c)}{\approx} \mathbb{E}_I\left[\Pr\left[S > T\left(I+\sigma^2+\frac{\sigma_c^2}{\nu}\right)\right]\right] \Pr[I > \mu] \\
&\qquad + \mathbb{E}_I\left[\Pr\left[S > \frac{\hat{\psi}}{(1-\nu)} - I - \sigma^2\right]\right] \Pr[I \leq \mu] \\
&= P_{\text{cov}}(\lambda, T, \nu)\tilde{P}_{\text{con}}(\lambda, \mu) + P_{\text{con}}(\lambda, \varphi)\left[1 - \tilde{P}_{\text{con}}(\lambda, \mu)\right] \qquad (3.36)
\end{aligned}$$

where the expectation in (a) is with respect to the interference I, (b) is obtained by further conditioning on I to be greater (or smaller) than a parameter μ which follows from the inequality $T\left(I+\sigma^2+\frac{\sigma_c^2}{\nu}\right) > \frac{\hat{\psi}}{(1-\nu)} - I - \sigma^2$. The approximation (or effectively an upperbound) in (c) results from dropping the conditions $I > \mu$ or $I \leq \mu$ while calculating the expectation. Finally, the SINR coverage probability $P_{\text{cov}}(\lambda, T, \nu)$ follows from Lemma 43, and the energy coverage probability $P_{\text{con}}(\lambda, \varphi)$ from Theorem 35. $\tilde{P}_{\text{con}}(\lambda, \mu)$ is the interference CCDF evaluated at μ.

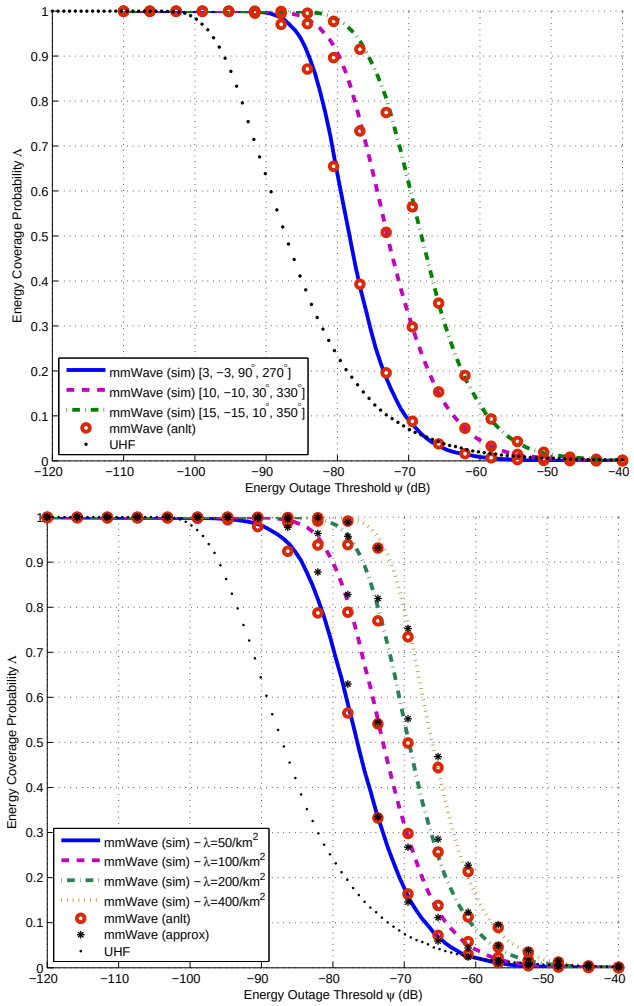

Figure 3.2: (a) Energy coverage probability $\Lambda(\epsilon, \psi, \lambda)$ for different transmit antenna beam patterns parameterized by $[M_{\mathrm{t}}, m_{\mathrm{t}}, \theta_{\mathrm{t}}, \bar{\theta}_{\mathrm{t}}]$ in a purely connected network ($\epsilon = 1$, $\lambda = 100/\mathrm{km}^2$). The performance improves with narrower beams for this case. $P_{\mathrm{t}} = 13$ dB, $W = 100$ MHz, $\alpha_{\mathrm{L}} = 2$, $\alpha_{\mathrm{N}} = 4$, $N_{\mathrm{L}} = 2$, $N_{\mathrm{N}} = 3$, and $r_g = 1$ m. There is a nice agreement between Monte Carlo simulation (sim) results and the analytical (anlt) results obtained using Theorem 1 with $N = 5$ terms. (b) Energy coverage probability $\Lambda(1, \psi, \lambda)$ for different network densities for connected users. Transmit beam pattern is fixed to $[10, -10, 30°, 330°]$. Other parameters are the same as given in Fig. 3.4.2. Also included are the results based on the analytical approximation (approx) in Proposition 1. The approximation becomes tighter as the density increases.

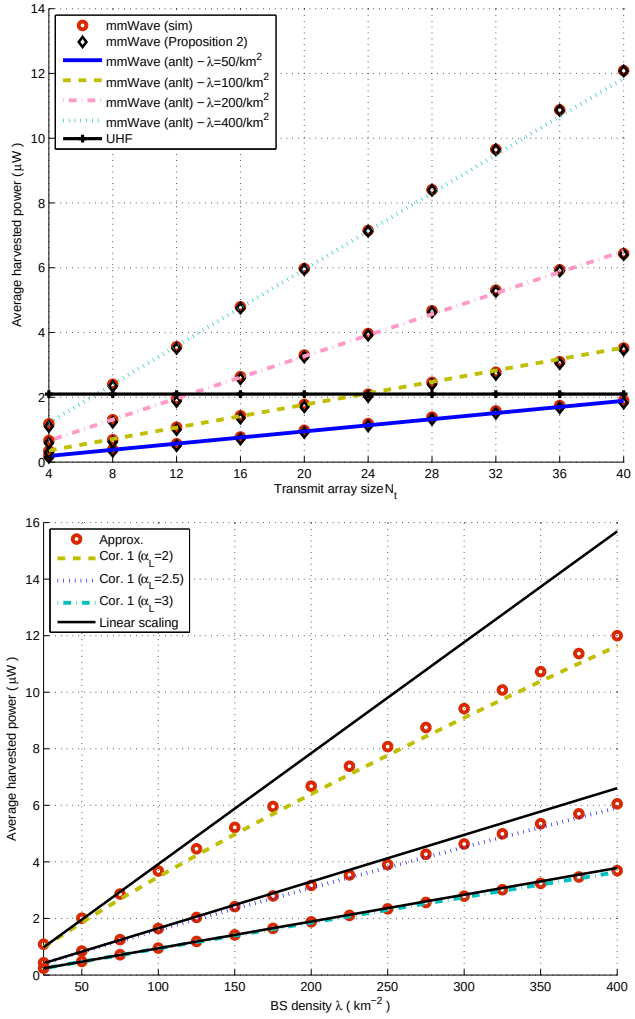

Figure 3.3: (a) The average harvested power in a connected mmWave network for different number of BS antennas N_{t} and deployment densities λ. Results based on Proposition 2 are obtained for $\psi = -35$ dBm. The analytical (anlt) results based on Corollary 1 ($\psi \to 0$) are validated using Monte Carlo simulations (sim); and closely approximate the average harvested energy obtained using Proposition 2. The transmit antenna beam patterns are calculated using the approximations used for obtaining Fig. 3.5. Other simulation parameters are the same as used in Fig. 3.4.2. For comparison, a plot for a UHF system is also included. (b) Plots the average harvested power (Corollary 1) vs. BS density for $N_{\mathrm{t}} = 32$. It validates the approximation in (3.13). For illustration, also included are the solid lines for the (hypothetical) case when average power scales linearly with density. The scaling tends to become linear as α_{L} is increased.

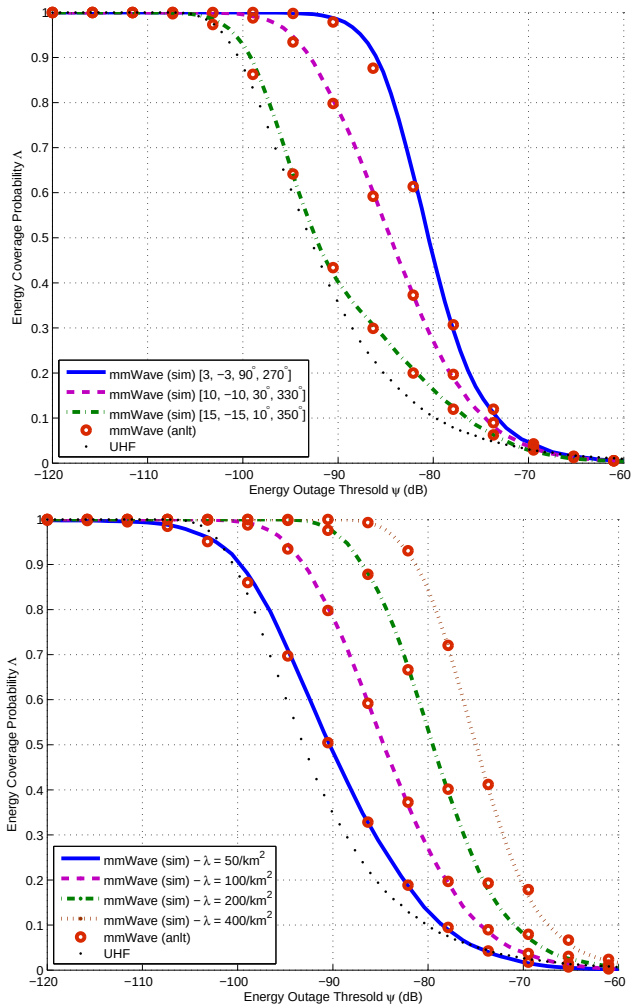

Figure 3.4: (a) Energy coverage probability $\Lambda(\epsilon, \psi, \lambda)$ for different transmit antenna beam patterns in a nonconnected network ($\epsilon = 0$, $\lambda = 100/\text{km}^2$). The performance improves with wider beams for this case. Other simulation parameters are same as given in Fig. 3.4.2. Monte Carlo simulation (sim) results validate the analytical (anlt) results obtained using Theorem 2 with $N = 5$ terms. (b) Energy coverage probability $\Lambda(0, \psi, \lambda)$ for different network densities for nonconnected users. Transmit beam pattern is fixed to $[10, -10, 30°, 330°]$. Other parameters are same as given in Fig. 3.4.2. Monte Carlo simulation (sim) results validate the analytical (anlt) results obtained using Theorem 2 with $N = 5$ terms.

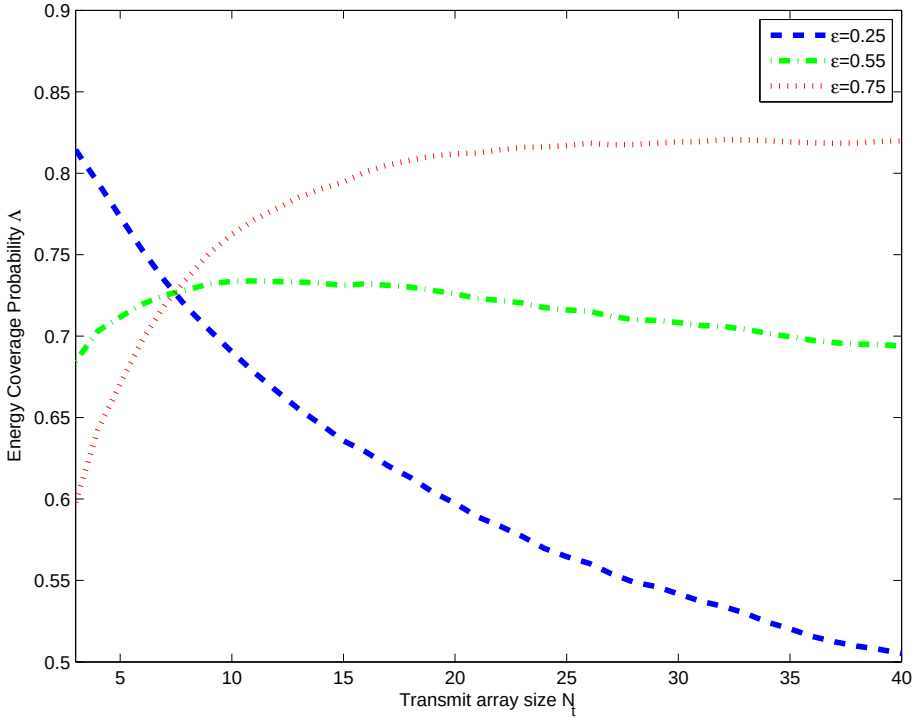

Figure 3.5: The overall energy coverage probability $\Lambda(\epsilon, \psi, \lambda)$ for different values of ϵ. Depending on the fraction of users operating in connected mode, the transmit array size (which controls the beamforming beamwidth in this example) can be optimized to maximize the network-wide energy coverage. This could translate into massive gains given that the number of served devices would be potentially large. The users are assumed to be equipped with a single omnidirectional receive antenna. The energy outage threshold ψ is -70 dB for $\Phi_{u,\mathrm{con}}$ and -85 dB for $\Phi_{u,\mathrm{ncon}}$. $P_{\mathrm{t}} = 13$ dB, $\lambda = 200/\mathrm{km}^2$. Channel parameters are the same as used in Fig. 3.4.2.

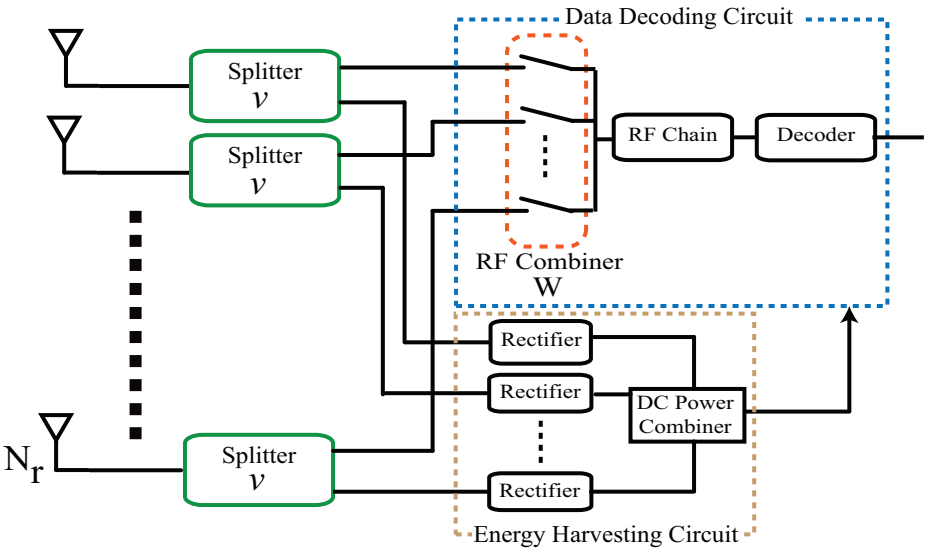

Figure 3.6: Low power receiver architecture for SWIPT.

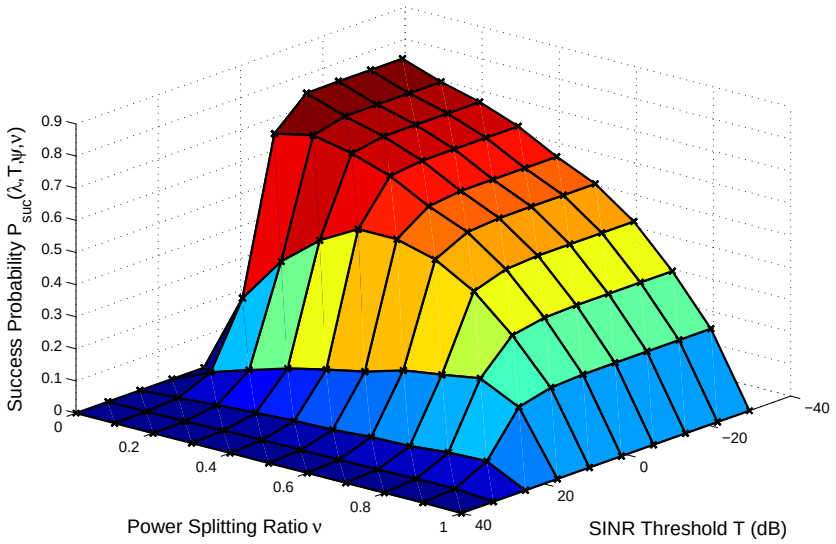

Figure 3.7: A 3D plot showing the interplay between the success probability, the power splitting ratio ν, and the SINR outage threshold T for a given energy outage threshold ψ and network density λ. As T gets large, the system becomes SINR-limited, and the optimum value of ν increases, suggesting that a larger fraction of received signal should be used for information extraction to optimize the overall success probability. The transmit antenna beam pattern is set to $A_{15,-15,10^\circ,350^\circ}$. Other parameters include $\psi = -70$ dB, $\sigma_c^2 = -80$ dB, $\lambda = 200/\text{km}^2$, and $P_\text{t} = 43$ dBm.

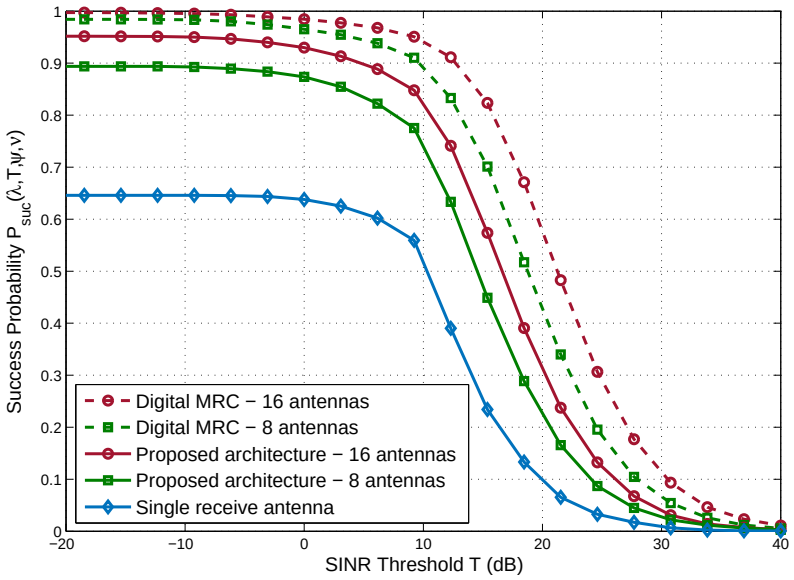

Figure 3.8: The success probability for different number of receive antennas N_{r} at the user given a fixed transmit beam pattern $A_{15,-15,10^{\circ},350^{\circ}}$ at the BSs. Proposed low-power architecture achieves good performance compared to superior receiver architectures. Other parameters include $\nu = 0.5$, $\psi = -70$ dB, $\sigma_c^2 = -80$ dB, $\lambda = 200/\mathrm{km}^2$, and $P_{\mathrm{t}} = 43$ dBm.

Chapter 4

Wireless-powered Communications with Massive MIMO

In this chapter[1], I investigate the power transfer efficiency and the energy efficiency of a wireless energy and information transfer system aided by massive MIMO. Using realistic models for energy harvesting and power consumption, this chapter characterizes the optimal values for system parameters such as the number of antennas, number of users, and transmit power. This research provides useful guidelines in configuring the system parameters for an energy efficient operation.

4.1 Prior Work and Motivation

Massive multiple-input multiple-output (MIMO) architecture is a key technology for enabling future 5G networks [107–109]. Due to its ability to beam energy towards desired spatial regions, massive MIMO is attractive for wireless energy transfer [15, 110, 111]. This could enable a wirelessly powered operation for the massive number of RF (radio frequency) energy harvesting devices in the future [1,6–8,16,18]. An RF or wireless energy harvesting device extracts energy from the incident RF sig-

[1]This chapter is based on my published work in [105,106]. This research was supervised by Prof. Robert W. Heath, Jr. The feedback from Dr. Ali Yazdan and Dr. Yael Maguire helped improve the quality of this research.

nals. Such wirelessly powered systems are becoming increasingly feasible due to the reduction in the power consumption requirements of devices and the advancement in energy harvesting technologies [3–6].

Energy efficiency has been a key consideration in the system-level analyses of massive MIMO systems [112–114]. It is often characterized by the ratio of the achievable data rate (bits/sec) and the total power consumption (watts). While deploying more antennas at the BS boosts the data rate, the additional antenna circuitry leads to increased power consumption. This motivates the need for an energy efficient system design. In [112], the energy efficiency of a massive MIMO system was analyzed while ignoring the circuit power consumption. It was shown that the energy efficiency improves as more antennas are added to the BS. Unlike [112] which considered the transmit power consumption only, the work in [113, 114] investigated the energy efficiency of a massive MIMO system while accounting for the BS circuit power consumption. In [113], it was shown that the transmit power should be increased with the number of antennas for an energy efficient system operation. Moreover, the energy efficiency eventually vanishes in the large-antenna regime. In [114], the downlink energy efficiency of a massive MIMO system was analyzed for a spatially correlated channel model. It was shown that the optimal transmit power is independent of the number of antennas in pilot-contaminated systems.

Similarly, the energy efficiency of wirelessly powered massive MIMO systems has also been investigated [115]. In [115], a single-user wireless information and power transfer system was considered. By jointly optimizing the power transfer duration and the transmit power, an energy efficient resource allocation strategy was proposed

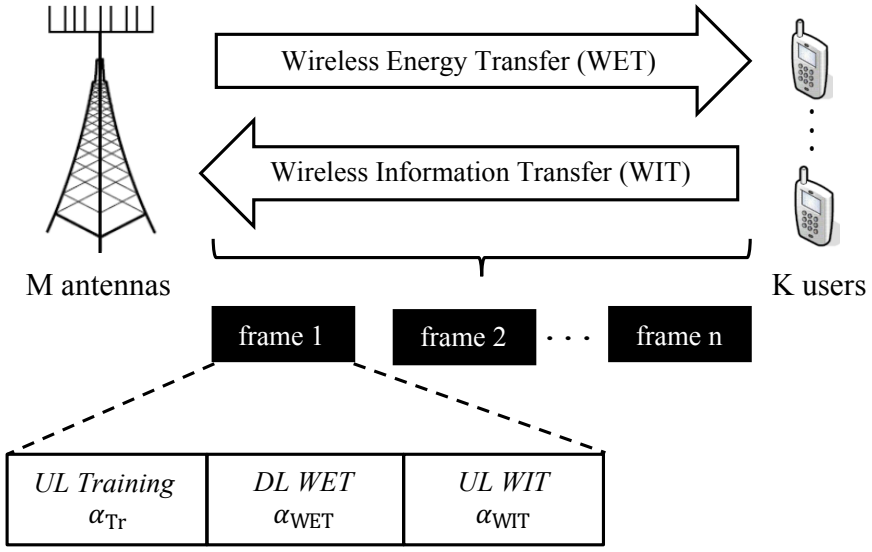

Figure 4.1: System Model.

under a delay constraint. In [116], the power transfer efficiency of a multi-user wireless energy transfer system was investigated. It was shown that the power transfer efficiency can be improved with opportunistic scheduling as the number of users is increased. In other related work, the throughput optimization of massive MIMO wireless information and power transfer systems has also been studied [111]. In [111], a throughput-optimal resource allocation policy was proposed for the large-antenna regime.

4.2 Contributions

In this chapter, I investigate the power transfer efficiency and the energy efficiency of a massive MIMO wireless information and power transfer system using a

scalable power consumption model. Using a piecewise linear energy harvesting model, I derive the average harvested power at a user while accounting for imperfect channel knowledge. I first focus on wireless energy transfer and analyze the system-level power transfer efficiency. I characterize the optimal number of BS antennas and users that maximize the power transfer efficiency. I find that the optimal design is guided by the BS power consumption as well as energy harvesting parameters. I then consider the case of wireless energy and information transfer where the users exploit the harvested energy to communicate with the BS. I analytically characterize the optimal BS transmit power for an energy efficient system operation. Moreover, I examine the interplay between energy efficiency and the key system parameters. Numerical results suggest that both power transfer efficiency and energy efficiency benefit from operating the system in the massive MIMO regime.

This chapter differs from other related work on several accounts. First, most prior work investigating the power transfer or energy efficiency of wireless-powered systems either ignores the BS circuit power consumption or treats it as a fixed component [111, 115, 116]. This could be misleading since the total power consumption varies with various system parameters such as the number of antennas, the number of users, and the choice of the transmit/receive filters. I address this concern by using a scalable power consumption model. Second, the existing analyses typically consider an ideal energy harvester, where the output power is a scalar multiple of the input. This affords analytical simplicity but it could be misleading in practice. This is because the output power of a practical energy harvester is a nonlinear function of the input. More recently, nonlinear energy harvesting models have been proposed to

address this concern [117,118]. In [117], a logistic function was considered for modeling the harvester, and a resource allocation algorithm was designed to maximize the harvested power. In [118], a similar model was used while studying the throughput maximization problem in a multi-user MIMO wireless-powered communication system with separate stations for energy transfer and data reception. In this chapter, I use a piecewise linear model for the energy harvester. This captures the key limitations of a practical energy harvester while keeping the analysis simple. With this motivation, I investigate the power transfer/energy efficiency of a remotely-powered system using realistic models for energy harvesting and power consumption.

The rest of this chapter is organized as follows. The system model is described in the next section. The average received power is derived in Section 4.4. Section 4.5 treats wireless energy transfer, whereas Section 4.6 deals with wireless energy and information transfer. Section 4.7 concludes this chapter.

4.3 System Model

Channel Model

I consider a wireless energy and information transfer system consisting of a BS with M antennas and K single-antenna users. I assume each user is equipped with an RF energy harvesting module. The BS charges the users on the downlink and the users exploit the harvested energy to communicate with the BS on the uplink. I assume a TDD (time division duplex) mode of operation consisting of a downlink wireless energy transfer (WET) phase, an uplink wireless information transfer (WIT) phase, and an uplink training phase (see Fig. 4.1) [111]. I assume the BS learns the uplink

channels for each user in the uplink training phase, and uses channel reciprocity to learn the downlink channels. It uses the estimated channel for decoding information on the uplink, and beamforming energy on the downlink. The energy harvesting users, however, are not assumed to have any channel knowledge.

I define $S = T_{\mathrm{c}} B_{\mathrm{c}}$ as the length of the coherence block or the frame size, where T_{c} and B_{c} denote the coherence time and the coherence bandwidth of the wireless channel. The frame is divided into three phases such that a fraction $\alpha_{\mathrm{Tr}} \in (0, 1)$ is reserved for uplink training, a fraction $\alpha_{\mathrm{WET}} \in (0, 1)$ for wireless energy transfer, and a fraction $\alpha_{\mathrm{WIT}} \in (0, 1)$ for wireless information transfer. Moreover, I assume that $\alpha_{\mathrm{WET}} + \alpha_{\mathrm{WIT}} + \alpha_{\mathrm{Tr}} = 1$, and set $\alpha_{\mathrm{Tr}} = \frac{\tau}{S}$ (where $K \leq \tau < S$) proportional to the number of users. I let $\mathbf{h}_i = [h_{i1}, \cdots, h_{iM}]^T \in \mathbb{C}^{M \times 1}$ be the uplink channel from a user i to the BS, where $i \in \{1, \cdots, K\}$. I assume a rich scattering environment with sufficiently spaced antennas such that $h_{ij} \sim \mathcal{CN}(0, 1)$ is a zero-mean complex gaussian random variable with unit variance, which is independent across i and j. I use $\beta_i = C d_i^{-\alpha}$ to model the average large-scale gain for the link between the BS and a user i where d_i denotes the link distance, $\alpha > 2$ is the path loss exponent, and $C > 0$ is the path loss intercept. I assume that the users are uniformly distributed around the BS in an annulus with inner radius $r_{\min}$ and outer radius $r_{\max}$ such that $d_i \in [r_{\min}, r_{\max}] \ \forall \ i \in \mathcal{I}_K$. By averaging over the user locations, it follows that $\mathbb{E}[{d_i}^{-\alpha}] = \frac{{r_{\max}}^{2-\alpha} - {r_{\min}}^{2-\alpha}}{(1-0.5\alpha)({r_{\max}}^2 - {r_{\min}}^2)}$. I further define $\mathbf{H} = \left[\mathbf{h}_1, \mathbf{h}_2, \cdots, \mathbf{h}_K\right] \in \mathbb{C}^{M \times K}$ and $\mathbf{G} = \left[\mathbf{g}_1, \mathbf{g}_2, \cdots, \mathbf{g}_K\right] \in \mathbb{C}^{M \times K}$ such that $\mathbf{G} = \mathbf{H}\mathbf{D}^{1/2}$, where $\mathbf{D}$ is a diagonal matrix with $(\beta_1, \cdots, \beta_K)$ as the entries of the main diagonal. For the downlink, I denote the BS transmit power (in watts) by $P_{\mathrm{dl}} = \alpha_{\mathrm{WET}} B p_{\mathrm{dl}}$, where p_{dl} gives the average transmit

symbol energy (in joules/symbol), while B denotes the system bandwidth. Similarly, for the uplink, $P_{\text{ul}} = \alpha_{\text{WIT}} B p_{\text{ul}}$ denotes the average transmit power (in watts) at a user, and p_{ul} gives the average transmit symbol energy (in joules/symbol). The user draws the uplink transmit power from the energy it harvests in the downlink. I let $\hat{\mathbf{G}} = \left[\hat{\mathbf{g}}_1, \hat{\mathbf{g}}_2, \cdots, \hat{\mathbf{g}}_K\right]$ denote the channel estimate of $\mathbf{G}$ at the BS.

Energy Harvesting Model

I assume that each user is equipped with an RF energy harvesting module with a sufficiently large battery. To simplify the analysis, prior work mostly assumes an *ideal* energy harvester where the harvested energy scales linearly with the input power. In practice, however, an energy harvester is a nonlinear device with a small operating range, which may lead to vastly different performance trends compared to the ideal case [117]. For example, the incident energy should be sufficiently high to activate the harvester; not all the incident energy can be harvested; and the harvester output eventually saturates beyond a certain input power. I, therefore, strengthen the analysis by parameterizing the harvester operation using $\{\theta_{\text{act}}, \theta_{\text{sat}}, \eta_{\text{EH}}\}$: θ_{act} is the harvester activation threshold (watts), θ_{sat} is the harvester saturation threshold (watts), and $\eta_{\text{EH}} \in (0, 1]$ is the rectifier efficiency. An ideal energy harvester has $\theta_{\text{act}} = 0$ and $\theta_{\text{sat}} = \infty$. I will often call a harvester in the active mode to be in the non-saturated mode.

Notation

For a positive integer K, I define the index set $\mathcal{I}_K = \{1, \cdots, K\}$. I use the superscripts $*$ and H to denote conjugate and conjugate transpose of a matrix. I use $\lceil x \rceil$ and $\lfloor x \rfloor$ to denote the integer ceiling or the integer floor of a real number x.

4.4 Average Received Energy

In this section, I analytically characterize the average received (incident) energy at the users assuming perfect and imperfect channel state information (CSI) at the BS. The corresponding harvested energy is characterized in the next section.

4.4.1 Average Received Energy: Perfect CSI

I assume that the BS transmits with the average transmit energy p_{dl} (in joules/symbol) in the downlink. The BS uses a weighted sum of conjugate beamformers for each user in the downlink, since it has been shown to be asymptotically optimal for wireless energy transfer [19]. The precoder $\mathbf{w}_{\text{dl}} = \sum_{i=1}^{K} \sqrt{\zeta_i} \frac{\mathbf{w}_i}{\|\mathbf{w}_i\|}$ where $\mathbf{w}_i = \hat{\mathbf{g}}_i$, and $\zeta_i \in (0,1)\ \forall\ i$ such that $\sum_{i=1}^{K} \zeta_i = 1$. Assuming the BS transmits a signal s with $\mathbb{E}[|s|^2] = p_{\text{dl}}$, the signal y_i received at user i can be expressed as

$$y_i = \mathbf{g}_i^{\text{H}} \mathbf{w}_{\text{dl}} s + n_i = \sqrt{\zeta_i} \mathbf{g}_i{}^{\text{H}} \frac{\hat{\mathbf{g}}_i}{\|\hat{\mathbf{g}}_i\|} s + \sum_{j \neq i}^{K} \sqrt{\zeta_j} \mathbf{g}_i^{\text{H}} \frac{\hat{\mathbf{g}}_j}{\|\hat{\mathbf{g}}_j\|} s + n_i, \tag{4.1}$$

where n_i is the receiver noise. A user harvests energy from the beam directed towards it, as well as from those directed towards other users. Assuming perfect channel

knowledge at the BS such that $\hat{\mathbf{g}}_i = \mathbf{g}_i \, \forall \, i \in \mathfrak{I}_K$, (4.1) simplifies to

$$y_i = \sqrt{\zeta_i}\|\mathbf{g}_i\| s + \sum_{j \neq i}^{K} \sqrt{\zeta_j} \mathbf{g}_i^{\mathrm{H}} \frac{\mathbf{g}_j}{\|\mathbf{g}_j\|} s + n_i. \tag{4.2}$$

The contribution from the noise term is usually negligible and is therefore ignored. This results in the following analytical expression for the average received energy $\bar{\gamma}_i = \alpha_{\mathrm{WET}} \, \mathbb{E}\left[|y_i|^2\right]$ at a user i.

Lemma 46 When a BS with M antennas serves K single-antenna energy harvesting users, the average received energy $\bar{\gamma}_i$ (in joules/symbol) at a user i, assuming perfect channel knowledge at the BS, is given by

$$\bar{\gamma}_i = \alpha_{\mathrm{WET}} \, p_{\mathrm{dl}} \, \beta_i \left(\zeta_i M + (1 - \zeta_i)\right) \tag{4.3}$$

where α_{WET} denotes the fraction reserved for downlink energy transfer, p_{dl} gives the transmit symbol energy (joules/symbol), and β_i gives the large-scale channel gain. I can take expectation with respect to the user locations by replacing β_i in (4.3) by $C\mathbb{E}[d_i^{-\alpha}]$ from Section 4.3.

Proof: The proof follows from the independence of the random vectors $\{\mathbf{g}_k\}_{k=1}^{K}$ and by further noting that the entries of $\mathbf{g}_k$ are independent and identically distributed (IID) with mean mean zero and variance β_k. □

The parameter α_{WET} captures the fact that the users receive energy for a fraction α_{WET} of the frame. The average received energy during the entire frame is given by $S\bar{\gamma}_i$. I note that the average received power $B\bar{\gamma}_i$ increases with an increase in the number of BS antennas M. Its dependency on the number of users is captured by

the energy allocation parameter ζ_i, which tends to decrease as more users are added to the system. Moreover, the term $\zeta_i M$ is due to the BS transmission intended for user i, while $1-\zeta_i$ results from the transmissions intended for other users.

Corollary 47 The average received energy $\bar{\gamma}_i \leq \alpha_{\text{WET}}\, p_{\text{dl}}\, \beta_i M$, which holds with equality for the single-user scenario where $\zeta_i = 1$.

Corollary 48 Under an equal transmit energy allocation at the BS, i.e., $\zeta_i = \frac{1}{K}\, \forall\, i \in \mathcal{I}_K$, the average received energy is given by

$$\bar{\gamma}_i = \alpha_{\text{WET}}\, p_{\text{dl}}\, \beta_i \left(1 + \frac{M-1}{K}\right). \tag{4.4}$$

Proof: This follows by plugging $\zeta_i = \frac{1}{K}$ in (4.3). □

Corollary 49 The average received energy converges to the limit

$$\lim_{M,K\to\infty} \bar{\gamma}_i = \alpha_{\text{WET}}\, p_{\text{dl}}\, \beta_i\, (1+r) \tag{4.5}$$

as both M and K grow large with $\frac{M}{K} = r > 1$ held constant.

Proof: The result follows directly from Corollary 48. □

Therefore, increasing the ratio r helps improve the average received energy at the users. This is because adding more antennas boosts the beamforming gain, and serving fewer users increases the per user energy allocation at the BS.

4.4.2 Average Received Energy: Imperfect CSI

I now characterize the average received energy while incorporating the channel estimation errors in the analysis. Imperfect channel estimation causes a reduction in the amount of energy reaching the harvesters. I recall that a fraction α_{Tr} of the frame is reserved for uplink training. I assume that the K users simultaneously transmit their training signals consisting of τ symbols, where $\tau \geq K$ and $\alpha_{\mathrm{Tr}} = \frac{\tau}{S}$. I define a $\tau \times K$ matrix $\mathbf{\Phi}$ where the ith column contains the training sequence of user i. I assume that the users transmit orthogonal training sequences such that $\mathbf{\Phi}^{\mathrm{H}}\mathbf{\Phi} = \mathbf{I}_{\mathrm{K}}$. Let us define a diagonal matrix $\mathbf{\Delta}$ with $\{\tau p_{\mathrm{Tr},1}, \cdots, \tau p_{\mathrm{Tr},K}\}$ as its diagonal entries, where $p_{\mathrm{Tr},i}$ denotes the training symbol energy of user i. The signal received at the BS during the training phase can be expressed as

$$\mathbf{Y}_{\mathrm{Tr}} = \mathbf{G}(\mathbf{\Phi}\mathbf{\Delta}^{\frac{1}{2}})^{\mathrm{T}} + \mathbf{N} \tag{4.6}$$

where the $M \times \tau$ matrix $\mathbf{N}$ denoting the BS thermal noise consists of IID Gaussian entries with mean zero and variance σ^2. For a user i, I define $\xi_i \in (0, 1)$ as the fraction of the total energy harvested $\bar{\delta}_i^{\mathrm{I}} S$ (treated in Lemma 56) in a frame that is reserved for uplink pilot transmission. Therefore, $\tau p_{\mathrm{Tr},i} = \eta_{\mathrm{PA}}^{\mathrm{EH}} \xi_i \bar{\delta}_i^{\mathrm{I}} S$, where $\eta_{\mathrm{PA}}^{\mathrm{EH}} \in (0, 1)$ is the user power amplifier (PA) efficiency.

4.4.2.1 LS Channel Estimation

I first consider the case where the BS estimates the UL channel from the K EHs using linear least squares (LS) approach. The resulting channel estimate $\hat{\mathbf{G}}_{\mathrm{LS}}$ is

given by

$$\hat{\mathbf{G}}_{\mathrm{LS}} = \mathbf{Y}_{\mathrm{Tr}}\boldsymbol{\Phi}^{*}\boldsymbol{\Delta}^{-\frac{1}{2}} = \mathbf{G} + \mathbf{N}\boldsymbol{\Phi}^{*}\boldsymbol{\Delta}^{-\frac{1}{2}}. \tag{4.7}$$

The corresponding estimation error matrix $\mathbf{E}_{\mathrm{LS}} = \hat{\mathbf{G}}_{\mathrm{LS}} - \mathbf{G}_{\mathrm{LS}} = \mathbf{N}\boldsymbol{\Phi}^{*}\boldsymbol{\Delta}^{-\frac{1}{2}}$ consists of independent Gaussian entries e_{ij}^{LS} $(i \in \mathcal{I}_M, j \in \mathcal{I}_K)$ with mean zero and variance $\frac{\sigma^2}{\tau p_{\mathrm{Tr},i}}$. The following expression characterizes the mean incident power at a user i.

Lemma 50 When the BS designs the downlink energy beamformer based on the LS channel estimate, the average received energy $\bar{\gamma}_i^{\mathrm{LS}}$ (in joules/symbol) at a user i is given by

$$\bar{\gamma}_i^{\mathrm{LS}} = \begin{cases} \psi_i^{\mathrm{LS,act}}, & \frac{\theta_{\mathrm{act}}}{B} \leq \psi_i^{\mathrm{LS,act}} < \frac{\theta_{\mathrm{sat}}}{B} \\ \psi_i^{\mathrm{LS,sat}}, & \psi_i^{\mathrm{LS,act}} \geq \frac{\theta_{\mathrm{sat}}}{B} \end{cases} \tag{4.8}$$

where

$$\psi_i^{\mathrm{LS,act}} = \frac{A_1 M + A_2 - A_3 + \sqrt{\left(A_1 M + A_2 - A_3\right)^2 + 4\left(A_1 + A_2\right)A_3}}{2}, \tag{4.9}$$

$$\psi_i^{\mathrm{LS,sat}} = A_1 M \left(1 - \frac{M-1}{M}\frac{1}{1+\frac{\theta_{\mathrm{sat}}}{BA_3}}\right) + A_2, \tag{4.10}$$

$$A_1 = \alpha_{\mathrm{WET}} p_{\mathrm{dl}} \beta_i \zeta_i, \tag{4.11}$$

$$A_2 = \alpha_{\mathrm{WET}} p_{\mathrm{dl}} \beta_i \left(1 - \zeta_i\right), \tag{4.12}$$

and

$$A_3 = \frac{\sigma^2}{\xi_i \beta_i \eta_{\mathrm{PA}}^{\mathrm{EH}} \eta_{\mathrm{EH}} S}. \tag{4.13}$$

Proof: See Appendix. □

I can interpret (4.8) as follows. The average received energy is given by the expression $\psi_i^{\mathrm{LS,act}}$ as long as the corresponding incident power falls within the linear range $[\theta_{\mathrm{act}}, \theta_{\mathrm{sat}})$ of the harvester. It is given by the expression $\psi_i^{\mathrm{LS,sat}}$ when the corresponding received power exceeds the saturation threshold of the harvester. When the incident power level is within the linear regime of the harvester, the harvested power increases with the incident power. As it exceeds the saturation threshold, however, the harvested power remains the same regardless of the incident power. This explains why different analytical expressions are required to characterize the incident energy. The following remark explains why the incident power - which is not the same as the harvested power - also depends on the harvesting parameters.

Remark 51 I note from (4.8)-(4.10) and (4.13) that the incident energy at a user also depends on the energy harvesting parameters. This is because the channel estimation error is a function of the uplink transmit power, which is drawn from the energy harvested in the previous frames. This introduces a dependency between the downlink energy beamformer and the energy harvesting parameters, as evident from the analytical expressions in Lemma 50. I further add that the average received energy could be smaller than $\frac{\theta_{\mathrm{act}}}{B}$. Since this amount would be insufficient to activate the harvester, I do not consider this case in Lemma 50. In principle, I may characterize this by assuming omnidirectional transmission, since the BS would not have any channel knowledge in the absence of uplink training.

Remark 52 The sum $A_1 M + A_2$ in Lemma 50 equals $\bar{\gamma}_i$, which is the average received energy with perfect CSI. Moreover, the term A_3 captures the dependency on the

EH parameters and the BS noise. As $\sigma^2 \to 0$, so does the estimation error and I recover the expression for the case with perfect CSI. Similarly, the degradation due to imperfect CSI vanishes as the frame size $S \to \infty$ and $A_3 \to 0$. This is because the users can afford a larger transmit power during pilot transmission due to an underlying increase in the energy harvested in a frame.

Finally, I note that the average received energy increases with an increase in the number of BS antennas, the EH conversion efficiency, as well as the PA efficiency at the user. It reduces with an increase in the number of users due to a decrease in the per-user transmit energy allocation at the BS.

4.4.2.2 MMSE Channel Estimation

I now consider the case where the BS estimates the uplink channel using (linear) minimum mean squared error (MMSE) estimation. The estimated channel is given by

$$\hat{\mathbf{G}}_{\text{MMSE}} = \mathbf{Y}_{\text{Tr}} \mathbf{\Phi}^* \left(\mathbf{D}\mathbf{\Delta} + \sigma^2 \mathbf{I}_K \right)^{-1} \mathbf{\Delta}^{\frac{1}{2}} \mathbf{D} \tag{4.14}$$

The corresponding estimation error matrix $\mathbf{E}_{\text{MMSE}} = \hat{\mathbf{G}}_{\text{MMSE}} - \mathbf{G}_{\text{MMSE}}$ consists of entries $e_{ij}^{\text{MMSE}} \, (i \in \mathcal{I}_M, j \in \mathcal{I}_K)$ with mean zero and variance $\frac{\beta_i}{1+\frac{\beta_i \tau p_{\text{Tr},i}}{\sigma^2}}$. This error variance is smaller than that obtained with LS estimation. Moreover, the matrices $\mathbf{E}_{\text{MMSE}}$ and $\hat{\mathbf{G}}_{\text{MMSE}}$ are independent by virtue of the orthogonality principle and the fact that uncorrelated Gaussian random variables are independent.

Remark 53 I note that the LS channel estimate is a scalar multiple of that obtained with the MMSE approach. Specifically, $\hat{\mathbf{g}}_i^{\text{LS}} = \left(1 + \frac{\sigma^2}{\beta_i \tau p_{\text{Tr},i}}\right) \hat{\mathbf{g}}_i^{\text{MMSE}}$ for $i \in \mathcal{I}_K$, which

follows by simplifying (4.7) and (4.14). In other words, the phase of the estimated channel remains the same with LS and MMSE.

The following expression characterizes the mean incident energy at a user i.

Lemma 54 When the BS designs the downlink energy beamformer based on the MMSE channel estimate, the average received energy at a user i is given by $\bar{\gamma}_i^{\mathrm{MMSE}} = \bar{\gamma}_i^{\mathrm{LS}}$, where $\bar{\gamma}_i^{\mathrm{LS}}$ follows from Lemma 50.

Proof: The proof follows from Remark 53 and by noting that the beamfomer in (4.1) consists of normalized vectors such that $\frac{\hat{\mathbf{g}}_i^{\mathrm{LS}}}{\|\hat{\mathbf{g}}_i^{\mathrm{LS}}\|} = \frac{\hat{\mathbf{g}}_i^{\mathrm{MMSE}}}{\|\hat{\mathbf{g}}_i^{\mathrm{MMSE}}\|}$, resulting in the same energy. □

The average received energy obtained with MMSE estimation is the same as that obtained with the LS approach. This is because the channel estimates obtained with both approaches differ only by a scaling factor. The downlink beamfomer in (4.1) consists of normalized vectors such that $\frac{\hat{\mathbf{g}}_i^{\mathrm{LS}}}{\|\hat{\mathbf{g}}_i^{\mathrm{LS}}\|} = \frac{\hat{\mathbf{g}}_i^{\mathrm{MMSE}}}{\|\hat{\mathbf{g}}_i^{\mathrm{MMSE}}\|}$. This means that the downlink energy beamformer and the received energy is the same with both approaches. In the rest of the chapter, I will not distinguish between LS or MMSE estimation. I use $\bar{\gamma}_i^{\mathrm{I}} \triangleq \bar{\gamma}_i^{\mathrm{MMSE}} = \bar{\gamma}_i^{\mathrm{LS}}$ to refer to the average received energy with imperfect channel knowledge.

4.5 Wireless Energy Transfer

In this section, I focus on wireless energy transfer where the BS attempts to charge users, but no information transfer is considered. I analyze the average

harvested energy and the power transfer efficiency in terms of the system parameters. Wireless energy and information transfer is treated in Section 4.6.

4.5.1 Average Harvested Energy

I now characterize the average harvested energy at a user. I use $\vartheta_{i,s}$ to denote the energy harvested by a user i in slot s $\left(s \in \mathcal{I}_{\lfloor \alpha_{\mathrm{WET}} S \rfloor}\right)$ during the harvesting phase of the frame. I let $\bar{\delta}_i = \alpha_{\mathrm{WET}} \mathbb{E}\left[\vartheta_i\right]$ denote the average harvested energy (in an arbitrary slot) at a user i, where I have dropped the subscript s as the mean is identical across the slots in the harvesting phase. Due to the piecewise linear energy harvesting model, the average harvested energy $\bar{\delta}_i$ (in joules/symbol) at a user i is given by

$$\bar{\delta}_i = \eta_{\mathrm{EH}} \bar{\gamma}_i \mathbb{1}_{\left[\frac{\theta_{\mathrm{act}}}{B} \leq \bar{\gamma}_i < \frac{\theta_{\mathrm{sat}}}{B}\right]} + \frac{\eta_{\mathrm{EH}} \theta_{\mathrm{sat}}}{B} \mathbb{1}_{\left[\bar{\gamma}_i \geq \frac{\theta_{\mathrm{sat}}}{B}\right]} \tag{4.15}$$

where $\mathbb{1}_{[\cdot]}$ is the indicator function which is 1 when the condition in the parenthesis is true, and zero otherwise. When the activation threshold θ_{act} is small and the saturation threshold θ_{sat} is large, the average harvested energy can be approximated as $\eta_{\mathrm{EH}} \bar{\gamma}_i$.

4.5.1.1 Perfect CSI

I first consider the case where the BS has perfect channel knowledge. Leveraging the analysis in Section 4.4, I provide an analytical expression for the average harvested energy $\hat{\gamma}_i$.

Lemma 55 The average harvested energy $\bar{\delta}_i$ at a user i can be expressed as

$$\bar{\delta}_i = \begin{cases} 0, & M < M_{\text{act},i} \\ \eta_{\text{EH}} \bar{\gamma}_i, & M_{\text{act},i} \leq M < M_{\text{sat},i} \\ \frac{\eta_{\text{EH}} \theta_{\text{sat}}}{B}, & M \geq M_{\text{sat},i} \end{cases} \tag{4.16}$$

where

$$M_{\text{act},i} = \left\lceil 1 + \frac{1}{\zeta_i} \left(\frac{\theta_{\text{act}}}{\alpha_{\text{WET}} B \beta_i p_{\text{dl}}} - 1 \right) \right\rceil = \left\lceil 1 + \frac{1}{\zeta_i} \left(\frac{\theta_{\text{act}}}{\beta_i P_{\text{dl}}} - 1 \right) \right\rceil$$

and

$$M_{\text{sat},i} = \left\lceil 1 + \frac{1}{\zeta_i} \left(\frac{\theta_{\text{sat}}}{\beta_i P_{\text{dl}}} - 1 \right) \right\rceil$$

give the minimum number of antennas needed to activate or saturate the harvester.

Proof: The proof follows from invoking Lemma 46 and the definition in (4.15). □

The antenna thresholds $\{M_{\text{act},i}, M_{\text{sat},i}\}$ depend on the downlink BS transmit power $\zeta_i P_{\text{dl}} = \zeta_i \alpha_{\text{WET}} B p_{\text{dl}}$ for user i and the link attenuation β_i. Increasing the BS transmit power, serving fewer users, or deploying a harvester with a smaller activation threshold reduces the number of required antennas. In other words, a minimum of $M_{\text{act},i}$ antennas are required for a successful wireless energy transfer to a user i, and at least $M_{\text{sat},i}$ antennas are required to operate the harvester at its maximum potential. In a multi-user system, the BS should have at least $M = \max_{i \in \mathcal{I}_K} M_{\text{act},i}$ antennas to ensure that all users are served. Similarly, having $M = \max_{i \in \mathcal{I}_K} M_{\text{sat},i}$ BS antennas ensures that each user attains the maximum possible harvested energy. With fewer than $M = \min_{i \in \mathcal{I}_K} M_{\text{act},i}$ antennas, all the transmitted energy will go waste as none of the harvesters will be activated. Likewise, having more than $M = \max_{i \in \mathcal{I}_K} M_{\text{sat},i}$ antennas

will not further improve the harvested energy since all the users will be in saturated mode. This behavior is markedly different from that observed with an (ideal) linear energy harvesting model where the average harvested energy keeps on increasing with M.

4.5.1.2 Imperfect CSI

I now characterize the average harvested energy while accounting for the channel estimation errors at the BS. Since LS/MMSE estimation results in the same received energy, I denote the harvested energy as $\bar{\delta}_i^{\mathrm{I}}$, where the superscript "I" signifies imperfect channel knowledge.

Lemma 56 With LS/MMSE channel estimation, the average harvested energy $\bar{\delta}_i^{\mathrm{I}}$ at a user i can be approximated as

$$\bar{\delta}_i^{\mathrm{I}} = \begin{cases} 0, & M < M_{\mathrm{act},i}^{\mathrm{I}} \\ \eta_{\mathrm{EH}} \bar{\gamma}_i^{\mathrm{I}}, & M_{\mathrm{act},i}^{\mathrm{I}} \leq M < M_{\mathrm{sat},i}^{\mathrm{I}} \\ \frac{\eta_{\mathrm{EH}} \theta_{\mathrm{sat}}}{B}, & M \geq M_{\mathrm{sat},i}^{\mathrm{I}} \end{cases} \tag{4.17}$$

where

$$M_{\mathrm{act},i}^{\mathrm{I}} = \min \left\{ M : \ \frac{\theta_{\mathrm{act}}}{B} \leq \bar{\gamma}_i^{\mathrm{I}} < \frac{\theta_{\mathrm{sat}}}{B} \right\} \tag{4.18}$$

and

$$M_{\mathrm{sat},i}^{\mathrm{I}} = \min \left\{ M : \ \bar{\gamma}_i^{\mathrm{I}} \geq \frac{\theta_{\mathrm{sat}}}{B} \right\} \tag{4.19}$$

denote the minimum number of antennas required to activate or saturate the harvesters.

Proof: The proof follow from invoking Lemma 50 and the definition in (4.15). □ As compared to the case with perfect CSI, a larger number of BS antennas is required to drive the users into activation or saturation mode. The expressions (4.18) and (4.19) characterize the required number of antennas with LS/MMSE channel estimation.

Remark 57 Let us consider the quantity $(1-\xi_i)\,\bar{\delta}_i^{\mathrm{I}}$, which represents the *effective* harvested energy at a user i. This is because a fraction ξ_i of the harvested energy is reserved for uplink training. On one hand, increasing ξ_i improves the channel estimation accuracy at the BS, thereby enhancing the incident power at the user. On the other hand, this means that a smaller fraction of the harvested energy will be available to the user. Therefore, ξ_i should be tuned so as to maximize the effective harvested energy at each user.

4.5.2 Power Transfer Efficiency

I define the system-level power transfer efficiency as the ratio of the total average power harvested by all users to the total average BS power consumption. I find the optimal number of antennas and the optimal number of users to maximize the system-level power transfer efficiency.

4.5.2.1 Perfect CSI

I first consider the case where the BS has perfect channel knowledge. For ease of exposition, I set β_i to the average $\mathbb{E}[\beta_i] = C\mathbb{E}[d_i^{-\alpha}] \triangleq \beta$, where $\mathbb{E}[d_i^{-\alpha}]$ is given in Section 4.3. As $\beta_i \triangleq \beta$ such that $\bar{\delta}_i \triangleq \bar{\delta}\ \forall\, i \in \mathfrak{I}_K$, I can equivalently view this as a

symmetric setup where the users are located on a circle of radius $(C\beta^{-1})^{\frac{1}{\alpha}}$ around the BS. I model the total BS power consumption as a sum of P_{TX} and P_{c}, where P_{TX} denotes the total average transmit (PA) power consumption (in watts) and P_{c} the total average circuit power consumption (in watts) at the BS. The PTE of overall system can be formulated as

$$\begin{aligned}\mathrm{PTE}\,(M,K) &= \frac{\sum_{i=1}^{K} B\bar{\delta}_i}{P_{\mathrm{TX}}+P_{\mathrm{c}}} \\ &= \frac{BK\bar{\delta}}{P_{\mathrm{TX}}+P_{\mathrm{FIX}}+MP_{\mathrm{BS}}+P_{\mathrm{CE}}+P_{\mathrm{LP}}}\end{aligned} \tag{4.20}$$

In particular, $P_{\mathrm{TX}} = \frac{P_{\mathrm{dl}}}{\eta_{\mathrm{PA}}^{\mathrm{BS}}} = \frac{\alpha_{\mathrm{WET}} p_{\mathrm{dl}} B}{\eta_{\mathrm{PA}}^{\mathrm{BS}}}$ where $\eta_{\mathrm{PA}}^{\mathrm{BS}} \in (0,1)$ denotes the BS PA efficiency. Note that the uplink transmit power, which is a fraction of the average harvested power, only appears in the numerator (via the expression for the harvested energy $\bar{\delta}$). This is because the energy harvesting users do not have any power source except for the wireless energy delivered by the BS. Inspired by [113], I allow the circuit power consumption P_c to scale with the key parameters such as M and K: P_{FIX} lumps the fixed power spent on running the BS; P_{BS} models the circuit power consumed by an RF chain such that MP_{BS} gives the total power consumed by the antenna circuitry. Let us use κ_{BS} to denote the BS computational efficiency in flops/watt, and recall that there are $\frac{B}{S}$ coherence blocks per second. Then, $P_{\mathrm{CE}} = M\tilde{P}_{\mathrm{CE}} = \frac{2MK^2B}{S\kappa_{\mathrm{BS}}}$ models the power consumed while computing the channel estimates on the uplink during each coherence block (includes the power consumed in multiplying an $M \times K$ received pilot signal with a length K pilot sequence for each of the K users [119, Appendix C]); $P_{\mathrm{LP}} = M\tilde{P}_{\mathrm{LP}} = \left(\frac{3MKB}{S\kappa_{\mathrm{BS}}}\right)$ accounts for the power consumption due to linear processing at the BS, i.e., for computing the downlink energy beamformer. I note

that the computational power consumption is usually negligible compared to the antenna power consumption in the large-antenna regime.

Optimal M

I now characterize the number of antennas required to optimize the power transfer efficiency, assuming the other parameters to be fixed. Let us denote this quantity by M^*_{PTE}.

Lemma 58 In a system with K users, the PTE-optimal number of antennas is given by $M^*_{\mathrm{PTE}} =$

$$\begin{cases} M_{\mathrm{act}} = \left\lceil 1 + K\left(\frac{\theta_{\mathrm{act}}}{\beta P_{\mathrm{dl}}} - 1\right)\right\rceil, & K \geq 1 + \frac{P_{\mathrm{TX}}+P_{\mathrm{FIX}}}{P_{\mathrm{BS}}+\tilde{P}_{\mathrm{CE}}+\tilde{P}_{\mathrm{LP}}} \\ M_{\mathrm{sat}} = \left\lceil 1 + K\left(\frac{\theta_{\mathrm{sat}}}{\beta P_{\mathrm{dl}}} - 1\right)\right\rceil, & K < 1 + \frac{P_{\mathrm{TX}}+P_{\mathrm{FIX}}}{P_{\mathrm{BS}}+\tilde{P}_{\mathrm{CE}}+\tilde{P}_{\mathrm{LP}}} \end{cases} \tag{4.21}$$

where M_{act} and M_{sat} are as defined in Lemma 55.

Proof: See Appendix. □ From the perspective of power transfer efficiency, it is optimal that the harvesters operate at the vertices of the linear regime. This is evident from Lemma 58 since $M^*_{\mathrm{PTE}} \in \{M_{\mathrm{act}}, M_{\mathrm{sat}}\}$. When M is smaller than M_{act}, the power transfer efficiency is (trivially) zero. When M is increased beyond M_{sat}, the total power consumption increases while the average harvested power remains the same, reducing the power transfer efficiency.

Remark 59 The PTE-optimal number of antennas depends on the number of users K as well as the BS power consumption. I note that M^*_{PTE} increases linearly with the number of users. This is because, with other parameters fixed, adding more

users reduces the per user average received energy. Therefore, a larger number of BS antennas are required to activate or saturate the harvesters. When $K = 1$, it is PTE-optimal to operate with M_{sat} antennas, since it maximizes the average harvested energy at the user. In a multi-user system, however, the condition $K \geq 1 + \frac{P_{\text{TX}}+P_{\text{FIX}}}{P_{\text{BS}}+\tilde{P}_{\text{CE}}+\tilde{P}_{\text{LP}}}$ informs the optimal solution. Here, $\frac{P_{\text{TX}}+P_{\text{FIX}}}{P_{\text{BS}}+\tilde{P}_{\text{CE}}+\tilde{P}_{\text{LP}}}$ is the ratio of the fixed power consumption to the scalable (circuit/computation) power consumption at the BS – normalized by the number of antennas. Note that this condition can be equivalently expressed as a cubic inequality in K as

$$\frac{2B}{S\kappa_{\text{BS}}}K^3 + \frac{B}{S\kappa_{\text{BS}}}K^2 + \left(P_{\text{BS}}\frac{3B}{S\kappa_{\text{BS}}}\right)K - (P_{\text{BS}} + P_{\text{TX}} + P_{\text{FIX}}) \geq 0. \tag{4.22}$$

Under some realistic assumptions, I obtain some useful insights from this relation. Typically, $\frac{P_{\text{TX}}+P_{\text{FIX}}}{P_{\text{BS}}+\tilde{P}_{\text{CE}}+\tilde{P}_{\text{LP}}} \approx \frac{P_{\text{TX}}+P_{\text{FIX}}}{P_{\text{BS}}}$ since the computational power consumption is usually much smaller than the antenna power consumption. This means that when the scalable power consumption exceeds the fixed power consumption, i.e., $P_{\text{BS}} > P_{\text{TX}} + P_{\text{FIX}}$, it is PTE-optimal to operate with the fewest possible (M_{act}) antennas. This is because the improvement in the harvested energy due to any additional antennas will be overshadowed by the increase in the BS power consumption. Conversely, when the fixed power consumption dominates the scalable power consumption *and* $K < 1 + \frac{P_{\text{TX}}+P_{\text{FIX}}}{P_{\text{BS}}}$, it is optimal to operate with M_{sat} antennas as it maximizes the net harvested energy.

Optimal K

I now characterize the number of users K^*_{PTE} required to optimize the power transfer efficiency, assuming the other parameters to be fixed. In a multi-user system,

there is a certain number of users a BS can simultaneously support. If a BS exceeds this limit, none of the harvesters will be activated due to insufficient received power. I can express this quantity $K_{\max}$ in terms of the system parameters as $K_{\max} = \left\lfloor \frac{M-1}{\frac{\theta_{\text{act}}}{P_{\text{dl}}\beta}-1} \right\rfloor$. Similarly, I define $K_{\text{sat}} = \left\lfloor \frac{M-1}{\frac{\theta_{\text{sat}}}{P_{\text{dl}}\beta}-1} \right\rfloor$ as the maximum number of allowed users such that each harvester operates in the saturated mode. The maximum sum harvested power $BK\bar{\delta}$ in the saturated mode is given by $K_{\text{sat}}\eta_{\text{EH}}\theta_{\text{sat}}$. Depending on the system parameters, serving more than K_{sat} users may decrease the total harvested power due to a reduction in the per-user harvested power in the non-saturated mode.

Lemma 60 Let us define $K^*_{\text{act}} = \min\left\{K_{\max}, \tilde{K}\right\}$ where $\tilde{K}$ is either the integer floor or the integer ceiling of $(M-1)\left[1+\sqrt{1+\frac{4}{(M-1)\dot{P}_{\text{CE}}}\left[\frac{P_{\text{TX}}+P_{\text{FIX}}+MP_{\text{BS}}}{M-1}-\dot{P}_{\text{LP}}\right]}\right]$, and $K^*_{\text{sat}} = \min\left\{K_{\text{sat}}, \hat{K}\right\}$ where $\hat{K}$ is either the integer floor or the integer ceiling of $\sqrt{\frac{P_{\text{TX}}+P_{\text{FIX}}+MP_{\text{BS}}}{\dot{P}_{\text{CE}}}}$. Here, $\dot{P}_{\text{CE}} = \frac{2MB}{S\kappa_{\text{BS}}}$ and $\dot{P}_{\text{LP}} = \frac{3MB}{S\kappa_{\text{BS}}}$ respectively denote the power required for channel estimation and precoding in a single-user system. With an M-antenna BS, the PTE-optimal number of users K^*_{PTE} is

$$K^*_{\text{PTE}} = \begin{cases} K^*_{\text{sat}}, & K^*_{\text{sat}} > \frac{[K^*_{\text{act}}+M-1]\beta P_{\text{dl}}}{\theta_{\text{sat}}} \frac{(K^*_{\text{sat}})^2\dot{P}_{\text{CE}}+K^*_{\text{sat}}\dot{P}_{\text{LP}}+P_{\text{TX}}+P_{\text{FIX}}+MP_{\text{BS}}}{(K^*_{\text{act}})^2\dot{P}_{\text{CE}}+K^*_{\text{act}}\dot{P}_{\text{LP}}+P_{\text{TX}}+P_{\text{FIX}}+MP_{\text{BS}}} \\ K^*_{\text{act}}, & \text{else} \end{cases} \tag{4.23}$$

Proof: See Appendix. □

The condition $K^*_{\text{sat}} > \frac{[K^*_{\text{act}}+M-1]\beta P_{\text{dl}}}{\theta_{\text{sat}}}$ implies that the aggregate user harvested power in the saturated mode exceeds that in the non-saturated mode. The fraction

$$\frac{(K^*_{\text{sat}})^2\dot{P}_{\text{CE}}+K^*_{\text{sat}}\dot{P}_{\text{LP}}+P_{\text{TX}}+P_{\text{FIX}}+MP_{\text{BS}}}{(K^*_{\text{act}})^2\dot{P}_{\text{CE}}+K^*_{\text{act}}\dot{P}_{\text{LP}}+P_{\text{TX}}+P_{\text{FIX}}+MP_{\text{BS}}}$$

is the ratio of the BS power consumption in the two modes. When the condition in (4.23) holds, it is PTE-optimal to operate the system in the saturated mode since serving more (than K^*_{sat}) users not only increases the BS power consumption, but also reduces the sum harvested power if the harvesters operate in the non-saturated mode. Under realistic values of the power consumption model, however, PTE typically improves as more users are added to the system. This is because the sum power delivered to the users grows with K, despite a decrease in the per-user harvested power. In contrast, the BS power consumption registers only a minor increase since the computational power is negligible compared to the hardware/transmit power. Therefore, it is PTE-optimal to serve the maximum allowed $K^*_{\text{PTE}} = K_{\max}$ users in typical systems.

4.5.2.2 Imperfect CSI

The PTE formulation for the case of imperfect CSI is similar to that of perfect CSI. It is, however, analytically challenging to derive the PTE-optimal solution for this case. Because the two solutions will be qualitatively similar, I do not elaborate this case further. I use simulation results in the following subsection to corroborate this observation.

4.5.3 Simulation Results

I now present the simulation results based on the analysis conducted in this section. I set the carrier frequency $f_c = 1.8$ GHz, coherence time $T_{\text{c}} = 180$ ms, coherence bandwidth $B_{\text{c}} = 10$ kHz, frame size $S = 1800$ symbols, system bandwidth

$B = 1$ MHz, BS transmit power $P_{\text{dl}} = 10$ W, noise power spectral density $\sigma^2 = -174$ dBm/Hz, BS computational efficiency $\kappa_{\text{BS}} = 20 \times 10^9$ flops/W [106], BS PA efficiency $\eta_{\text{PA}}^{\text{BS}} = 0.39$ [113], user PA efficiency $\eta_{\text{PA}}^{\text{EH}} = 0.3$ [113], BS RF chain power consumption $P_{\text{BS}} = 1$ W [113], BS fixed power consumption $P_{\text{FIX}} = 1$ W [113], EH conversion efficiency $\eta_{\text{EH}} = 0.5$, EH activation threshold $\theta_{\text{act}} = 10$ μW, EH saturation threshold $\theta_{\text{sat}} = 1$ mW, energy splitting parameter $\xi = 0.1$, path-loss exponent $\alpha = 3.2$, path-loss intercept $C = 1.76 \times 10^{-4}$ (for a reference distance of 1 m), $r_{\min} = 5$ m, and $r_{\max} = 20$ m, unless noted otherwise. I set $\alpha_{\text{Tr}} = \frac{K}{S}$, $\alpha_{\text{WET}} = 1 - \alpha_{\text{Tr}}$, and $\alpha_{\text{WIT}} = 0$.

Average harvested power vs. M

In Fig. 4.2, I examine how the average harvested power $B\bar{\delta}_i$ at a user varies as a function of the number of BS antennas M and users K. I consider the ideal case where the BS has perfect channel knowledge, and the realistic case where it has imperfect channel knowledge due to LS/MMSE estimation. I obtain the analytical (anl) results using Lemma $55 - 56$, and the simulation (sim) results using Monte Carlo simulations for 10^4 trials. I include the results for both single-user ($K = 1$) and multi-user systems ($K = 2$).

I can draw several useful insights from Fig. 4.2. First, with K fixed and $M \geq M_{\text{act}}$ (which is 7 for $K = 1$ and 13 for $K = 2$), the average harvested power increases with M, until the harvester saturates. For example, for $K = 1$, the harvested power saturates at $M = M_{\text{sat}} = 1089$ antennas (and at $M = 2177$ antennas for $K = 2$ which is not shown). I caution that this trend will not hold when M/K is fixed, as the harvested power remains almost constant as M and K are increased (Corollary

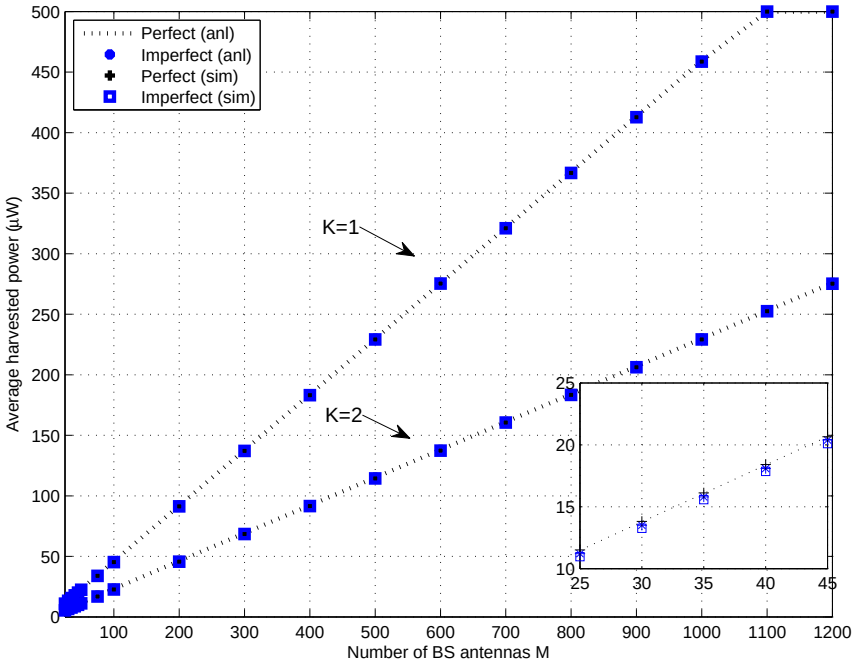

Figure 4.2: The average harvested power $B\bar{\delta}_i$ increases with the number of BS antennas M, and decreases with the number of users K. The inset shows a zoomed-in version of the curves for $K = 1$. Imperfect channel knowledge (LS/MMSE channel estimation) causes a minor degradation versus perfect channel knowledge. Simulation-based (sim) results validate the analytical (anl) results.

49). Second, adding more users reduces the harvested energy at each user. This is due to a reduction in the energy beamformed at each user. Third, imperfect channel knowledge causes only a minor loss in the harvested energy. This suggests that the insights drawn with perfect channel knowledge may be applicable to realistic scenarios with imperfect channel knowledge. Finally, the simulation-based results validate the analysis conducted in this section.

PTE vs. M

In Fig. 4.3, I plot the power transfer efficiency versus M for single-user and multi-user systems. It reveals how PTE behaves in terms of key system parameters, confirming the insights drawn in Lemma 58. First, I observe that there is an optimal M that maximizes the PTE. In a single-user case, it is optimal to operate with the maximum possible antennas M_{sat} in the linear regime, beyond which the PTE tends to decrease. In a multi-user system, this is not necessarily the case. For example, in the considered multi-user case $K = 40$, the PTE is maximized using the fewest possible M_{act} antennas. This is because, for this example, the boost in harvested power due to additional antennas is overshadowed by the increase in the BS circuit power consumption. With fewer than M_{act} antennas, the PTE is zero as the received power fails to meet the activation threshold. Second, I observe that imperfect channel knowledge results in a minor degradation in PTE, which is more evident in the multi-user scenario. Moreover, imperfect knowledge requires a larger number of antennas to activate the system compared to the ideal case with perfect channel knowledge. Third, I observe that multi-user system yields a higher PTE than the single-user system. Though the individual harvested power is reduced, the sum power increases as more users are added to the system. This trend holds as long as the number of users do not exceed $K_{\max}$, beyond which the individual harvested power – and therefore the PTE – drops to zero. This trend is in line with Lemma 60.

Optimizing energy splitting parameter ξ

I now consider the effective harvested power at a user, after discounting the amount used for uplink pilot transmission (see Remark 57). In Fig. 4.4, I set $M = 500$, $S = 100$, $P_{\text{dl}} = 20$ W, $r_{\max} = 50$ m, and plot the effective harvested power at a user versus the energy splitting parameter ξ for various values of K. I recall that the energy splitting parameter ξ is the fraction of the harvested energy that a user reserves for pilot transmission. For the considered system, I observe that dedicating around 1% of the harvested power maximizes the effective power available to the user. I note that this fraction will be even smaller in systems with a larger frame size. Moreover, deviating from this optimal value may cause a significant degradation in effective harvested power: allocating a smaller fraction will reduce the uplink transmit power, decreasing the channel estimation accuracy at the BS. The resulting BS transmission based on the inaccurate channel knowledge sacrifices the beamforming gain, reducing the harvested power at the user. Conversely, allocating more energy for uplink training will improve the harvested power. This improvement, however, is insufficient to justify the underlying increase in the uplink transmit power. As a result, the effective harvested power will reduce nonetheless. This trend is in line with the discussion in Remark 57. I further note that the optimal value is insensitive to the number of users. This suggests that a user does not need to tune this parameter when other users enter/leave the system. Finally, I observe that the effective harvested power at a user decreases as more users are being served. As explained earlier, this is due to a reduction in the energy beamformed to each user.

4.6 Wireless Energy and Information Transfer

In this section, I consider wireless-powered communications where the BS charges users in the downlink, and the users leverage the harvested energy to communicate with the BS on the uplink. This is different from the previous section where no information transfer was considered on the uplink.

4.6.1 Uplink Achievable Rate

I now provide analytical expressions for the uplink achievable rate for a wirelessly powered user. Note that the total harvested energy is used for sending both training and data symbols during uplink transmission. As defined previously, $\xi_i \in (0,1)$ is the fraction of the harvested energy $\bar{\delta}_i$ at a user i reserved for the uplink pilot transmission, while the remaining fraction $1-\xi_i$ of the harvested energy is used for uplink data transmission. I assume that a user i transmits uplink data symbols with an average energy $p_{\text{ul}}^i = \frac{\eta_{\text{PA}}^{\text{EH}}(1-\xi_i)\bar{\delta}_i}{\alpha_{\text{WIT}}}$ (in joules/symbol). Here, $\eta_{\text{PA}}^{\text{EH}} \in (0,1]$ denotes the user PA efficiency. At the users, while I explicitly model only the transmit power consumption, any additional power consumption (e.g., due to computation) could be equivalently handled by tuning (i.e., further reducing) the parameter $\eta_{\text{PA}}^{\text{EH}}$. While I account for the training overhead, I ignore the loss in harvested power due to channel estimation errors. This simplifies the analysis, and could be justified since the imperfect channel knowledge causes only a minor loss in the harvested power (Section 4.5.3). For uplink detection, I assume that the BS uses a Zero-forcing (ZF) receive filter. Leveraging the convexity of the function $\log(1+x^{-1})$ where $x > 0$, I use Jensen's inequality to obtain a lower bound on the ergodic uplink achievable rate,

and call it the achievable rate in the ensuing analysis [112].

Lemma 61 With an M-antenna BS serving $K < M$ users, the uplink achievable rate R_i for a remotely-powered user i is given by

$$R_i = \begin{cases} 0 & M < M_{\text{act},i} \\ \alpha_{\text{WIT}} B \log_2 \left(1 + (1-\xi_i)\,\beta_i\,\eta_{\text{PA}}^{\text{EH}}\,\frac{\eta_{\text{EH}}\bar{\gamma}_i}{\alpha_{\text{WIT}}\sigma^2}\,(M-K)\right), & M_{\text{act},i} \leq M < M_{\text{sat},i} \\ \alpha_{\text{WIT}} B \log_2 \left(1 + (1-\xi_i)\,\beta_i\,\eta_{\text{PA}}^{\text{EH}}\,\frac{\eta_{\text{EH}}\theta_{\text{sat}}}{B\alpha_{\text{WIT}}\sigma^2}\,(M-K)\right), & M \geq M_{\text{sat},i} \end{cases} \tag{4.24}$$

where $\bar{\gamma}_i$ is the average received energy as defined in Lemma 46. When $\zeta_i = \frac{1}{K}$, the achievable rate for $M_{\text{act},i} \leq M < M_{\text{sat},i}$ can be further simplified to

$$R_i = \alpha_{\text{WIT}} B \log_2 \left(1 + \rho_i\,[M-K]\left[1 + \frac{M-1}{K}\right]\right), \tag{4.25}$$

where

$$\rho_i \triangleq \frac{(1-\xi_i)\,p_{\text{dl}}\,\alpha_{\text{WET}}\,\eta_{\text{EH}}\,\eta_{\text{PA}}^{\text{EH}}\,\beta_i^2}{\alpha_{\text{WIT}}\sigma^2} = \frac{P_{\text{dl}}\,(1-\xi_i)\;\eta_{\text{EH}}\,\eta_{\text{PA}}^{\text{EH}}\,\beta_i^2}{B\alpha_{\text{WIT}}\sigma^2}. \tag{4.26}$$

captures the effect of the system parameters (other than M and K) on the uplink SNR.

Proof: This follows by noting that $\frac{p_{\text{ul}}^i}{\sigma^2} = \frac{\eta_{\text{PA}}^{\text{EH}}(1-\xi_i)\bar{\delta}_i}{\alpha_{\text{WIT}}\sigma^2}$ is the uplink (transmit) signal-to-noise ratio (SNR) for user i, applying Lemma 1, and invoking the result in [112, Proposition 3]. □

I note that the uplink rate is expressed in terms of the downlink transmit symbol energy p_{dl} since the user exploits the harvested energy to power its uplink transmission. This further means that the uplink communication link will typically operate in the low-SNR regime due to the limited energy available at the user. This case is further elaborated in the following corollary.

Corollary 62 Let us consider a user in the linear mode such that $M_{\text{act},i} \leq M < M_{\text{sat},i}$. In the low-SNR regime, i.e., when $R_i \approx \alpha_{\text{WIT}} B \rho_i (M-K)\left(1+\frac{M-1}{K}\right)$, the uplink achievable rate is the most susceptible to path loss — being proportional to the *square* of the large-scale channel gain β_i. Fortunately, additional antennas are the most beneficial also in this regime as the rate approximately grows with the square of M.

Proof: This follows from (4.26) and by noting that $\log(1+x) = x + \mathcal{O}(x^2)$ for $|x| \leq 0.5$. □

Remark 63 The achievable rate reports a faster growth with M in the non-saturated mode than the saturated mode. This follows from (4.24) by noting that the effective uplink SNR grows approximately with the square of M in the non-saturated mode, but only linearly in the saturated mode. In the linear mode, more antennas help improve the downlink energy transfer as well as the uplink information detection. This is not the case in the saturated mode where only the uplink detection benefits from more antennas. I further note that, unlike the harvested power, the achievable rate does *not* saturate in the saturated mode.

4.6.2 Energy Efficiency

I now characterize the total energy efficiency of the considered system by leveraging the power consumption model used in (4.20). Similar to Section 4.5.2, I set $\beta_i \; \forall \; i \in \mathcal{I}_K$ to the average $\mathbb{E}[\beta_i] = C\mathbb{E}[d_i^{-\alpha}] \triangleq \beta$, where $\mathbb{E}[d_i^{-\alpha}]$ is given in Section 4.3. I assume all users have the same value for the energy splitting parameter $\xi_i \triangleq \xi$

such that $\rho_i \triangleq \rho$. With these simplifying assumptions, the users achieve an identical average rate, i.e., $R_i \triangleq R \; \forall \; i \in \mathfrak{I}_K$. I define the total energy efficiency (EE) of the overall system (in bits/joule) as the ratio of the average uplink sum rate to the total average power consumed, i.e.,

$$\begin{aligned} \mathrm{EE}\,(M,K) &= \frac{KR}{P_{\mathrm{TX}} + P_{\mathrm{c}}} \\ &= \frac{KR}{P_{\mathrm{TX}} + P_{\mathrm{FIX}} + MP_{\mathrm{BS}} + P_{\mathrm{CE}} + P_{\mathrm{LP}} + P_{\mathrm{DEC}}KR} \end{aligned} \tag{4.27}$$

where the power consumption model is similar to (4.20) except for two components: i) P_{LP} is modified to account for additional BS linear processing, i.e., in addition to the power required for computing the downlink precoder $\left(\frac{3MKB}{S\kappa_{\mathrm{BS}}}\right)$, it also includes the power required for computing the uplink ZF filter $\left(\frac{B(\frac{K^3}{3}+3MK^2+MK)}{S\kappa_{\mathrm{BS}}}\right)$ once per coherence block, and for evaluating a matrix-vector multiplication for each data symbol $\frac{2\alpha_{\mathrm{WIT}}MKB}{\kappa_{\mathrm{BS}}}$ [113, 119]; ii) $P_{\mathrm{DEC}}KR$ is introduced to model the power consumed in decoding the received data, where P_{DEC} parameterizes the BS decoder power consumption (in W/bit/s) [113]. These terms were absent in (4.20) since no uplink data transmission was considered. I note that the computational power consumption is usually negligible compared to the antenna power consumption in the large-antenna regime. Moreover, the uplink transmit power, which is a fraction of the average harvested power, only appears in the numerator (via the expression for the achievable rate R). This is because the energy harvesting users do not have any power source except for the wireless energy delivered by the BS.

Remark 64 I observe from (4.27) that EE eventually vanishes in the large M regime. This is because the data rate in the numerator grows only logarithmically whereas

the power consumption in the denominator grows linearly with M.

Energy Efficiency Optimization

I now characterize the optimal BS transmit power that maximizes the total energy efficiency for a given number of antennas and users.

Lemma 65 When the harvesters operate in the non-saturated mode, the EE-optimal transmit power at the BS is given by $P_{\mathrm{dl}}^{*} = \alpha_{\mathrm{WET}} B p_{\mathrm{dl}}^{*}$ where

$$p_{\mathrm{dl}}^{*} = \frac{e^{1+\mathrm{W}\left[\frac{\eta_{\mathrm{PA}}^{\mathrm{BS}}\tilde{\rho}(\tilde{C}+M\tilde{D})(M-K)\left(1+\frac{M-1}{K}\right)}{eB\alpha_{\mathrm{WET}}}-\frac{1}{e}\right]}-1}{\tilde{\rho}\,(M-K)\left(1+\frac{M-1}{K}\right)}, \tag{4.28}$$

and $\mathrm{W}[\cdot]$ is the Lambert-W function. The constants $\tilde{\rho} = \frac{(1-\xi_i)\,\alpha_{\mathrm{WET}}\,\eta_{\mathrm{EH}}\,\eta_{\mathrm{PA}}^{\mathrm{EH}}\,\beta_i^2}{\alpha_{\mathrm{WIT}}\sigma^2}$, $\tilde{C} = P_{\mathrm{FIX}} + \frac{BK^3}{3S\delta_{\mathrm{BS}}}$, and $\tilde{D} = P_{\mathrm{BS}} + \frac{2B}{\delta_{\mathrm{BS}}}(1+\frac{2}{S})K + \frac{3B}{S\delta_{\mathrm{BS}}}K^2$.

Proof: See Appendix. □

Remark 66 The expression in (4.28) is applicable when the harvesters operate in the linear mode. When $M < M_{\mathrm{act}}$, I should increase the BS transmit power to activate the harvesters, resulting in a non-zero EE i.e., set $P_{\mathrm{dl}} = \frac{\theta_{\mathrm{act}}K}{\beta(M+K-1)}$. Similarly, when P_{dl}^{*} satisfies $M > M_{\mathrm{sat}}$, reducing the transmit power to be at least as small as $\frac{\theta_{\mathrm{act}}K}{\beta(M+K-1)}$ helps improve the energy efficiency. This is because once the harvesters get saturated, the excess power only increases the power consumption without bringing any improvement in the achievable rate. Using this principle, Algorithm 2 provides a procedure for jointly selecting the number of antennas and the transmit power for energy efficient operation.

Algorithm 2 EE-optimal selection of P_{dl} and M

procedure
Initialize $M \leftarrow K+1, \mathrm{flag} \leftarrow 0, \mathrm{EE}_{\mathrm{old}} \leftarrow 1$
  While flag $= 1$
  Update:
  $p_{\mathrm{act}} \leftarrow \frac{K\theta_{\mathrm{act}}}{\alpha_{\mathrm{WET}} B\beta(M+K-1)}$, $p_{\mathrm{sat}} \leftarrow \frac{K\theta_{\mathrm{sat}}}{\alpha_{\mathrm{WET}} B\beta(M+K+1)}$
  $p_{\mathrm{dl}} \leftarrow \frac{e^{1+\mathrm{W}\left[\frac{\eta_{\mathrm{PA}}^{\mathrm{BS}}\tilde{\rho}(\tilde{C}+M\tilde{D})(M-K)\left(1+\frac{M-1}{K}\right)}{eB\alpha_{\mathrm{WET}}}-\frac{1}{e}\right]-1}}{\tilde{\rho}(M-K)\left(1+\frac{M-1}{K}\right)}$
  $M_{\mathrm{act}} \leftarrow \left\lceil \frac{K\theta_{\mathrm{act}}}{\alpha_{\mathrm{WET}} B\beta p_{\mathrm{dl}}} - (K-1) \right\rceil$,
  $M_{\mathrm{sat}} \leftarrow \left\lfloor \frac{K\theta_{\mathrm{sat}}}{\alpha_{\mathrm{WET}} B\beta p_{\mathrm{dl}}} - (K-1) \right\rfloor$
  If $M > M_{\mathrm{sat}}$
    $p_{\mathrm{dl}} \leftarrow \min\left(p_{\mathrm{sat}}, p_{\mathrm{dl}}\right)$
  else
    $p_{\mathrm{dl}} \leftarrow \max\left(p_{\mathrm{act}}, p_{\mathrm{dl}}\right)$
  end
  Compute energy efficiency $\mathrm{EE}(M, p_{\mathrm{dl}})$
  If $\mathrm{EE}_{\mathrm{old}} > \mathrm{EE}(M, p_{\mathrm{dl}})$
    flag $\leftarrow 0$
  else
    $\mathrm{EE}_{\mathrm{old}} \leftarrow \mathrm{EE}(M, p_{\mathrm{dl}})$
    $M \leftarrow M+1$
  end
 end
  $P_{\mathrm{dl}}^{*} \leftarrow \alpha_{\mathrm{WET}} p_{\mathrm{dl}} B$, $M^{*} \leftarrow M$

4.6.3 Simulations

I now present simulation results to verify the analytical insights in this section. The simulation parameters are the same as described in Section 4.5.3, unless noted otherwise. I set $P_{\text{FIX}} = 18$ W (I expect an increased fixed power consumption at the BS compared to Section 4.5.3 since it now has to deal with data reception on the uplink similar to a traditional BS) [113], $P_{\text{DEC}} = 10^{-9}$ W/bits/sec [113], $r_{\min} = 5$ m, $r_{\max} = 50$ m, and $K = 2$. In the following figures, "ideal" curve is for ideal (linear) energy harvesters with $\theta_{\text{act}} \to 0$ and $\theta_{\text{sat}} \to \infty$. Similarly, "practical" curve corresponds to the case where practical energy harvesters are deployed in a system optimized for ideal energy harvesters.

EE-optimal BS transmit power vs. M: In Fig. 4.5, I plot the EE-optimal transmit power against M for both ideal and practical energy harvesters. I note that the EE-optimal transmit power selection assuming ideal energy harvesters could be very misleading for practical energy harvesters. Let us first consider the case when M is large (say > 2000 in Fig. 4.5): it is EE-optimal to reduce the transmit power with M for practical harvesters. This helps avoid the energy wastage when the energy harvesters operate in the saturated mode. This is contrary to the ideal case where the EE-optimal transmit power increases with M. Let us now consider the case when M is small (say < 90): it is EE-optimal to use a larger transmit power than the ideal case. A sufficient increase in the transmit power helps activate the nodes, resulting in a nonzero data rate and EE. I also note that the transmit power selection based on Algorithm 2 closely approximates the optimal solution. Similarly, Fig. 4.6 shows how the per-antenna transmit power scales with M. Unlike the total transmit power

which may increase with M, the EE-optimal per-antenna transmit power typically reduces as M is increased.

Maximal EE vs. M: In Fig. 4.7, I plot the maximal EE versus M. I note that a system designed assuming energy harvester to be ideal could result in severe performance degradation in the presence of practical energy harvesters. For example, when M is small (say < 90 in Fig. 4.5 and 4.7), the EE will be zero for practical energy harvesters. This is because the transmit power, though EE-optimal for an ideal harvester, is insufficient to wake up a practical harvester. With a practical harvester, EE-optimality warrants increasing the transmit power, so that the uplink rate and the EE could be improved. Conversely, when M is large (say > 2000 in Fig. 4.5 and 4.7), the maximal EE is attained by sufficiently reducing the transmit power to avoid saturating the harvesters. I note that the EE achieved using Algorithm 2 closely approximates the optimal solution. In line with Remark 64, EE will eventually vanish in the large antenna regime due to excessive power consumption. Finally, there exists an optimal M that maximizes the EE. I further observe that the EE-optimal operating point indeed lies in the massive MIMO regime.

Uplink sum rate vs. M: In Fig. 4.8, I plot the uplink sum rate obtained using the EE-optimal policy considered in the previous figures. In contrast to the EE, the sum rate improves monotonically with M. Further, the rate grows with M at a slower pace in the saturated mode (Remark 63). This is because the harvested power does not increase with M in the saturated mode, leaving only the uplink detection to benefit from additional BS antennas.

4.7 Conclusions

In this chapter, I optimized the system-level power transfer efficiency and energy efficiency of wireless energy and/or information transfer in a multi-user network, where a BS equipped with a massive antenna array remotely powers multiple single-antenna energy harvesting users. Using a piecewise linear model for the energy harvesters, I derived the average harvested power at a user in terms of the system parameters. I then analyzed the power transfer efficiency of the overall system, while using a scalable power consumption model at the BS. I found that the overall PTE may increase or decrease by adding more BS antennas, depending on the system parameters such as the number of users, energy harvester specification, and the transmit/circuit power consumption at the BS. I also found that it tends to improve by adding more users to the system. I analytically characterized the PTE-optimal values for the number of BS antennas and users. The results suggest that it is PTE-optimal to operate the system in the massive antenna regime.

I also studied the energy efficiency of the overall system when the users communicate with the BS using the harvested energy. I characterized the EE-optimal BS transmit power for energy efficient system operation. The analysis, aided by simulations, revealed several useful insights. While the energy efficiency eventually vanishes as the number of antennas becomes large, results suggest that it is energy efficient to operate the system in the massive MIMO regime. Moreover, increasing the transmit power helps improve the energy efficiency as the number of antennas is increased.

Appendix

Proof of Lemma 50: Let us consider a user i transmitting a training signal over τ symbols with an average symbol energy $p_{\mathrm{Tr},i}$. Assuming the BS uses MMSE channel estimation, the mean received energy $\bar{\gamma}_i^{\mathrm{I}} = \alpha_{\mathrm{WET}}\,\mathbb{E}\left[|y_i|^2\right]$ (where y_i follows from (4.1)) can be expressed as

$$\bar{\gamma}_i^{\mathrm{I}} = A_1 M \left[1 - \frac{M-1}{M}\frac{1}{1+\frac{\beta_i \tau p_{\mathrm{Tr},i}}{\sigma^2}}\right] + A_2. \tag{4.29}$$

Here, similar to [111, Appendix B], I have leveraged the independence of random vectors $\{\mathbf{g}_i\}_i$, and the fact that the variance of the estimation error is $\frac{\beta_i}{1+\frac{\beta_i \tau p_{\mathrm{Tr},i}}{\sigma^2}}$ (see discussion following (4.14)). I recall that $\tau p_{\mathrm{Tr},i} = \eta_{\mathrm{PA}}^{\mathrm{EH}} \xi_i \bar{\delta}_i^{\mathrm{I}} S$ since the user employs a fraction ξ_i of the per-frame average harvested energy for uplink transmission. For the non-saturated mode, I apply Lemma 56 and substitute $\bar{\delta}_i^{\mathrm{I}} = \eta_{\mathrm{EH}} \bar{\gamma}_i^{\mathrm{I}}$ to obtain a quadratic equation in $\bar{\gamma}_i^{\mathrm{I}}$. The solution of this quadratic equation yields (4.9). Similarly, I substitute $\bar{\delta}_i^{\mathrm{I}} = \frac{\eta_{\mathrm{EH}} \theta_{\mathrm{sat}}}{B}$ for the saturated mode to obtain (4.10).

Proof of Lemma 58: First, note that the PTE is sub-optimal when $M \notin [M_{\mathrm{act}}, M_{\mathrm{sat}}]$, as it is zero for $M < M_{\mathrm{act}}$ and is upper bounded by $\mathrm{PTE}\left(M_{\mathrm{sat}}, K\right)$ for $M > M_{\mathrm{sat}}$. The next step is to solve the linear fractional program $\max\limits_{x} f(x) = \max\limits_{x} \frac{N_1 x + N_2}{D_1 x + D_2}$ under the constraint $x \in [M_{\mathrm{act}}, M_{\mathrm{sat}}]$, where $N_1 = BKA_1$, $N_2 = BKA_2$, $D_1 = P_{\mathrm{BS}} + \tilde{P}_{\mathrm{CE}} + \tilde{P}_{\mathrm{LP}}$, and $D_2 = P_{\mathrm{TX}} + P_{\mathrm{FIX}}$. I note that $f(x)$ is quasilinear and monotonic in x [119, Section 4.3], [120]. When $N_1 D_2 > N_2 D_1$ such that $\frac{\partial}{\partial x} f(x) > 0$, $x^* = M_{\mathrm{sat}}$ as $f(x)$ is an increasing function of x. Conversely, when $N_1 D_2 \leq N_2 D_1$, $x^* = M_{\mathrm{act}}$ maximizes $f(x)$.

Proof of Lemma 60: The proof follows by noting that the function $f(x) = \frac{N_1 x + N_2}{D_1 x^2 + D_2 x + D_3}$ is quasiconcave for $x \in \mathbb{R}$ when the superlevel sets $\mathcal{S}_\nu = \{x : f(x) \geq \nu\}$ are convex for any $\nu \in \mathbb{R}$ [119, Section 3.4]. Using differentiation, I can prove the convexity of the superlevel sets for nonnegative values of $\{N_i\}_{i=1,2}$ and $\{D_i\}_{i=1,2,3}$, where $D_1 = \dot{P}_{\mathrm{CE}}$, $D_2 = \dot{P}_{\mathrm{LP}}$, and $D_3 = P_{\mathrm{TX}} + P_{\mathrm{FIX}} + MP_{\mathrm{BS}}$. $N_1 = \eta_{\mathrm{EH}}\theta_{\mathrm{sat}}$ and $N_2 = 0$ in the saturated mode, whereas $N_1 = \eta_{\mathrm{EH}} P_{\mathrm{dl}} \beta$ and $N_2 = \eta_{\mathrm{EH}} P_{\mathrm{dl}} \beta \left(M - 1\right)$ in the non-saturated mode. Solving $\frac{\partial}{\partial K} f(K) = 0$, I obtain the optimal K for the saturated (K^*_{sat}) or non-saturated mode (K^*_{act}), which follows from (i) the quasiconcavity of $f(K)$ since it is an increasing (or decreasing) function of K for $K < K^*$ (or $K > K^*$) where K^* is the stationary point of $f(K)$; and (ii) because $K \leq K_{\mathrm{sat}}$ and $K \leq K_{\max}$ in the saturated or non-saturated mode. Finally, the condition in (4.23) is obtained by comparing the maximal PTE in the saturated and non-saturated modes.

Proof of Lemma 65: The proof follows by casting the EE expression in (4.27) in the form $f(z) = \frac{g \log(1+bz)}{c + dz + h \log(1+bz)}$, where the constants $c, h \geq 0$, and $b, d, g > 0$. Using the quasiconcavity of the function $f(z)$, it was shown in [113, Lemma 3] that the optimal solution to the problem $\max\limits_{z > -\frac{1}{b}} f(z) = \frac{g \log(1+bz)}{c + dz + h \log(1+bz)}$ is given by $z^* = \frac{e^{\mathrm{W}\left[\frac{bc}{de} - \frac{1}{e}\right] + 1} - 1}{b}$, which completes the proof.

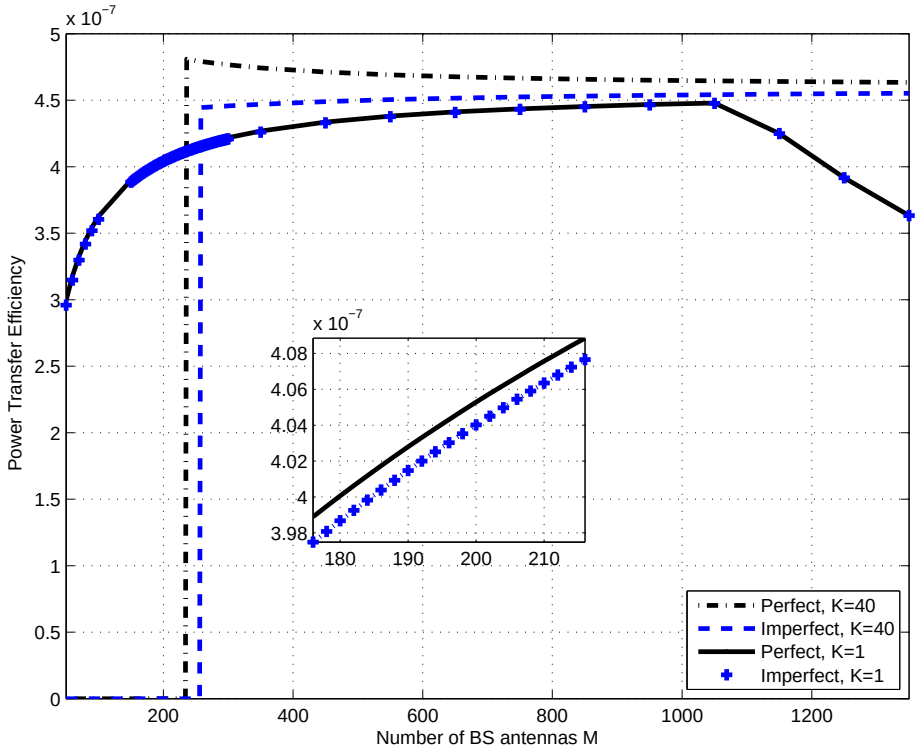

Figure 4.3: Power transfer efficiency PTE vs. the number of BS antennas M for $K = 1$ and $K = 40$ users. There is an optimal M that maximizes the PTE, as reported in Lemma 58: For single-user system, PTE is optimized by operating with maximum possible antennas in the linear regime. For the considered multi-user system, operating with fewest possible antennas maximizes the PTE. The inset shows a zoomed-in version of the curves for $K = 1$. Imperfect channel knowledge (LS/MMSE channel estimation) causes a minor degradation versus perfect channel knowledge.

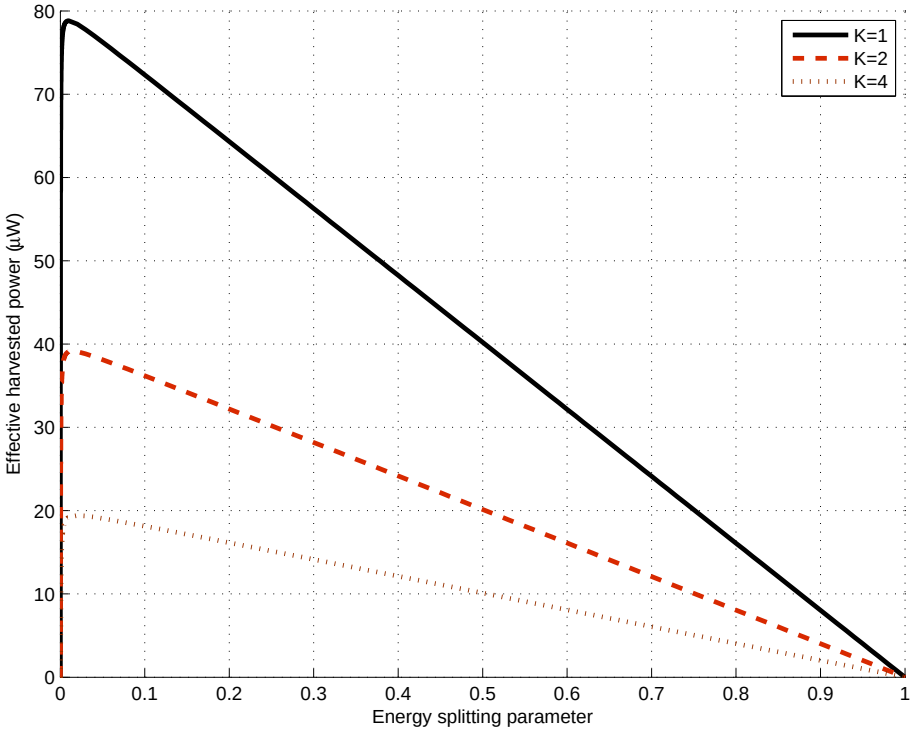

Figure 4.4: Effective harvested power vs. energy splitting parameter ξ for $M = 500$. A user can maximize the effective harvested power by allocating the right amount of harvested energy for uplink pilot transmission. The optimal value is not particularly sensitive to the number of users in the system. The harvested power decreases as more users are added to the system.

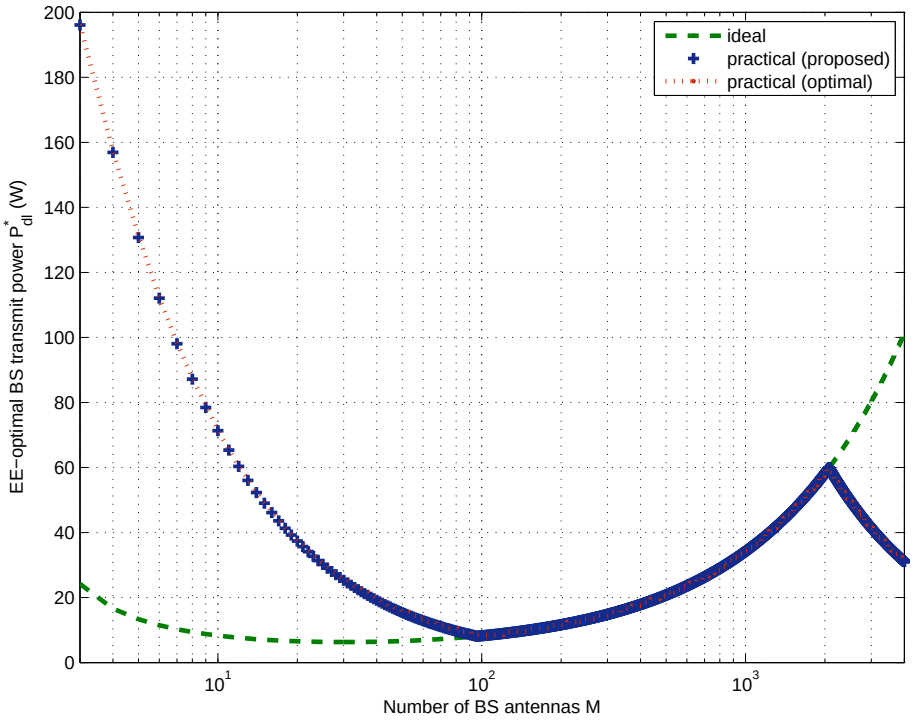

Figure 4.5: EE-optimal transmit power vs. the number of BS antennas for ideal as well as practical energy harvesters. The EE-optimal approach for the ideal (linear) case could be very misleading for the practical (nonlinear) case: It is EE-optimal to i) sufficiently increase the transmit power to wake up the users; and ii) decrease it in the saturated mode to avoid energy wastage. The proposed approach closely approximates the optimal solution.

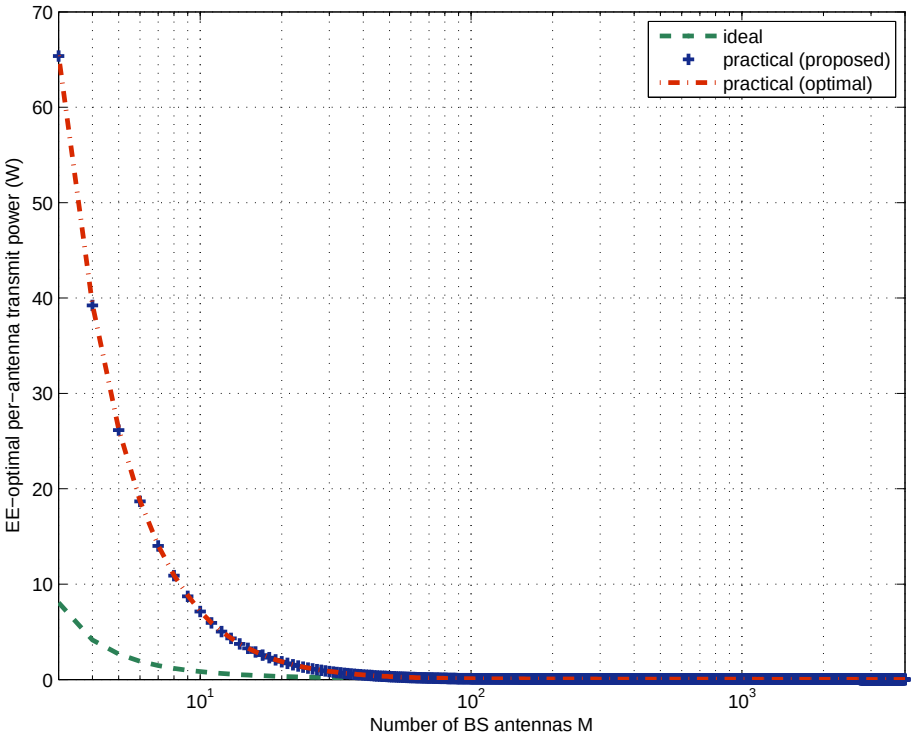

Figure 4.6: The EE-optimal per-antenna transmit power vs. the number of BS antennas. The per-antenna optimal transmit power tends to decrease with M for both ideal and practical cases.

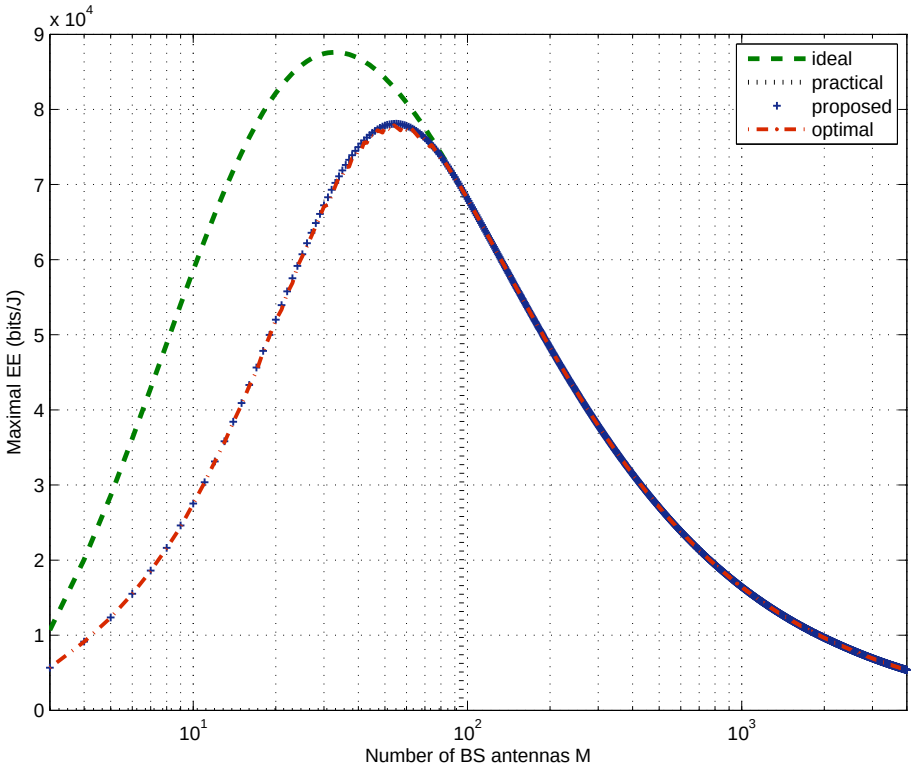

Figure 4.7: The maximal EE vs. the number of BS antennas. A comparison between "ideal" and "practical' shows the performance actually achieved with practical energy harvesters in a system designed for ideal (linear) energy harvesters. The EE-optimal approach for the ideal case could be very misleading for the practical case. Note that the proposed solution significantly improves the EE, and closely approximates the optimal solution. Moreover, there exists an optimal M that maximizes the EE.

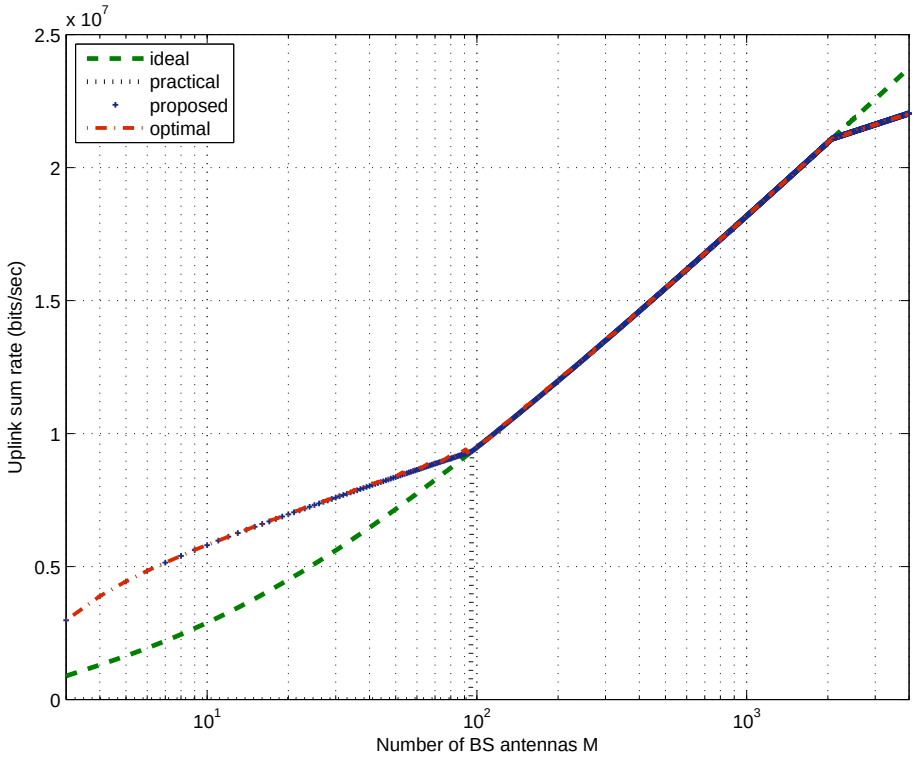

Figure 4.8: Uplink achievable rate vs. the number of BS antennas. The proposed solution yields uplink rate almost similar to that obtained using the EE-optimal solution. The rate increases monotonically with M even in the saturated mode due to improved uplink detection.

Chapter 5

Concluding Remarks

In this chapter, I conclude this dissertation with a summary of my contributions, followed by some potential research directions for future work.

5.1 Summary

This dissertation focused on the design and analysis of energy harvesting wireless communications systems. My broad goal was to investigate the performance of wireless-powered communications in the context of emerging technologies for 5G: IoT, mmWave and massive MIMO. First, I characterized the performance of a remotely-powered system in the finite blocklength regime. Using analytical expressions for the energy supply probability and the achievable rate as well as numerical simulations, I investigated the interplay between key system parameters such as the harvest blocklength, the transmit blocklength, the error probability, and the power ratio. For the case of a single power beacon, I showed that the harvest blocklength should be scaled proportionally to the transmit blocklength in order to maintain the ϵ-achievable rate. The rate of growth is characterized by the power ratio as well as the target error probability. Moreover, I derived closed-form expression for the optimal transmit power in the asymptotic blocklength regime. Numerical results show that using the

asymptotically optimal transmit power can substantially improve the achievable rate even in the finite blocklength regime. I also extended the analysis to a large-scale network with Poisson-distributed power beacons. Numerical results reveal that the performance is sensitive to the blocklength, confirming that the asymptotic analyses of wireless-powered systems fail to capture the behavior in the short packet regime.

In the second contribution, I analyzed the performance of wireless energy and information transfer to energy harvesting nodes powered by a mmWave cellular network. Using a stochastic geometry framework, I derived analytical expressions characterizing the performance of mmWave energy and information transfer in terms of system, channel, and network parameters. Simulation results were used to validate the accuracy of the derived expressions. Leveraging the analytical framework, I also provided useful network and device level design insights. For the connected case when the transmitter and receiver beams are aligned, results show that the energy coverage improves with narrower beams. In contrast, wider beams provide better energy coverage when the receivers are not aligned with a particular transmitter. This trade-off is evident in the more general scenario having both types of receivers, where there typically exists an optimal beamforming beamwidth that maximizes the network-wide energy coverage. Moreover, I found that several device-related parameters can significantly impact the system performance. For example, the performance can be substantially improved by optimizing over the power splitting ratio and by leveraging large antenna arrays. To allow using multiple antennas at the mmWave receivers while keeping the power consumption low, I proposed a low-power receiver architecture for mmWave energy and information transfer using antenna switches.

Simulation results show that the energy harvesting receiver performs well with the proposed architecture. Simulation results also reveal that mmWave cellular networks could potentially provide better energy coverage than lower frequency solutions.

In the third contribution, I characterized the system-level power transfer efficiency and energy efficiency of wireless energy and information transfer in a multi-user network, where a BS equipped with a massive antenna array remotely powers multiple single-antenna energy harvesting users. Using a piecewise linear model for the energy harvesters, I derived the average harvested power at a user in terms of the system parameters. I then analyzed the power transfer efficiency of the overall system, while using a scalable power consumption model at the BS. I found that the overall PTE may increase or decrease by adding more BS antennas, depending on the system parameters such as the number of users, the energy harvesting parameters, and the transmit/circuit power consumption at the BS. I also found that it tends to improve by adding more users to the system. I analytically characterized the PTE-optimal values for the number of BS antennas and the number of users. The results suggest that it is PTE-optimal to operate the system in the massive antenna regime. I also analyzed the system-level energy efficiency for the case where the users exploit the harvested energy to communicate with the BS. I derived the EE-optimal BS transmit power required for an energy efficient system operation. In the non-saturated mode, increasing the transmit power typically helps improve the energy efficiency as the number of antennas is increased. While the energy efficiency eventually vanishes as the number of antennas becomes large, results suggest that it is energy efficient to operate the system in the massive antenna regime.

5.2 Future Work

There are several possible directions for future research.

Wireless-powered communications with short packets In Chapter 2, I characterized the achievable rate of a remotely-powered communication system in the finite blocklength regime. The considered setup is applicable to many scenarios, but there is room to further extend the scope of this work. One such direction is to incorporate variable rate and variable power transmission in the analysis. This is nontrivial because adaptive transmission results in a different underlying communication channel. Because the finite-blocklength behaviour of a system strongly depends on the communication channel, the insights obtained in Chapter 2 for non-adaptive transmission may not be applicable to the adaptive case.

In Chapter 2, I assumed the available power at the energy harvester to be independent across the transmission frames. Depending on the transmitted codeword, it is possible to have some left-over or residual energy at the end of the data transmission phase. The independence assumption is plausible when the residual energy is dedicated to support other tasks at the harvester such as sensing and computation. It is equally interesting to analyze the case where the residual energy is saved to support future data transmissions. The ensuing analysis is nontrivial since the available transmit power, which is accumulated across transmission frames, is no longer independent across transmission frames. Another possible extension is to incorporate finite battery size in the analysis. It will also be beneficial to explicitly account for the sensing operation in the analysis.

Wireless-powered communications with mmWave In Chapter 3, I characterized the performance of mmWave wireless information and power transfer in an outdoor cellular network with building blockages. There are several possible directions for future work. For example, it will be useful to expand the scope of this work to other network scenarios such as mmWave ad hoc/wearable networks. This extension is nontrivial since it will require a different stochastic geometry framework to model the network topology and a different analytical model to entertain additional sources of signal blockages. In a wearable mmWave network, a major analytical challenge is to incorporate human-body blockage in the analysis. This is because the transmitter/receiver density will be coupled with the blockage density. For such networks, it will be useful to characterize the performance of wireless information and power transfer in terms of the system parameters such as network density, array size, and blockage/propagation conditions. In addition to the considered metrics (energy coverage probability and achievable rate), analyzing the performance from the perspective of other metrics such as power transfer efficiency or energy efficiency will be a welcome contribution.

Another promising direction is to incorporate additional practical limitations in the analysis. For example, Chapter 3 considered analog beamforming at the mmWave BS. The design and analysis of hybrid analog/digital architectures for mmWave wireless information and power transfer requires further research. Similarly, designing low-power mmWave receiver architectures for joint information and energy reception warrants more attention. Another possibility is to devise novel channel estimation algorithms tailored for mmWave wireless information and power transfer.

It will also be useful to incorporate the impact of training overhead in the analysis.

Wireless-powered communications with massive MIMO In Chapter 4, I characterized the power transfer efficiency and the energy efficiency of a wireless-powered system aided by massive MIMO. There are several possible directions to extend this work. I treated a single-cell network with a fixed topology under Rayleigh fading conditions. A natural extension is to include multi-cell scenarios with more general (Nakagami) fading conditions and to incorporate random geometries using tools from stochastic geometry. This may help establish the scaling behavior of the power transfer efficiency or energy efficiency with system parameters such as the number of antennas or the node density. The resulting insights may contribute towards the design of an energy efficient remotely-powered large-scale network.

Another useful extension is to incorporate backscatter communication in the analysis. This is because it enables remotely-powered communications while requiring minimal power consumption at the energy harvesting device. This, however, comes at the expense of a reduced communication range as the energy harvester simply reflects a portion of the incident signal to communicate information. This extension is also nontrivial since it requires a different modeling approach due to differences in the mode of data transmission and signal propagation. Finally, it will also be useful to devise optimal waveforms for each of the considered wireless-powered system.

Bibliography

[1] S. Ulukus, A. Yener, E. Erkip, O. Simeone, M. Zorzi, P. Grover, and K. Huang, "Energy harvesting wireless communications: A review of recent advances," *IEEE J. Sel. Areas Commun.*, vol. 33, no. 3, pp. 360–381, Mar. 2015.

[2] R. Vullers, R. van Schaijk, I. Doms, C. V. Hoof, and R. Mertens, "Micropower energy harvesting," *Solid-State Electronics*, vol. 53, no. 7, pp. 684 – 693, 2009. [Online]. Available: ''http://www.sciencedirect.com/science/article/pii/S0038110109000720".

[3] M. Pinuela, P. Mitcheson, and S. Lucyszyn, "Ambient RF energy harvesting in urban and semi-urban environments," *IEEE Trans. Microw. Theory Techn.*, vol. 61, no. 7, pp. 2715–2726, Jul. 2013.

[4] C. Valenta and G. Durgin, "Harvesting wireless power: Survey of energy-harvester conversion efficiency in far-field, wireless power transfer systems," *IEEE Microw. Mag.*, vol. 15, no. 4, pp. 108–120, Jun. 2014.

[5] V. Talla, B. Kellogg, B. Ransford, S. Naderiparizi, J. R. Smith, and S. Gollakota, "Powering the next billion devices with Wi-Fi," *Commun. ACM*, vol. 60, no. 3, pp. 83–91, Feb. 2017. [Online]. Available: http://doi.acm.org/10.1145/3041059

[6] S. Gollakota, M. Reynolds, J. Smith, and D. Wetherall, "The emergence of RF-powered computing," *Computer*, vol. 47, no. 1, pp. 32–39, Jan. 2014.

[7] V. Talla, B. Kellogg, S. Gollakota, and J. R. Smith, "Battery-free cellphone," *Proc. ACM Interact. Mob. Wearable Ubiquitous Technol.*, vol. 1, no. 2, pp. 25:1–25:20, Jun. 2017. [Online]. Available: http://doi.acm.org/10.1145/3090090

[8] A. Zanella *et al.*, "Internet of Things for smart cities," *IEEE Internet Things J.*, vol. 1, no. 1, pp. 22–32, Feb. 2014.

[9] M. Gorlatova, J. Sarik, G. Grebla, M. Cong, I. Kymissis, and G. Zussman, "Movers and shakers: Kinetic energy harvesting for the internet of things," *IEEE J. Sel. Areas Commun.*, vol. 33, no. 8, pp. 1624–1639, Aug. 2015.

[10] "RF energy harvesting and wireless power for low-power applications." [Online]. Available: http://www.powercastco.com/PDF/powercast-overview%20(2012).pdf.

[11] K. Huang and X. Zhou, "Cutting the last wires for mobile communications by microwave power transfer," *IEEE Commun. Mag.*, vol. 53, no. 6, pp. 86–93, Jun. 2015.

[12] Y. Zeng, B. Clerckx, and R. Zhang, "Communications and signals design for wireless power transmission," *IEEE Trans. Commun.*, vol. 65, no. 5, pp. 2264–2290, May 2017.

[13] X. Lu, P. Wang, D. Niyato, D. I. Kim, and Z. Han, "Wireless networks with RF energy harvesting: A contemporary survey," *IEEE Commun. Surveys Tuts.*, vol. 17, no. 2, pp. 757–789, May 2015.

[14] O. Georgiou, K. Mimis, D. Halls, W. H. Thompson, and D. Gibbins, "How many Wi-Fi APs does it take to light a lightbulb?" *IEEE Access*, vol. 4, pp. 3732–3746, Jan. 2016.

[15] S. Bi, C. Ho, and R. Zhang, "Wireless powered communication: opportunities and challenges," *IEEE Commun. Mag.*, vol. 53, no. 4, pp. 117–125, Apr. 2015.

[16] I. Krikidis, S. Timotheou, S. Nikolaou, G. Zheng, D. W. K. Ng, and R. Schober, "Simultaneous wireless information and power transfer in modern communication systems," *IEEE Commun. Mag.*, vol. 52, no. 11, pp. 104–110, Nov. 2014.

[17] L. R. Varshney, "Transporting information and energy simultaneously," in *Proc. 2008 IEEE Int. Symp. Inf. Theory*, Jul. 2008, pp. 1612–1616.

[18] O. Galinina, H. Tabassum, K. Mikhaylov, S. Andreev, E. Hossain, and Y. Koucheryavy, "On feasibility of 5G-grade dedicated RF charging technology for wireless-powered wearables," *IEEE Wireless Commun.*, vol. 23, no. 2, pp. 28–37, Apr. 2016.

[19] R. Zhang and C. K. Ho, "MIMO broadcasting for simultaneous wireless information and power transfer," *IEEE Trans. Wireless Commun.*, vol. 12, no. 5, pp. 1989–2001, May 2013.

[20] X. Zhou, R. Zhang, and C. K. Ho, "Wireless information and power transfer: Architecture design and rate-energy tradeoff," *IEEE Trans. Commun.*, vol. 61, no. 11, pp. 4754–4767, Nov. 2013.

[21] H. Ju and R. Zhang, "Throughput maximization in wireless powered communication networks," *IEEE Trans. Wireless Commun.*, vol. 13, no. 1, pp. 418–428, Jan. 2014.

[22] J. Park and B. Clerckx, "Joint wireless information and energy transfer in a two-user MIMO interference channel," *IEEE Trans. Wireless Commun.*, vol. 12, no. 8, pp. 4210–4221, Aug. 2013.

[23] L. Liu, R. Zhang, and K.-C. Chua, "Wireless information transfer with opportunistic energy harvesting," *IEEE Trans. Wireless Commun.*, vol. 12, no. 1, pp. 288–300, Jan. 2013.

[24] A. A. Nasir, X. Zhou, S. Durrani, and R. A. Kennedy, "Throughput and ergodic capacity of wireless energy harvesting based DF relaying network," in *Proc. 2014 IEEE Int. Conf. Commun.*, Jun. 2014, pp. 4066–4071.

[25] A. A. Nasir *et al.*, "Relaying protocols for wireless energy harvesting and information processing," *IEEE Trans. Wireless Commun.*, vol. 12, no. 7, pp. 3622–3636, Jul. 2013.

[26] I. Flint *et al.*, "Performance analysis of ambient RF energy harvesting with repulsive point process modeling," *IEEE Trans. Wireless Commun.*, vol. 14, no. 10, pp. 5402–5416, Oct. 2015.

[27] S. Lee, R. Zhang, and K. Huang, "Opportunistic wireless energy harvesting in cognitive radio networks," *IEEE Trans. Wireless Commun.*, vol. 12, no. 9, pp. 4788–4799, Sep. 2013.

[28] A. Sakr and E. Hossain, "Cognitive and energy harvesting-based D2D communication in cellular networks: Stochastic geometry modeling and analysis," *IEEE Trans. Commun.*, vol. 63, no. 5, pp. 1867–1880, May 2015.

[29] I. Krikidis, "Relay selection in wireless powered cooperative networks with energy storage," *IEEE J. Sel. Areas Commun.*, vol. 33, no. 12, pp. 2596–2610, Dec. 2015.

[30] K. Huang and V. Lau, "Enabling wireless power transfer in cellular networks: Architecture, modeling and deployment," *IEEE Trans. Wireless Commun.*, vol. 13, no. 2, pp. 902–912, Feb. 2014.

[31] K. Huang and E. Larsson, "Simultaneous information and power transfer for broadband wireless systems," *IEEE Trans. Signal Process.*, vol. 61, no. 23, pp. 5972–5986, Dec. 2013.

[32] I. Krikidis, "Simultaneous information and energy transfer in large-scale networks with/without relaying," *IEEE Trans. Commun.*, vol. 62, no. 3, pp. 900–912, Mar. 2014.

[33] Y. Shi, L. Xie, Y. T. Hou, and H. D. Sherali, "On renewable sensor networks with wireless energy transfer," in *Proc. 2011 IEEE INFOCOM*, Apr. 2011, pp. 1350–1358.

[34] K. W. Choi, D. I. Kim, and M. Y. Chung, "Received power-based channel estimation for energy beamforming in multiple-antenna RF energy transfer system," *IEEE Trans. Signal Process.*, vol. 65, no. 6, pp. 1461–1476, Mar. 2017.

[35] C. K. Ho and R. Zhang, "Optimal energy allocation for wireless communications with energy harvesting constraints," *IEEE Trans. Signal Proces.*, vol. 60, no. 9, pp. 4808–4818, Sep. 2012.

[36] D. T. Hoang, D. Niyato, P. Wang, and D. I. Kim, "Performance optimization for cooperative multiuser cognitive radio networks with RF energy harvesting capability," *IEEE Trans. Wireless Commun.*, vol. 14, no. 7, pp. 3614–3629, Jul. 2015.

[37] H. Tabassum, E. Hossain, M. J. Hossain, and D. I. Kim, "On the spectral efficiency of multiuser scheduling in RF-powered uplink cellular networks," *IEEE Trans. Wireless Commun.*, vol. 14, no. 7, pp. 3586–3600, Jul. 2015.

[38] H. Son and B. Clerckx, "Joint beamforming design for multi-user wireless information and power transfer," *IEEE Trans. Wireless Commun.*, vol. 13, no. 11, pp. 6397–6409, Nov. 2014.

[39] Q. Shi, L. Liu, W. Xu, and R. Zhang, "Joint transmit beamforming and receive power splitting for MISO SWIPT systems," *IEEE Trans. Wireless Commun.*, vol. 13, no. 6, pp. 3269–3280, Jun. 2014.

[40] L. Liu, R. Zhang, and K.-C. Chua, "Multi-antenna wireless powered communication with energy beamforming," *IEEE Trans. Commun.*, vol. 62, no. 12, pp.

4349–4361, Dec. 2014.

[41] Y. Zeng and R. Zhang, "Optimized training design for wireless energy transfer," *IEEE Trans. Commun.*, vol. 63, no. 2, pp. 536–550, Feb. 2015.

[42] Z. Ding, C. Zhong, D. W. K. Ng, M. Peng, H. A. Suraweera, R. Schober, and H. V. Poor, "Application of smart antenna technologies in simultaneous wireless information and power transfer," *IEEE Commun. Mag.*, vol. 53, no. 4, pp. 86–93, Apr. 2015.

[43] D. W. K. Ng, E. S. Lo, and R. Schober, "Wireless information and power transfer: Energy efficiency optimization in OFDMA systems," *IEEE Trans. Wireless Commun.*, vol. 12, no. 12, pp. 6352–6370, Dec. 2013.

[44] T. A. Khan, R. W. Heath Jr, and P. Popovski, "On wirelessly powered communications with short packets," *Proc. 2016 IEEE Globecom Workshops*, pp. 1–6, Dec. 2016.

[45] T. A. Khan, R. W. Heath, and P. Popovski, "Wirelessly powered communication networks with short packets," *IEEE Trans. Commun.*, vol. PP, no. 99, pp. 1–1, 2017.

[46] G. Durisi, T. Koch, and P. Popovski, "Toward massive, ultrareliable, and low-latency wireless communication with short packets," *Proc. IEEE*, vol. 104, no. 9, pp. 1711–1726, Sep. 2016.

[47] J. Yang, "Achievable rate for energy harvesting channel with finite blocklength," in *Proc. 2014 IEEE Int. Symp. Inf. Theory*, Jun. 2014, pp. 811–815.

[48] S. L. Fong, V. Y. F. Tan, and J. Yang, "Non-asymptotic achievable rates for energy-harvesting channels using save-and-transmit," *IEEE J. Sel. Areas Commun.*, vol. 34, no. 12, pp. 3499–3511, Dec. 2016.

[49] Y. Polyanskiy, H. V. Poor, and S. Verdu, "Channel coding rate in the finite blocklength regime," *IEEE Trans. Inf. Theory*, vol. 56, no. 5, pp. 2307–2359, May 2010.

[50] K. G. Shenoy and V. Sharma, "Finite blocklength achievable rates for energy harvesting AWGN channels with infinite buffer," in *Proc. 2016 IEEE Int. Symp. Inf. Theory*, Jul. 2016, pp. 465–469.

[51] A. Guo, H. Yin, and W. Wang, "Performance analysis of energy harvesting wireless communication system with finite blocklength," *IEEE Commun. Lett.*, vol. 20, no. 2, pp. 324–327, Feb. 2016.

[52] B. Makki, T. Svensson, and M. Zorzi, "Wireless energy and information transmission using feedback: Infinite and finite block-length analysis," *IEEE Trans. Commun.*, vol. 64, no. 12, pp. 5304–5318, Dec. 2016.

[53] E. MolavianJazi and A. Yener, "Low-latency communications over zero-battery energy harvesting channels," in *Proc. 2015 IEEE Global Commun. Conf.*, Dec. 2015, pp. 1–6.

[54] V. Y. F. Tan, "Asymptotic estimates in information theory with non-vanishing error probabilities," *Found. Trends Commun. Inf. Theory*, vol. 11, no. 1-2, pp. 1–184, Sep. 2014. [Online]. Available: http://dx.doi.org/10.1561/0100000086

[55] O. Ozel and S. Ulukus, "Achieving AWGN capacity under stochastic energy harvesting," *IEEE Trans. Inf. Theory*, vol. 58, no. 10, pp. 6471–6483, Oct. 2012.

[56] O. Ozel and S. Ulukus, "AWGN channel under time-varying amplitude constraints with causal information at the transmitter," in *Proc. 2011 Asilomar Conf. Signals, Systems and Computers*, Nov. 2011, pp. 373–377.

[57] W. Mao and B. Hassibi, "On the capacity of a communication system with energy harvesting and a limited battery," in *Proc. 2013 IEEE Int. Symp. Inf. Theory*, Jul. 2013, pp. 1789–1793.

[58] V. Jog and V. Anantharam, "An energy harvesting AWGN channel with a finite battery," in *Proc. 2014 IEEE Int. Symp. Inf. Theory*, Jun. 2014, pp. 806–810.

[59] Y. Dong, F. Farnia, and A. Ozgur, "Near optimal energy control and approximate capacity of energy harvesting communication," *IEEE J. Sel. Areas Commun.*, vol. 33, no. 3, pp. 540–557, Mar. 2015.

[60] O. Ozel, K. Tutuncuoglu, S. Ulukus, and A. Yener, "Fundamental limits of energy harvesting communications," *IEEE Commun. Mag.*, vol. 53, no. 4, pp. 126–132, Apr. 2015.

[61] B. Klar, "A note on gamma difference distributions," *Journal of Statistical Computation and Simulation*, vol. 85, no. 18, pp. 3708–3715, 2015.

[62] R. M. Corless, G. H. Gonnet, D. E. Hare, D. J. Jeffrey, and D. E. Knuth, "On the Lambert W function," *Advances in Computational mathematics*, vol. 5, no. 1, pp. 329–359, 1996.

[63] M. Haenggi, *Stochastic geometry for wireless networks*. Cambridge University Press, 2012.

[64] A. Prudnikov, *Integrals and series: special functions*.

[65] S. Noschese and P. E. Ricci, "Differentiation of multivariable composite functions and Bell polynomials," *Journal of Computational Analysis and Applications*, vol. 5, no. 3, pp. 333–340, 2003.

[66] J. Abate and W. Whitt, "Numerical inversion of Laplace transforms of probability distributions," *ORSA Journal on computing*, vol. 7, no. 1, pp. 36–43, 1995.

[67] Y.-C. Ko, M.-S. Alouini, and M. K. Simon, "Outage probability of diversity systems over generalized fading channels," *IEEE Trans. Commun.*, vol. 48, no. 11, pp. 1783–1787, Nov. 2000.

[68] J. Guo, S. Durrani, and X. Zhou, "Outage probability in arbitrarily-shaped finite wireless networks," *IEEE Trans. Commun.*, vol. 62, no. 2, pp. 699–712, Feb. 2014.

[69] T. Khan, R. W. Heath Jr, and P. Popovski, "Wirelessly powered communication networks with short packets," *arXiv preprint arXiv:1610.07672*, 2016.

[70] H. ElSawy, A. Sultan-Salem, M. S. Alouini, and M. Z. Win, "Modeling and analysis of cellular networks using stochastic geometry: A tutorial," *IEEE Commun. Surveys Tuts.*, vol. 19, no. 1, pp. 167–203, Firstquarter 2017.

[71] T. A. Khan, A. Alkhateeb, and R. W. Heath, "Energy coverage in millimeter wave energy harvesting networks," in *Proc. 2015 IEEE Globecom Workshops*, Dec. 2015, pp. 1–6.

[72] T. A. Khan, A. Alkhateeb, and R. Heath, "Millimeter wave energy harvesting," *IEEE Trans. Wireless Commun.*, vol. 15, no. 9, pp. 6048–6062, Sep. 2016.

[73] T. S. Rappaport, R. W. Heath Jr, R. C. Daniels, and J. N. Murdock, *Millimeter Wave Wireless Communications*. Pearson Education, 2014.

[74] T. Bai, A. Alkhateeb, and R. Heath, "Coverage and capacity of millimeter-wave cellular networks," *IEEE Commun. Mag.*, vol. 52, no. 9, pp. 70–77, Sep. 2014.

[75] S. Rangan, T. Rappaport, and E. Erkip, "Millimeter-wave cellular wireless networks: Potentials and challenges," *Proc. IEEE*, vol. 102, no. 3, pp. 366–385, Mar. 2014.

[76] F. Baccelli, B. Blaszczyszyn, and P. Muhlethaler, "An Aloha protocol for multihop mobile wireless networks," *IEEE Trans. Inf. Theory*, vol. 52, no. 2, pp. 421–436, Feb. 2006.

[77] S. Weber, J. Andrews, and N. Jindal, "An overview of the transmission capacity of wireless networks," *IEEE Trans. Commun.*, vol. 58, no. 12, pp. 3593–3604, Dec. 2010.

[78] H. ElSawy, E. Hossain, and M. Haenggi, "Stochastic geometry for modeling, analysis, and design of multi-tier and cognitive cellular wireless networks: A survey," *IEEE Commun. Surveys Tuts.*, vol. 15, no. 3, pp. 996–1019, Jul. 2013.

[79] J. Andrews, F. Baccelli, and R. Ganti, "A tractable approach to coverage and rate in cellular networks," *IEEE Trans. Commun.*, vol. 59, no. 11, pp. 3122–3134, Nov. 2011.

[80] H. S. Dhillon, R. K. Ganti, F. Baccelli, and J. G. Andrews, "Modeling and analysis of K-tier downlink heterogeneous cellular networks," *IEEE J. Sel. Areas Commun.*, vol. 30, no. 3, pp. 550–560, Apr. 2012.

[81] S. Akoum and R. W. Heath, "Interference coordination: Random clustering and adaptive limited feedback," *IEEE Trans. Signal Process.*, vol. 61, no. 5-8, pp. 1822–1834, Apr. 2013.

[82] F. Baccelli and A. Giovanidis, "A stochastic geometry framework for analyzing pairwise-cooperative cellular networks," *IEEE Trans. Wireless Commun.*, vol. PP, no. 99, pp. 1–1, 2014.

[83] G. Nigam, P. Minero, and M. Haenggi, "Coordinated multipoint joint transmission in heterogeneous networks," *IEEE Trans. Commun.*, vol. 62, no. 11, pp. 4134–4146, Nov. 2014.

[84] R. Tanbourgi, S. Singh, J. G. Andrews, and F. K. Jondral, "A tractable model for non-coherent joint-transmission base station cooperation," *arXiv preprint*

arXiv:1308.0041, 2013.

[85] L. Wang, M. Elkashlan, R. W. Heath, M. D. Renzo, and K. K. Wong, "Millimeter wave power transfer and information transmission," in *Proc. 2015 IEEE Global Commun. Conf.*, Dec. 2015, pp. 1–6.

[86] K. Huang, "Spatial throughput of mobile ad hoc networks powered by energy harvesting," *IEEE Trans. Inf. Theory*, vol. 59, no. 11, pp. 7597–7612, Nov. 2013.

[87] R. Vaze, "Transmission capacity of wireless ad hoc networks with energy harvesting nodes," in *IEEE Global Conf. Signal Inf. Process.*, Dec. 2013, pp. 353–358.

[88] H. Dhillon, Y. Li, P. Nuggehalli, Z. Pi, and J. Andrews, "Fundamentals of heterogeneous cellular networks with energy harvesting," *IEEE Trans. Wireless Commun.*, vol. 13, no. 5, pp. 2782–2797, May 2014.

[89] F. Parzysz, M. D. Renzo, and C. Verikoukis, "Power-availability-aware cell association for energy-harvesting small-cell base stations," *IEEE Trans. Wireless Commun.*, vol. 16, no. 4, pp. 2409–2422, Apr. 2017.

[90] Y. Deng, L. Wang, M. Elkashlan, M. D. Renzo, and J. Yuan, "Modeling and analysis of wireless power transfer in heterogeneous cellular networks," *IEEE Trans. Commun.*, vol. 64, no. 12, pp. 5290–5303, Dec. 2016.

[91] T. A. Khan, P. V. Orlik, K. J. Kim, R. W. Heath, and K. Sawa, "A stochastic geometry analysis of large-scale cooperative wireless networks powered by en-

ergy harvesting," *IEEE Trans. Commun.*, vol. 65, no. 8, pp. 3343–3358, Aug. 2017.

[92] T. A. Khan, P. Orlik, and K. J. Kim, "A stochastic geometry analysis of cooperative wireless networks powered by energy harvesting," in *Proc. 2015 IEEE Int. Conf. Commun.*, Jun. 2015, pp. 1988–1993.

[93] T. Bai and R. Heath, "Coverage and rate analysis for millimeter-wave cellular networks," *IEEE Trans. Wireless Commun.*, vol. 14, no. 2, pp. 1100–1114, Feb. 2015.

[94] S. Singh, M. Kulkarni, A. Ghosh, and J. Andrews, "Tractable model for rate in self-backhauled millimeter wave cellular networks," *IEEE J. Sel. Areas Commun.*, vol. 33, no. 10, pp. 2196–2211, Oct. 2015.

[95] T. Bai, R. Vaze, and R. Heath, "Analysis of blockage effects on urban cellular networks," *IEEE Trans. Wireless Commun.*, vol. 13, no. 9, pp. 5070–5083, Sep. 2014.

[96] A. Hunter, J. Andrews, and S. Weber, "Transmission capacity of ad hoc networks with spatial diversity," *IEEE Trans. Wireless Commun.*, vol. 7, no. 12, pp. 5058–5071, Dec. 2008.

[97] M. Tabesh *et al.*, "A power-harvesting pad-less millimeter-sized radio," *IEEE J. Solid-State Circuits*, vol. 50, no. 4, pp. 962–977, Apr. 2015.

[98] J. Charthad, N. Dolatsha, A. Rekhi, and A. Arbabian, "System-level analysis of far-field radio frequency power delivery for mm-sized sensor nodes," *IEEE Trans. Circuits Syst. I: Reg. Papers*, vol. 63, no. 2, pp. 300–311, Feb. 2016.

[99] T. Wu, T. S. Rappaport, and C. M. Collins, "The human body and millimeter-wave wireless communication systems: Interactions and implications," *arXiv preprint arXiv:1503.05944*, 2015.

[100] A. Ghosh, J. Zhang, J. G. Andrews, and R. Muhamed, *Fundamentals of LTE*. Pearson Education, 2010.

[101] H. L. Van Trees, *Detection, estimation, and modulation theory, optimum array processing*. John Wiley & Sons, 2004.

[102] R. Méndez-Rial, C. Rusu, A. Alkhateeb, N. González-Prelcic, and R. W. Heath Jr, "Channel estimation and hybrid combining for mmWave: Phase shifters or switches?" in *Proc. 2015 Inf. Theory and Applications Workshop*, Feb. 2015, pp. 90–97.

[103] R. Méndez-Rial, C. Rusu, N. González-Prelcic, A. Alkhateeb, and R. W. Heath, "Hybrid MIMO architectures for millimeter wave communications: Phase shifters or switches?" *IEEE Access*, vol. 4, pp. 247–267, Jan. 2016.

[104] H. Alzer, "On some inequalities for the incomplete gamma function," *Mathematics of Computation of the American Mathematical Society*, vol. 66, no. 218, pp. 771–778, 1997.

[105] T. A. Khan, A. Yazdan, Y. Maguire, and R. W. Heath, "Energy efficiency of wireless information and power transfer with massive MIMO," in *Proc. 2017 IEEE 85th Veh. Tech. Conf. (VTC-Spring)*, Jun. 2017, pp. 1–6.

[106] A. Yazdan *et al.*, "Energy-efficient massive MIMO: Wireless-powered communication, multiuser MIMO with hybrid precoding, and cloud radio access network with variable-resolution ADCs," *IEEE Microw. Mag.*, vol. 18, no. 5, pp. 18–30, Jul. 2017.

[107] F. Boccardi *et al.*, "Five disruptive technology directions for 5G," *IEEE Commun. Mag.*, vol. 52, no. 2, pp. 74–80, Feb. 2014.

[108] T. L. Marzetta, "Noncooperative cellular wireless with unlimited numbers of base station antennas," *IEEE Trans. Wireless Commun.*, vol. 9, no. 11, pp. 3590–3600, Nov. 2010.

[109] J. Andrews, S. Buzzi, W. Choi, S. Hanly, A. Lozano, A. Soong, and J. Zhang, "What will 5G be?" *IEEE J. Sel. Areas Commun.*, vol. 32, no. 6, pp. 1065–1082, Jun. 2014.

[110] S. Kashyap *et al.*, "On the feasibility of wireless energy transfer using massive antenna arrays," *IEEE Trans. Wireless Commun.*, vol. 15, no. 5, pp. 3466–3480, May 2016.

[111] G. Yang *et al.*, "Throughput optimization for massive MIMO systems powered by wireless energy transfer," *IEEE J. Sel. Areas Commun.*, vol. 33, no. 8, pp. 1640–1650, Aug. 2015.

[112] H. Q. Ngo *et al.*, "Energy and spectral efficiency of very large multiuser MIMO systems," *IEEE Trans. Commun.*, vol. 61, no. 4, pp. 1436–1449, Apr. 2013.

[113] E. Bjornson *et al.*, "Optimal design of energy-efficient multi-user MIMO systems: Is massive MIMO the answer?" *IEEE Trans. Wireless Commun.*, vol. 14, no. 6, pp. 3059–3075, Jun. 2015.

[114] W. Liu, S. Han, and C. Yang, "Is massive MIMO energy efficient?" *arXiv preprint arXiv:1505.07187*, 2015.

[115] X. Chen *et al.*, "Energy-efficient optimization for wireless information and power transfer in large-scale MIMO systems employing energy beamforming," *IEEE Wireless Commun. Lett.*, vol. 2, no. 6, pp. 667–670, Dec. 2013.

[116] M. Xia and S. Aissa, "On the efficiency of far-field wireless power transfer," *IEEE Trans. Signal Process.*, vol. 63, no. 11, pp. 2835–2847, Jun. 2015.

[117] E. Boshkovska, D. W. K. Ng, N. Zlatanov, and R. Schober, "Practical non-linear energy harvesting model and resource allocation for SWIPT systems," *IEEE Commun. Lett.*, vol. 19, no. 12, pp. 2082–2085, Dec. 2015.

[118] E. Boshkovska *et al.*, "Robust resource allocation for MIMO wireless powered communication networks based on a non-linear EH model," *IEEE Trans. Commun.*, vol. 65, no. 5, pp. 1984–1999, May 2017.

[119] S. Boyd and L. Vandenberghe, *Convex optimization*. Cambridge Univ. Press, 2004.

[120] A. Charnes and W. W. Cooper, "Programming with linear fractional functionals," *Naval Research Logistics (NRL)*, vol. 9, no. 3-4, pp. 181–186, 1962.

Vita

Talha Ahmed Khan is a PhD candidate at the University of Texas at Austin. He graduated with a Bachelor of Science in Electrical Engineering from University of Engineering and Technology, Lahore in 2010. He started his professional career as an RF Optimization Engineer at Mobilink. Before beginning his graduate studies in 2012, he was affiliated with the Department of Electrical Engineering at Lahore University of Management Sciences, where he worked as a wireless researcher. He was a research intern at Connectivity Lab, Facebook, Menlo Park in the summer of 2016. He interned with Mitsubishi Electric Research Labs, Cambridge during the summer of 2014. He has also interned with the Mobile and Wireless Group at Broadcom, San Diego. His research interests broadly span the areas of wireless communications and networking, with a current focus on energy harvesting communications system.

Permanent address: talhakhan@utexas.edu

This dissertation was typeset with LaTeX[†] by the author.

[†]LaTeX is a document preparation system developed by Leslie Lamport as a special version of Donald Knuth's TeX Program.